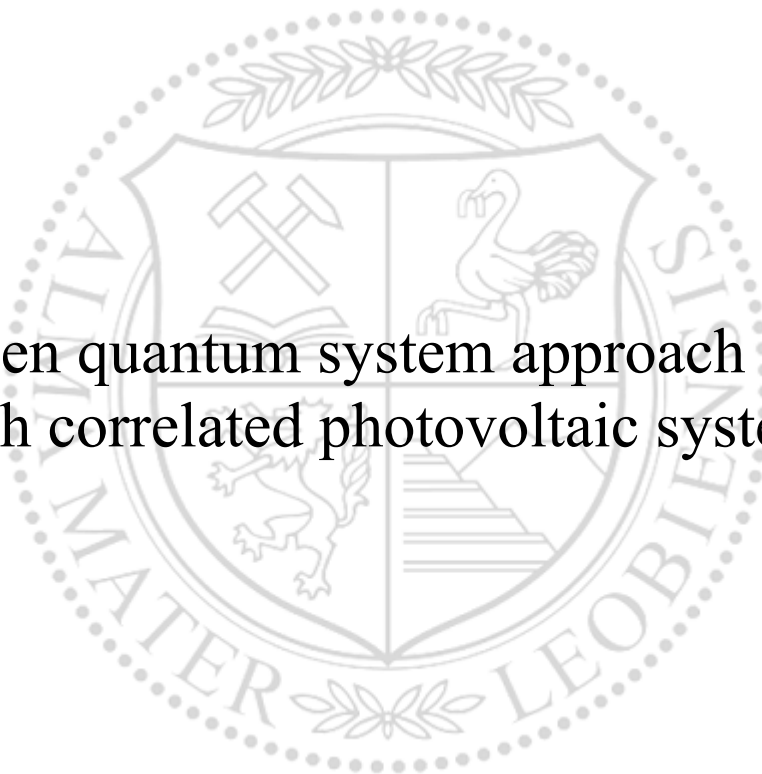Chair of Physics

Master's Thesis

An open quantum system approach to deal with correlated photovoltaic systems

Daniel Werner, BSc

November 2021

EIDESSTATTLICHE ERKLÄRUNG

Ich erkläre an Eides statt, dass ich diese Arbeit selbständig verfasst, andere als die angegebenen Quellen und Hilfsmittel nicht benutzt, und mich auch sonst keiner unerlaubten Hilfsmittel bedient habe.

Ich erkläre, dass ich die Richtlinien des Senats der Montanuniversität Leoben zu "Gute wissenschaftliche Praxis" gelesen, verstanden und befolgt habe.

Weiters erkläre ich, dass die elektronische und gedruckte Version der eingereichten wissenschaftlichen Abschlussarbeit formal und inhaltlich identisch sind.

Datum 09.11.2021

Unterschrift Verfasser/in
Daniel Werner

Daniel Werner, BSc

An open quantum system approach to deal with correlated photovoltaic systems

MASTERARBEIT

zur Erlangung des akademischen Grades

Master of Science

Masterstudium Werkstoffwissenschaft

eingereicht an der

Montanuniversität Leoben

Betreuer

Prof. Enrico Arrigoni

Institute of Theoretical and Computational Physics
Technische Universität Graz

Leoben, November 2021

1 Acknowledgements

This work has been supervised by Prof. Enrico Arrigoni of the Institute of Theoretical and Computational Physics at the TU Graz, whom I also want to thank for giving me the opportunity to do this thesis. I also would have never even asked in the first place, if I had not been encouraged to do so by one of my previous flatmates, namely Valerie, and I also want to thank her for this. Another aspect I very much appreciate is, that Enrico provided me with a place in an already full exercise group for Advanced Quantum Mechanics, without which I might had not gained the knowledge to even start this thesis.

Furthermore, I want to thank my family. No matter what I choose to do, I can always rely on their support. I always take this for granted, but I know that by far not everyone has such loving family members.

Doing this thesis was not the most straightforward path, considering that I studied material science in Leoben. Also for my Bachelor thesis I did something atypical for this field of study at my university, where Prof. Josef Oswald, who also co-supervised this thesis, gave me the opportunity to deal with quantum mechanics in a bit more detail, than is usually done in material science.

A lot of thanks also goes to someone I never met in reality, Prof. Zwiebach, who provides all his quantum mechanics lecture and exercise material online, which allowed me to get a much more detailed basic knowledge, which was the basis for successfully participating in Enrico's Advanced Quantum Mechanics course.

Furthermore, I also want to thank my colleagues at the TU Graz, Jan, Paolo, and Tommaso, because whenever I had any questions they would immediately help me, and they were also amazing colleagues in any other regard. It felt really nice being among people with an interest in theory, and it made me realize even more that physics should have been my choice from the very start. I also want to thank Enrico, Jan, Josef, and Mariia for their comments on my written thesis, since it taught me quite a lot.

2 Abstract

In this master thesis, our goal is to simulate a simplified photovoltaic setup, and to study the average current as a function of the frequency of a monochromatic light source. Physically, we may imagine our system as a semiconductor, which is influenced by the periodic electric field, connected to two metallic leads, where the energy of the left lead is smaller than the one of the right lead and application of electron-magnetic radiation provides the energy to move electrons from the left to the right lead, allowing for energy harvesting. In two of our setups we have a band gap due to a specific structure and parameter choice. For the third setup the gap is caused by electron-electron interaction, which is the case we are most interested in.

The energy of the left lead, and the lower band of the semiconductor are chosen to overlap, as well as the energy of the right lead and the upper band gap of the semiconductor. Therefore, electrons coming in from the left can easily find a state in the lower band of the central region they can occupy.

To simulate this open quantum system, the Lindblad equation has been used, which means we must assume that the influence of the system on the environment is negligible, compared to the reveres process. If we want to take into account electron-electron interaction, we must perform the exact diagonalization of the many body density-matrix to solve this equation, which is strongly limiting the system size. For the non-interacting case, we can use the equations of motion, which allow for larger setups.

The shape of the average current as a function of frequency, reflected the respective band gaps quite well in most cases. One of our main findings is, that we found maxima in the average current plots, that lie at a fraction (1/2, 1/3) of the gap size, and increase with intensity, which are interpreted in terms of excitations due to the absorption of two or more photons.

Contents

3 Introduction

We will investigate a model for a system which features a gap, which can be alternatively produced by band effects or by correlation effects. To this system we apply a monochromatic light source, and it is connected to two metallic leads, which represent the environment. The main motivation is to address photovoltaic effects in a system with strong electron correlation, which is not present in conventional semiconductors. In correlated systems one has to take into account the full many-body Hilbert space. The central region cannot be too large in size, and that is why the environment is treated via the Lindblad equation. Therefore, we are simulating simplified photovoltaics systems, similar to [1, 2, 3, 4, 5, 6, 7], but here we only investigate direct excitations, use a less sophisticated approach, and do not take into account phonons.

The observable we are interested in, is the average current. This means that there are interactions with the environment, since an average current is only nonzero, if we have a net in-/outflow at some point. The connection with the environment means, we have to take into account coupling between the system we are interested in, and the its surroundings. Provided the influence of the system on the environment is negligible, compared to the reveres process, we can approximate such a setup reasonably well via the Lindblad equation, and we assume this to be the case. Furthermore, our system is considered to consist of atoms, in which only one orbital is relevant. For simplicity we deal with chain like structures, which are connected to a reservoir at their start and ending points.

There are different approaches for solving the Lindblad equation, and, thereby, how to obtain values for observables, and we will use two of them. If we want to take into account electron-electron interaction, we have to use the exact diagonalization of the many body density-matrix, but this only allows for small system sizes, due to the strong exponential increase of the matrix size, with the number of sites. The other method we use are the equations of motion (EOM), which allow for significantly larger systems, but electron-electron interaction cannot be taken into account, if we want to obtain a closed set of equations.

The setup of our configurations is always the same. We have a central part, corresponding to a semiconductor, in which we have a band gap, which is under the influence of the periodic electric field, and this central system is weakly coupled to a lead at the beginning and the end. The term "lead" means a 1D chain, which mimics a metallic lead, where no electron-electron interaction takes place, and which have a certain on-site energy. The continuation of these metallic leads is modelled by Lindblad equation via the reservoirs connected to the 1D chains. The reason for the weak coupling between the leads, and the central part is, that we want to cause minimal disturbance of the semiconductor's band structure.

For the non-interacting systems, we have to design them in a way, such that a band gap arises. One possibility to do this, is to create a ladder like structure, in which we use different hopping parameters for the direction of chain extension, and normal to the direction of chain extension, as depicted in figure 10. This gives a band structure, in which we have only a single energy, for which a direct band transition is possible. Another structure that gives a band gap, is a one dimensional one, where we alternate the hopping parameter, which is shown in figure 29. For this latter band structure, we get an energy interval, where a continuous direct band transition is possible. In the case of interacting electrons, a gap is created due to the electron repulsion, but in that case large systems can not be considered, and we are limited to a maximum of five sites for the system. These correlated systems are also the ones we are most interested in, however, treating such setups is quite challenging, which is why only part of this thesis is devoted to them.

Since we have a gap, we can excite low energy electrons in the semiconductor from the lower to the higher band, when the applied time periodic electric field has sufficiently high frequency. The left lead then supplies us with more low energy electrons, and the high energy electrons can escape through the right lead, which has a high energy.

4 Theoretical approaches

4.1 Lindblad equation and its derivation

In this chapter we are following the treatment by [8], [9], [10], [11], [12], and [13]. The theoretical basis of this thesis is the Lindblad equation, since this equation allows us to take into account the interaction of a system with its environment, provided the approximations we will discuss in this chapter are fulfilled to a reasonable degree. Therefore, we will start by deriving it. We use the Lioville-von-Neumann equation for the quantum mechanical case[8]:

$$\rho = -i[H, \rho], \tag{1}$$

where H is the Hamiltonian of the system, and ρ the density matrix. H can be split up in three parts: H_S which purely acts on the system, H_E which purely acts on the environment, and V which connects the system and the environment:

$$H = H_S \otimes I + I \otimes H_E + V = H_0 + \alpha V. \tag{2}$$

H_S and H_E have been collected in H_0, and α has been factored out from V, which describes the strength of the coupling between system and environment. V is a combination of system, and environment operators, and, therefore, can be written as:

$$V = \sum_i S_i \otimes E_i, \tag{3}$$

where S_i exists in the system's Hilbert space, and E_i exists in the environment's Hilbert space. ρ can be written as a superposition of projection operators of product states. Since we are only interested in how the system changes over time, the trace over the environment is performed[13, p.132]:

$$
\begin{aligned}
\rho_S = Tr_E(\rho) &= \sum_i \sum_j P_j \langle E_i | \Psi_j \rangle \langle \Psi_j | E_i \rangle \\
&= \sum_i \sum_j \sum_k P_{jk} | S_j \rangle \langle E_i | E_k \rangle \langle S_j | \langle E_k | E_i \rangle \\
&= \sum_j \sum_k P_{jk} | S_j \rangle \langle S_j | .
\end{aligned}
\tag{4}
$$

In the second line the substitution $|\Psi_j\rangle = |E_l\rangle |S_k\rangle$ has been used, where $|\Psi_j\rangle$ are product states. It is more convenient to work in the interaction picture, therefore the necessary substitutions to get there are performed in the following equation[13, p.138]:

$$
\begin{aligned}
\rho_I(t) &= e^{iH_0 t} e^{-iHt} \rho e^{iHt} e^{-iH_0 t}, \\
O_I(t) &= e^{iH_0 t} O e^{-iH_0 t},
\end{aligned}
\tag{5}
$$

with O being an arbitrary operator, and the index I indicating the interaction picture. In this picture equation (1) becomes [13, p.138]:

$$\frac{d\rho_I(t)}{dt} = -i\alpha[V_I(t), \rho_I(t)]. \tag{6}$$

By integrating eq. (6) one obtains [13, p.139]

$$\rho_I(t + \Delta t) = \rho_I(t) - i\alpha \int_t^{t+\Delta t} dt' [V_I(t'), \rho_I(t')], \tag{7}$$

which can be reinserted into itself[13, p.138], giving:

$$\rho_I(t + \Delta t) = \rho_I(t) - i\alpha \int_t^{t+\Delta t} dt' \left[V_I(t'), \rho_I(t) - i\alpha \int_t^{t'} dt''[V_I(t''), \rho_I(t'')] \right]$$

$$= \rho_I(t) - i\alpha \int_t^{t+\Delta t} dt'[V_I(t'), \rho_I(t)] - \alpha^2 \int_t^{t+\Delta t} \int_t^{t'} dt''dt'[V_I(t'), [V_I(t''), \rho_I(t'')]] \quad (8)$$

$$\rightarrow \Delta\rho_I(t) = \rho_I(t + \Delta t) - \rho_I(t)$$

$$= -i\alpha \int_t^{t+\Delta t} dt'[V_I(t'), \rho_I(t)] - \alpha^2 \int_t^{t+\Delta t} \int_t^{t'} dt''dt'[V_I(t'), [V_I(t''), \rho_I(t'')]].$$

ρ_I can be written as $\rho_{SI} \otimes \rho_{EI0} + \rho_{corr}$ [13, p.139]. It is assumed that the environment is so large, that it is negligibly affected by the system [14, p.17]. This allows us to set ρ_{corr} to zero. Furthermore, it is assumed that the environment is in its equilibrium distribution, which means ρ_{EI} does not have any time dependency[13, p.139].

As a next step, the trace of the environment over the density matrix is used, to get the density matrix purely for the system [13, p.139]:

$$\Delta\rho_{SI}(t) = -i\alpha \int_t^{t+\Delta t} dt' Tr_E[V_I(t'), \rho_I(t)] - \alpha^2 \int_t^{t+\Delta t} \int_t^{t'} dt''dt' Tr_E[V_I(t'), [V_I(t''), \rho_I(t'')]]. \quad (9)$$

It can be shown, that the first term in eq. (9) can be taken to be zero[13, p.139]:

$$Tr_R[V_I(t'), \rho_I(t)] = Tr_E[V_I(t'), \rho_{SI}(t) \otimes \rho_E] = \sum_i [S_{Ii} \otimes Tr_E E_{Ii}(t'), \rho_{SI}(t) \otimes Tr_E\rho_E]$$

$$= \sum_i [S_{Ii} \otimes Tr_E E_{Ii}, \rho_{SI}(t) \otimes Tr_E\rho_E] = \sum_i [S_{Ii}, \rho_{SI}(t)]r_i. \quad (10)$$

Since the trace of an hermitian operator is preserved, the time dependence of E_{Ii} vanishes. From the trace over the environment two constants are obtained, which can be pulled out of the commutator, and their product is denoted as r_i[13, p.139]. These r_i can be chosen to be zero, by just reabsorbing the excess part in the non-interacting Hamiltonian[13, p.139]:

$$R_i' = R_i - r_i \mathbb{1}$$

$$\rightarrow V = \alpha \sum_i (R_i' + r_i\mathbb{1}) \otimes S_i = \alpha \sum_i (R_i' \otimes S_i + r_i\mathbb{1} \otimes S_i) \quad (11)$$

To proceed, another approximation has to be made. The remaining term contains a $\rho_{SI}(t'')$, and there is an integration over t''. But if Δt is small, compared to the time over which significant change appears in the system, which is assumed to be the case, then the density matrix is approximately constant over this time interval, and the following substitution can be performed $\rho_{SI}(t'') \rightarrow \rho_{SI}(t)$ [13, p.141]. Then one obtains

$$\frac{\Delta\rho_{SI}(t)}{\Delta t} = -\alpha^2 \int_t^{t+\Delta t} \int_t^{t'} dt''dt' Tr_E[V_I(t'), [V_I(t''), \rho_I(t'')]]. \quad (12)$$

Since the system operators are not affected by the trace, they can be pulled out of it, and so only the environment operators, and the environment density matrix are left in the trace. Therefore, there are only permutations of

$$Tr_E(V_I(t'')V_I(t')\rho_I) = \sum_{ij} Tr_E(S_i(t'') \otimes E_j(t'') \cdot S_j(t') \otimes E_i(t') \cdot \rho_{SI}(t) \otimes \rho_E)$$

$$= \sum_{ij} S_i(t'')S_j(t')\rho_{SI}(t) \otimes Tr_E(E_j(t'')E_i(t')\rho_E)$$

$$= \sum_{ij} S_i(t'')S_j(t')\rho_{SI}(t) \langle E_j(t'')E_i(t') \rangle = \sum_{ij} S_i(t'')S_j(t')\rho_{SI}(t)C_{ij}(t'-t''),$$

$$(13)$$

inside of the integral [13, p.140]. The environment is expected to be invariant under time translation. Therefore, only the time difference is of importance for the functions $C_{ij}(t'-t'')$. What is obtained, are so called environment self-correlation functions [14, p.17]. Since the E_i are part of V, they are related to the coupling between system and environment. Eq. (13) measures how correlated the measurements of the E_i over time would be, if performed, and, therefore, also how much "memory" the environment has of its interaction with the system, after a certain time [14, p.17]. The "memory" of the environment must decay over a time scale τ_E, that is much smaller than the time scale over which the "memory" of the system decays [13, p.141].

Since $C_{ij}(t'-t'')$ only depends on the time difference, the substitution $\tau = t'-t''$ can be performed. With this one gets:

$$\frac{\Delta\rho_{SI}(t)}{\Delta t} = -\int_0^{\Delta t} d\tau \frac{1}{\Delta t}\int_{t+\tau}^{t+\Delta t} dt'\alpha^2 \sum_{ij}\{S_i(t')S_j(t'-\tau)\rho_{SI}(t)C_{ij}(\tau)$$
$$-S_i(t')\rho_{SI}(t)S_j(t'-\tau)C_{ji}(-\tau) \qquad (14)$$
$$-S_j(t'-\tau)\rho_{SI}(t)S_i(t')C_{ij}(\tau)$$
$$+\rho_{SI}(t)S_j(t'-\tau)S_i(t')C_{ji}(-\tau)\}.$$

Eq. (14) can be rewritten in terms of commutators:

$$\frac{\Delta\rho_{SI}(t)}{\Delta t} = -\int_0^{\Delta t} d\tau \frac{1}{\Delta t}\int_{t+\tau}^{t+\Delta t} dt'\alpha^2 \sum_{ij}\{C_{ij}(\tau)[S_i(t'),S_j(t'-\tau)\rho_{SI}(t)]$$
$$+C_{ji}(-\tau)[\rho_{SI}(t)S_j(t'-\tau),S_i(t')].\} \qquad (15)$$

Since both integrals in eq. (15) run over an interval equal to or below Δt, and Δt is supposed to be small compared to time scales over which significant changes occur in the system, the following approximation can be made: $S(t') \approx S(t'-\tau) \approx S(t)$ [13, p.143]. Now, the only thing that is being integrated over are the correlation functions. The next step is to change the integral boundaries, by performing more approximations[13, p.141]. The integrals are

$$\int_0^{\Delta t} d\tau \int_{t+\tau}^{t+\Delta t} dt', \qquad (16)$$

and the correlation functions decay on a time scale τ_E, which must be much smaller than Δt, to make the approximation $\rho_I = \rho_{SI} \otimes \rho_{EI0}$ valid [13, p.145-146]. This means the integration boundary of the leftmost integral in eq. (16) may be changed from Δt to something negligible compared to Δt, but still large compared to τ_E, and, thereby, allows one to change the rightmost integral to:

$$\int_t^{t+\Delta t} dt'. \qquad (17)$$

Now there is no more τ dependence in the rightmost integral, but still the upper border of the leftmost integral in eq. (16) is high enough to contain all the area of the correlation functions. Therefore, the upper border can be taken to be infinite:

$$\int_0^{\infty} d\tau. \qquad (18)$$

There are no more functions depending on t', so one only gets a Δt from this integral. If one combines everything that has been discussed here, the result is:

$$\frac{\Delta\rho_{SI}(t)}{\Delta t} = -\alpha^2 \sum_{ij} \{[S_i(t), S_j(t)\rho_{SI}(t)] \int_0^\infty d\tau C_{ij}(\tau)$$
$$+ [\rho_{SI}(t)S_j(t), S_i(t)] \int_0^\infty d\tau C_{ji}(-\tau)\} \tag{19}$$

The integral over the correlation functions is in fact just a constant, so one may substitute [13, p.141]:

$$C_{ij}^\pm \equiv \int_0^\infty d\tau C_{ij}(\pm\tau). \tag{20}$$

Up to now, the result is in the interaction picture, it is, however, more useful in the Schrödinger picture, therefore, the according transformation is performed[13, p.143]:

$$\rho_{SI}(t) = e^{iH_S t}\rho_S(t)e^{-iH_S t}$$
$$\rightarrow \frac{d\rho_{SI}(t)}{dt} = e^{iH_S t}\left(i[H_S, \rho_S(t)] + \frac{\rho_S(t)}{dt}\right)e^{-iH_S t} \tag{21}$$
$$\rightarrow \frac{d\rho_S(t)}{dt} = -i[H_S, \rho_S(t)] + e^{-iH_S t}\frac{\rho_{SI}(t)}{dt}e^{iH_S t}.$$

Instead of $d\rho_{SI}(t)/dt$ eq. (19) can be used, since the Δ expressions are approximately the derivative [13, p.143]. Before inserting it into eq. (21), it is convenient to rewrite it as[13, 143]:

$$S_i(t)S_j(t)\rho_{SI}(t) = e^{iH_S t}S_i e^{-iH_S t}e^{iH_S t}S_j e^{-iH_S t}e^{iH_S t}\rho_S(t)e^{-iH_S t}$$
$$= e^{iH_S t}S_i S_j \rho_S(t)e^{-iH_S t}. \tag{22}$$

It can be seen, that the exponential functions cancel out, when inserting eq. (19) into eq. (21), and one obtains:

$$\frac{d\rho_S(t)}{dt} = -i[H_S, \rho_S] - \alpha^2 \sum_{ij}\left(C_{ij}^+[S_i, S_j\rho_S] + C_{ij}^-[\rho_S S_i, S_j]\right). \tag{23}$$

After performing some substitutions that will not be discussed here in detail, but can be found in [13, p.144-145], one gets a more familiar form of the Lindblad equation [13, p.145]:

$$\frac{d\rho_S(t)}{dt} = -i[\tilde{H}_S, \rho_S] + \sum_{ij}\Gamma_{ij}\left(S_j\rho_S S_i^\dagger - \frac{1}{2}\{S_i^\dagger S_j, \rho_S]\}\right),$$
$$= L_H\rho_S + L_D\rho_S = L\rho_S, \tag{24}$$

where $\tilde{H}_S = H_S + \frac{1}{2}\sum_{ij}\sigma_{ij}S_i S_j^\dagger$, and Γ and σ contain the correlation functions and coupling factor α.

For a fermionic system, the σ correspond to an integral of the coupling constants times the occupation probability, and it is assumed here that this expression is a symmetric function, which then means the σ become zero [13, p.149].

4.2 Superfermion representation

4.2.1 Introduction

Here we follow the treatment by [15], [16] and [13]. The superfermion representation is a more convenient way of using the Lindblad equation. The main idea is to describe the density matrix in terms of a state that lives in a doubled Hilbert space [13, p.150]. The usual density matrix can be written as

$$\rho = \sum_{nm} |n\rangle \langle m| \, \rho_{nm}. \tag{25}$$

By using some "trick" one wants to change the ket into a bra. To do this, the so-called left vacuum is introduced [13, p.150]:

$$|I\rangle = \sum_m |m\rangle |\tilde{m}\rangle . \tag{26}$$

Now, one can define the state vector corresponding to the density matrix [13, p.150]:

$$\begin{aligned}
\rho \to |\rho\rangle = \rho \otimes \tilde{I} \, |I\rangle &= \sum_{nm} \rho_{nm} |n\rangle \langle m| \otimes \tilde{I} \cdot \sum_j |j\rangle |\tilde{j}\rangle \\
&= \sum_{nmj} \rho_{nm} |n\rangle \langle m|j\rangle \otimes |\tilde{j}\rangle = \sum_{nm} \rho_{nm} |n\rangle \otimes |\tilde{m}\rangle .
\end{aligned} \tag{27}$$

4.2.2 Phase factors

As the next step, one wants to define the creation and annihilation operators of the tilde space in such a way, that the following relations hold [17, p.4]:

$$a_j \, |I\rangle = -i\tilde{a}_j^\dagger \, |I\rangle \qquad a_j^\dagger \, |I\rangle = -i\tilde{a}_j \, |I\rangle . \tag{28}$$

Each state in the superfermion space, corresponds to some operator in the normal space [17, p.3]:

$$|m\rangle \otimes |\tilde{n}\rangle \cong |m\rangle \otimes \langle n| \equiv a_i^\dagger ... a_g^\dagger |0\rangle \langle 0| \, a_j ... a_h. \tag{29}$$

Now it can be seen, that a creation operator in tilde space is acting from the left on a ket, therefore, in the normal space it corresponds to an annihilation operator acting on the bra from the right [17, p.3]. This can be expressed as:

$$\tilde{a}_k^\dagger \, |mn\rangle \cong i(-1)^\mu a_i^\dagger ... a_g^\dagger |0\rangle \langle 0| \, a_j ... a_h a_k. \tag{30}$$

Where μ is the amount of all normal and tilde operators [17, p.3]. The following example should provide an intuitive idea for the phase one obtains from the tilde operators. One can rewrite $a_4^\dagger \tilde{a}_3^\dagger \, |00\rangle$ as $a_4^\dagger (|0\rangle \langle 0| \, a_3)$. If one wants to further rewrite it as $(|0\rangle \langle 0| \, a_3 a_4)$ one would swap the operators a_3, and a_4, resulting in a phase of -1.

This is equally true for

$$\tilde{a}_k \, |mn\rangle \cong i(-1)^\mu a_i^\dagger ... a_g^\dagger |0\rangle \langle 0| \, a_j ... a_h a_k^\dagger. \tag{31}$$

For the tilde annihilation, as well as creation operator a phase factor of i is added, which solely serves as a means to make eqs. (28) true, as we will see next.

Using the previous results, one can express the occupation number representation of the state in the superfermion space in terms of creation and annihilation operators [17, p.4]:

$$|mn\rangle = (-i)^{n^2} a_{k_1}^\dagger ... a_{k_g}^\dagger \tilde{a}_{k_1}^\dagger ... \tilde{a}_{k_h}^\dagger |00\rangle . \tag{32}$$

The additional factor in the beginning compensates all the phases one obtains from the tilde operators, as is shown in the following. The first creation operator only contributes a factor of i, all the others additionally a factor $(-1)^j$, where j is the distance between the current, and the rightmost operator, minus one. Therefore, the total phase factor is:

$$i \prod_{j=1}^{n-1} i(-1)^j = i \prod_{j=1}^{n-1} i\, i^{2j} = i^n i^{2\frac{n^2-n}{2}} = i^{n^2} = (-i)^{-n^2}. \tag{33}$$

This precisely cancels with the factor in eq. (33).

The states in the sum of the left vacuum (eq. (26)) can be expanded as [13, p.152]:

$$|n\tilde{n}\rangle = (-i)^{\sum_i n_i}(a_1^\dagger \tilde{a}_1^{\ \dagger})^{n_1}...(a_N^\dagger \tilde{a}_N^{\ \dagger})^{n_N}|00\rangle. \tag{34}$$

Since in the above equation the operators are not correctly ordered, the prefactor is different. It can, however, be seen that the (-1) factors are precisely canceled, since each tilde operator gets the same phase from passing by the normal operators, as it gets from acting on the tilde space. Only the i remain, and these are equal to $i^{\sum_i n_i}$, which cancels the prefactor in eq. (34).
Now the tilde conjugation rules have been established [17, p.152]:

$$
\begin{aligned}
a_j |I\rangle &= \sum_{n:n_j=1} (-i)^{\sum_i n_i}...\, a_j(a_j^\dagger \tilde{a}_j^\dagger)...|00\rangle \\
&= \sum_{n:n_j=1} (-i)^{\sum_i n_i}...\, (1 - \underbrace{a_j^\dagger a_j}_{\text{This part is zero}}) \tilde{a}_j^\dagger ...|00\rangle = -i\tilde{a}_j^\dagger \sum_{n:n_j=0} |n\tilde{n}\rangle \\
&= -i\tilde{a}_j^\dagger |I\rangle
\end{aligned}
\tag{35}
$$

This requires some explanation. Since a_j annihilates all states that have $n_j = 0$, one does not need to consider them anymore. Furthermore, when pulling a_j to its appropriate position, it always passes through pairs of tilde, and normal operators, so there is no additional phase.
In the second line, one commutes $a_j a_j^\dagger$, and pulls out $\tilde{a}_j$. Then the sum contains all the states that have $n_j = 0$, since the normal and tilde space operators of index j have just been removed. This is also the reason why one pulls out the $-i$ factor, since now $\sum_i n_i$ is one less than before, since one less tilde operator inside the sum acts on the vacuum, which then needs one less $-i$ to compensate. As a last step, one adds all the states with $n_j = 1$, which one can do for free, since all of those are anyway annihilated by the tilde creation operator, and, therefore, one gets the left vacuum again. This procedure works similarly for the tilde annihilation operator.

4.2.3 Lindblad operator in superfermion representation

What has just been done, shows that eq. (28) is indeed fulfilled. Most importantly, one can use these relations for all operators that can be constructed from creation and annihilation operators, and its is assumed that this is the case for all operators being used in the Lindblad equation.

To transform the Lindblad operator in the superfermion representation, one needs to know how to transform the following two special cases [13, p.153]:

$$
\begin{aligned}
S_i \rho S_j |I\rangle &= S_i \rho(-i)\tilde{S}_j^{\ \dagger}|I\rangle = -iS_i\tilde{S}_j^{\ \dagger}\rho|I\rangle = -iS_i\tilde{S}_j^{\ \dagger}|\rho\rangle \\
\rho S_i S_j |I\rangle &= \rho S_i(-i)\tilde{S}_j^{\ \dagger}|I\rangle = i\tilde{S}_j^{\ \dagger}\rho S_i|I\rangle = i\tilde{S}_j^{\ \dagger}(-i)\tilde{S}_i^{\ \dagger}|\rho\rangle = \tilde{S}_j^{\ \dagger}\tilde{S}_i^{\ \dagger}|\rho\rangle.
\end{aligned}
\tag{36}
$$

For the second equation one can more generally say, that for any even number of fermionic operators one has [13, p.153]:

$$\rho\, O\, |I\rangle = \tilde{O}^\dagger |\rho\rangle. \tag{37}$$

After transferring an operator to the tilde space, one can swap it with those of the normal space, since they live in different Hilbert spaces. However, they are still fermionic operators, and, therefore, anti-commute, which gives an additional minus sign.

Now everything needed to perform the transformation of the Lindblad equation from the normal to the superfermion representation has been obtained [13, p.154]:

$$
\begin{aligned}
\frac{\mathrm{d}\rho}{\mathrm{d}t} &= -i[H,\rho] + \sum_{ij} \Gamma_{ij} \left(S_j \rho S_i^\dagger - \frac{1}{2}\{S_i^\dagger S_j, \rho]\} \right) \\
&\rightarrow -iH\rho\,|I\rangle + i\rho H\,|I\rangle + \sum_{ij} \Gamma_{ij} \left(S_j \rho S_i^\dagger\,|I\rangle - \frac{1}{2}(S_i^\dagger S_j \rho\,|I\rangle + \rho S_i^\dagger S_j\,|I\rangle) \right) \\
&= -i(H\,|\rho\rangle - \tilde{H})\,|\rho\rangle + \sum_{ij} \Gamma_{ij} \left(-i S_j \tilde{S}_i\,|\rho\rangle - \frac{1}{2}S_i^\dagger S_j\,|\rho\rangle - \frac{1}{2}\tilde{S}_j^{\,\dagger}\tilde{S}_i\,|\rho\rangle \right) \\
&= -i(H - \tilde{H})\,|\rho\rangle + \sum_{ij} \Gamma_{ij} \left(-i S_j \tilde{S}_i - \frac{1}{2}S_i^\dagger S_j - \frac{1}{2}\tilde{S}_j^{\,\dagger}\tilde{S}_i \right)|\rho\rangle . \\
&= L_H\,|\rho\rangle + L_D\,|\rho\rangle = L\,|\rho\rangle
\end{aligned}
\tag{38}
$$

4.2.4 The Hubbard Model

In this thesis we approximate the reality by using the Hubbard model [18, p.238]. It assumes that the orbitals are strongly localized, and that the Coulomb interaction is strongly screened. The electrons can "hop" to one of their nearest neighbour sites (if free), and the Coulomb interaction among electrons themselves is only relevant for the respective site i.e. it doesn't affect the neighbouring sites. The Hamiltonian of such a system can be written as [18, p.243]:

$$
H = \sum_i \varepsilon_{ij}(t) a_{i\sigma}^\dagger a_{i\sigma} - \sum_{\langle i,j \rangle} t_{ij}(t) a_{i\sigma}^\dagger a_{j\sigma} + U \sum_i n_{i\downarrow} n_{i\uparrow} - \mu N.
\tag{39}
$$

With ε_{ij} the on-site energy, t_{ij} the hopping parameter between two neighbouring sites i and j (We do not allow hopping to non-neighbouring sites), U the Coulomb interaction between electrons, $a_{\mu\sigma}^\dagger$, and $a_{\mu\sigma}$ the creation and the annihilation operators for a particle at site μ with spin σ respectively, N the particle number operator, and μ the chemical potential. Since we now know the form of our Hamiltonian, we can write down the specific Lindblad operator that will be relevant for this thesis, since eq. (38) is still very general. The Hamiltonian part is already known, therefore, we will only write down the dissipative part of eq. (38) [19, p.4]:

$$
L_D = -2 \sum_{\mu\nu}^{N_B} \sum_\sigma \left[\Gamma_{\nu\mu}^{(1)} \left(i a_{\mu\sigma} \tilde{a_{\nu\sigma}} + \frac{1}{2} a_{\nu\sigma}^\dagger a_{\mu\sigma} + \frac{1}{2} \tilde{a_{\mu\sigma}}^{\,\dagger} \tilde{a_{\nu\sigma}} \right) + \Gamma_{\nu\mu}^{(2)} \left(i a_{\nu\sigma}^\dagger \tilde{a_{\mu\sigma}}^{\,\dagger} + \frac{1}{2} a_{\mu\sigma} a_{\nu\sigma}^\dagger + \frac{1}{2} \tilde{a_{\nu\sigma}} \tilde{a_{\mu\sigma}}^{\,\dagger} \right) \right],
\tag{40}
$$

where the more general operators S, and $S^\dagger$ have been replaced by the creation and annihilation operators, a and $a^\dagger$. The term that is multiplied by $\Gamma^{(1)}$ is the one removing particles from the system, and the one multiplied by $\Gamma^{(2)}$ adds particles to the system.

4.3 Exact Diagonalization of the many body density-matrix

4.3.1 Basis

To diagonalize the many body density-matrix, one must first create this matrix, and for that one needs to choose some basis. We represent basis states in a discrete position basis, and, additionally include spin information. Eq. (41) gives an example for a basis state:

$$|011001\rangle \otimes |101\tilde{1}10\rangle, \tag{41}$$
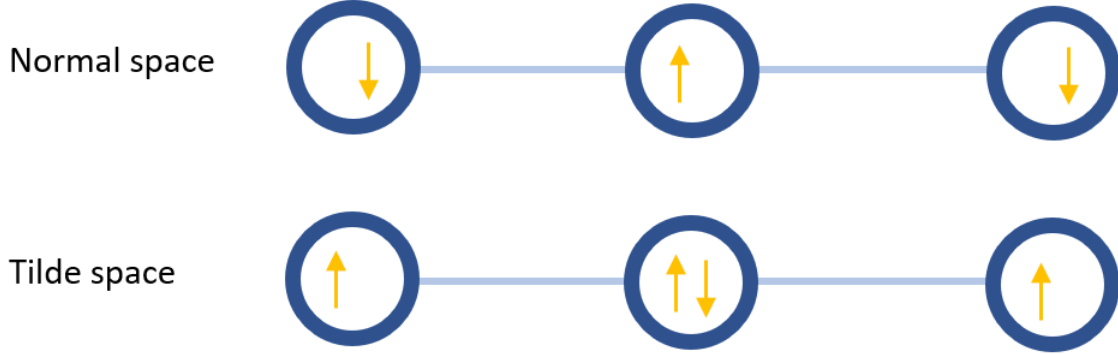
and figure 1 visualizes this it.

Figure 1: Visual interpretation of the state described by eq. (41)

The number of these basis states increases exponentially with the number of sites. More specifically:

$$n_{basis} = 2^{n_{sites} \cdot \underbrace{2}_{\text{from spin}} \cdot \underbrace{2}_{\text{from tilde states}}}. \tag{42}$$

This means an enormous increase in computing time for each additional site we add. Therefore, if we could decrease the states which are relevant to us, this would be very beneficial, and in fact we do only need the $n_{\text{normal}} - n_{\text{tilde}} = 0$ subspace [19, p.7]. The left vacuum has the eigenvalue zero, as is shown in e.g. [13, p.154]. There is also a right eigenvector with eigenvalue zero, which is called steady state, since it fulfills the equation $d |\rho_\infty\rangle /dt = L |\rho_\infty\rangle = 0$, where L is given in eq. (38). It is also known, that the left vacuum consists of a linear combination of states of the form $\langle n| \langle \tilde{n}|$. That means, they conserve the particle number difference between normal, and tilde states, and in this case we have that $n_{\text{normal}} - n_{\text{tilde}} = 0$. This conservation should also show in eq. (38), which can be checked straightforwardly. There are only two terms that do not preserve particle number, however they do still preserve $n_{\text{normal}} - n_{\text{tilde}}$, as expected. Having verified this, we can draw the following conclusion. Since left and right eigenvectors are not orthogonal to each other, at least one state in the steady state must be from the $n_{\text{normal}} - n_{\text{tilde}} = 0$ space. Therefore, all other states of which the steady state consists must be in the same subspace, since otherwise we would combine states with different $n_{\text{normal}} - n_{\text{tilde}}$ value.

4.3.2 Matrix

We must apply the Lindblad operator to each state of the subspace in which $n_{\text{normal}} - n_{\text{tilde}} = 0$ is fulfilled. What we get is in general a superposition of states that are all part of this subspace, since the Lindbladian itself conserves the particle difference between normal, and tilde space. All states are orthonormal to each other, therefore, we know that only the corresponding bra will give a result that is nonzero. But this already gives us all the information about where which resulting value belongs within our matrix. For each state we chose an index, which refers to the position of the respective column, or row in the matrix. Knowing the indices of the initial, and final states we can insert the respective value in its appropriate place in the matrix. Figure 2 illustrates this.

$$|1011\rangle|\widetilde{1101}\rangle \xrightarrow{\;L(t)\;} t_{ijkl}|1101\rangle|\widetilde{1101}\rangle + (e_{ij} + e_{og}(t) + e_{uf})|1011\rangle|\widetilde{1101}\rangle + U|1011\rangle|\widetilde{1101}\rangle + \Gamma_{ij}^{(1)}|1010\rangle|\widetilde{1100}\rangle$$

states		...	$|1011\rangle|\widetilde{1101}\rangle$	...	$|1101\rangle|\widetilde{1101}\rangle$	...	$|1101\rangle|\widetilde{1101}\rangle$	...
	indices	...	23	...	31	...	74	...
$\vdots$	$\vdots$							
$\langle 1011|\langle\widetilde{1101}|$	23	...	$e_{ij} + e_{og}(t) + e_{uf} + U$	...	t_{ijkl}	...	$\Gamma_{ij}^{(1)}$	...
$\vdots$	$\vdots$							
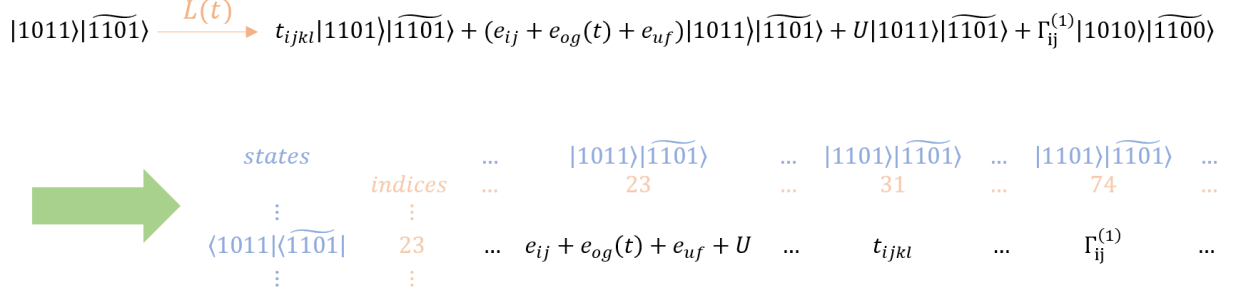
Figure 2: Creation of the Lindblad matrix.

Having the matrix, we can get the steady state by calculating the eigenvector with eigenvalue zero.

4.3.3 Observables

We eventually want to calculate the expectation values of observables. Most importantly, the electron current. In the superfermion space the expectation value is given by $\langle I|O|\rho\rangle = Tr(O\rho)$ [13, p.151], with O being an arbitrary operator. Since the number operator is $a^\dagger a$, its expectation value is therefore given by $\langle I|a^\dagger a|\rho\rangle$. To get the current into/out of the system we can use the time derivative of this expression. However, purely the time derivative is not useful, since in the steady state the sum of all currents must be zero. Therefore, one just takes into account the part of the Lindblad operator relevant for either outflow, or inflow, into/from the environment [13, p.155]:

$$I_i^{\text{out}} = -\frac{\mathrm{d}}{\mathrm{d}t}\langle n_i\rangle_{L_{\text{out}}} = -\langle I|n_i\frac{\mathrm{d}}{\mathrm{d}t}|\rho\rangle_i = -\langle I|n_i L_{\text{out}}|\rho\rangle,$$
$$I_i^{\text{in}} = -\langle I|n_i L_{\text{in}}|\rho\rangle. \tag{43}$$

For the current between neighbouring sites, we can use the current operator given as [15, p.5]:

$$I_{ij}^{\text{neighbour}} = -it_{ij}\left(a_j^\dagger a_i - a_i^\dagger a_j\right). \tag{44}$$

Where the indices i, and j give the sites between which the current flows, and t_{ij} is the hopping parameter between those sites. The result is the current flowing from site j to site i.

When applying time periodic driving, we let the Lindbladian act on an arbitrary state, which will then be evolved into the single "stable" periodic response. Then we get a density matrix state for each time point we calculate. Extracting an observable from this works the same way as shown in eqs. (43), and (44).

4.4 Equations of Motion

4.4.1 Introduction

Another way to solve the time dependent Lindblad equation is via the equations of motion, which is what we will discuss in this chapter. This approach is only useful if one eventually gets a closed system of equations, which cannot be taken for granted. However, in the case of a Hubbard model in which electrons do not interact with one another, a closed set can be obtained. One starts by writing down the equation of motion for an arbitrary operator of the system [20, p.1]:

$$
\begin{aligned}
b(t) &= \langle B(t) \rangle = \mathrm{Tr} B \rho(t) \\
&\rightarrow \frac{\mathrm{d}b}{\mathrm{d}t} = \mathrm{Tr} B \frac{\mathrm{d}\rho}{\mathrm{d}t} = \mathrm{Tr} B (\mathcal{L}\rho) \\
&= -i \mathrm{Tr} B [H, \rho] + \sum_i \mathrm{Tr} (B L_i \rho L_i^\dagger - \frac{1}{2} B \{ L_i^\dagger L_i, \rho \}).
\end{aligned}
\tag{45}
$$

Our goal is to get an equation without ρ, i.e. just containing B. To do this one has to perform some rearranging [20, p.1]:

$$
\begin{aligned}
\mathrm{Tr} B [H, \rho] &= \mathrm{Tr} (BH\rho - B\rho H) = \mathrm{Tr} (BH\rho - HB\rho) = Tr(-[H, B]\rho), \\
\mathrm{Tr} (B L_i \rho L_i^\dagger) &= \mathrm{Tr} (L_i^\dagger B L_i \rho), \\
\mathrm{Tr} (B \{ L_i^\dagger L_i, \rho \}) &= \mathrm{Tr} (B L_i^\dagger L_i \rho + B \rho L_i^\dagger L_i) = \mathrm{Tr} (B L_i^\dagger L_i \rho + L_i^\dagger L_i B \rho) = \mathrm{Tr} (\{ L_i^\dagger L_i, B \} \rho).
\end{aligned}
\tag{46}
$$

Using these relations one can rewrite eq. (45) as:

$$
\frac{\mathrm{d}b}{\mathrm{d}t} = i \mathrm{Tr}([H, B]\rho) + \sum_i \mathrm{Tr}(L_i^\dagger B L_i \rho - \frac{1}{2} B \{ L_i^\dagger L_i, B \} \rho).
\tag{47}
$$

The general expressions one gets on the right-hand side are of the form $\mathrm{Tr}(C\rho)\, (= \mathrm{d}c(t)/\mathrm{d}t)$, but for $\mathrm{Tr}(C\rho)$, one can again write an equation of motion in a similar manner, that again contains expressions of this type, and so on. As mentioned before, this whole process only makes sense if in the end one gets a closed set of equations.

4.4.2 Algorithm

Having established this general form, we can now discuss the special case we will deal with in this thesis. In our case, L is the one given in eq. (38), and what is B in eq. (45) is $c_i^\dagger c_j$, with i and j integer numbers from one to the maximum number of sites. Our goal is to obtain the most general formula, because it can be used to write an algorithm which creates the coefficient matrix.

We first want to observe which parts will eventually become zero. Let us start with the Hamiltonian part. All the operators contained are of the form $c_k^\dagger c_l$. Since there are now always two fermionic operators being swapped, it behaves like a bosonic operator, and one easily sees:

$$
[c_k^\dagger c_l, c_i^\dagger c_j] = 0 \quad \forall\, i, j \in \mathbb{N} \text{ with } i \neq l \text{ and } j \neq k.
\tag{48}
$$

Now let us show that the same is true for L_D:

$$
c_k^\dagger c_i^\dagger c_j c_k - \frac{1}{2}(c_k^\dagger c_k c_i^\dagger c_j + c_i^\dagger c_j c_k^\dagger c_k) = c_i^\dagger c_j c_k^\dagger c_k - \frac{1}{2} c_i^\dagger c_j c_k^\dagger c_k - \frac{1}{2} c_i^\dagger c_j c_k^\dagger c_k = 0 \quad \forall\, i, j \in \mathbb{N} \text{ with } i, j \neq k.
\tag{49}
$$

Again, we only moved two operators simultaneously, which does not change the sign.

There is one more simplification we can make, since we only care for the case in which there is interaction of the first, and the last site of the internal system with the environment. Furthermore, we take $\Gamma_1^{(1)} = \Gamma_{\text{end}}^{(2)}$, and $\Gamma_1^{(2)} = \Gamma_{\text{end}}^{(1)}$. Where the Γ's describe the rate with which particles are either inserted ($\Gamma_1^{(2)}$ for the left lead, and $\Gamma_1^{(1)}$ for the right), or removed ($\Gamma_1^{(1)}$ for the left lead, and $\Gamma_1^{(2)}$ for the right). We also consider 2D configurations, because we will deal with a ladder like structure, therefore we set $c_i \to c_{ij}$, but everything we showed before also applies there. With this we get:

$$
\begin{aligned}
\frac{\mathrm{d}\left\langle c_{ij}^\dagger c_{lk}\right\rangle}{\mathrm{d}t} = \left\langle L c_{ij}^\dagger c_{lk}\right\rangle = \Big\langle & i\varepsilon_{ij}(t)[c_{ij}^\dagger c_{ij}, c_{ij}^\dagger c_{lk}] + i\varepsilon_{ij}(t)[c_{lk}^\dagger c_{lk}, c_{ij}^\dagger c_{lk}] \\
& + it_{l+1,k,l,k}[c_{l+1,k}^\dagger c_{lk}, c_{ij}^\dagger c_{lk}] + it_{l,k,l+1,k}[c_{lk}^\dagger c_{l+1,k}, c_{ij}^\dagger c_{lk}] \\
& + it_{i+1,j,i,j}[c_{i+1,j}^\dagger c_{ij}, c_{ij}^\dagger c_{lk}] + it_{i+1,j,i,j}[c_{ij}^\dagger c_{i+1,j}, c_{ij}^\dagger c_{lk}] \\
& + it_{l-1,k,l,k}[c_{l-1,k}^\dagger c_{lk}, c_{ij}^\dagger c_{lk}] + it_{l,k,l-1,k}[c_{lk}^\dagger c_{l-1,k}, c_{ij}^\dagger c_{lk}] \\
& + it_{i-1,j,i,j}[c_{i-1,j}^\dagger c_{ij}, c_{ij}^\dagger c_{lk}] + it_{i,j,i-1,j}[c_{ij}^\dagger c_{i-1,j}, c_{ij}^\dagger c_{lk}] \\
& + it_{l,k+1,l,k}[c_{l,k+1}^\dagger c_{lk}, c_{ij}^\dagger c_{lk}] + it_{l,k,l,k+1}[c_{lk}^\dagger c_{l,k+1}, c_{ij}^\dagger c_{lk}] \\
& + it_{i,j+1,i,j}[c_{i,j+1}^\dagger c_{ij}, c_{ij}^\dagger c_{lk}] + it_{i,j,i,j+1}[c_{ij}^\dagger c_{i,j+1}, c_{ij}^\dagger c_{lk}] \\
& + it_{l,k-1,l,k}[c_{l,k-1}^\dagger c_{lk}, c_{ij}^\dagger c_{lk}] + it_{l,k,l,k-1}[c_{lk}^\dagger c_{l,k-1}, c_{ij}^\dagger c_{lk}] \\
& + it_{i,j-1,i,j}[c_{i,j-1}^\dagger c_{ij}, c_{ij}^\dagger c_{lk}] + it_{i,j,i,j-1}[c_{ij}^\dagger c_{i,j-1}, c_{ij}^\dagger c_{lk}] \\
& + \Gamma_1^{(1)}(c_1^\dagger c_{ij}^\dagger c_{lk} c_1 - \frac{1}{2}\{c_{ij}^\dagger c_{lk}, c_1^\dagger c_1\}) + \Gamma_1^{(2)}(c_1 c_{ij}^\dagger c_{lk} c_1^\dagger - \frac{1}{2}\{c_{ij}^\dagger c_{lk}, c_1 c_1^\dagger\}) \\
& + \Gamma_1^{(2)}(c_{\text{end}}^\dagger c_{ij}^\dagger c_{lk} c_{\text{end}} - \frac{1}{2}\{c_{ij}^\dagger c_{lk}, c_{\text{end}}^\dagger c_{\text{end}}\}) + \Gamma_1^{(1)}(c_{\text{end}} c_{ij}^\dagger c_{lk} c_{\text{end}}^\dagger - \frac{1}{2}\{c_{ij}^\dagger c_{lk}, c_{\text{end}} c_{\text{end}}^\dagger\})\Big\rangle.
\end{aligned}
\tag{50}
$$

The ε have a time dependence, because we want to use this formula to describe the current when a time periodic electric field is being applied. The current between sites is given by eq. (44), and we want to calculate its expectation value. This provides us with the initial two operators, from which the (closed) system of differential equations is obtained. Since in this special case there is only current flowing into and out of the system from the first and the last site, we only need to calculate the current between two neighbouring sites, since it must be equal everywhere else, at least for the 1D case. In two dimension as similar approach can be used.

Eventually, we need to create an algorithm which produces the coefficient matrix, therefore, eq. (50) is not practicable yet. We want to know which commutator leads to which function. First, we observe that we can neglect all terms of the form

$$
\begin{aligned}
& [c_{j\pm1}^\dagger c_j, c_i^\dagger c_j], \\
& [c_i^\dagger c_{i\pm1}, c_i^\dagger c_j].
\end{aligned}
\tag{51}
$$

They are clearly zero for $i \neq j$. If $i = j$, then some commutators in eq. (50) coincide. That means eq. (50) is not fully valid then, since we have double counting of some operators in the Lindblad equation. Luckily, however, this eventually only means we also have to neglect all commutators of the form shown in eq. (51) in the case of $i = j$.

Now we can set up some general rules that can be applied. For easier notation we will discuss this in 1D, but it can straightforwardly be applied to 2D, which we need, because we also want to simulate a ladder structure.

$$[c_k^\dagger c_i, c_i^\dagger c_j] = c_k^\dagger c_i c_i^\dagger c_j + c_k^\dagger (1 - c_i c_i^\dagger) c_j = c_k^\dagger c_j \quad \forall\, j \in \mathbb{N} \text{ with } j \neq k.$$

$$[c_j^\dagger c_k, c_i^\dagger c_j] = -[c_i^\dagger c_j, c_j^\dagger c_k] = -c_i^\dagger c_k \quad \forall\, i \in \mathbb{N} \text{ with } i \neq k.$$

$$[c_j^\dagger c_i, c_i^\dagger c_j] = c_j^\dagger c_i c_i^\dagger c_j - c_i^\dagger (1 - c_j^\dagger c_j) c_i = c_i c_i^\dagger c_j^\dagger c_j - c_i^\dagger c_i + (1 - c_i c_i^\dagger) c_j^\dagger c_j) = c_j^\dagger c_j - c_i^\dagger c_i$$

$$c_k^\dagger c_k^\dagger c_j c_k - \frac{1}{2}\{c_k^\dagger c_j, c_k^\dagger c_k\} = c_k^\dagger c_k^\dagger c_j c_k - \frac{1}{2} c_k^\dagger c_k^\dagger c_j c_k - \frac{1}{2} c_k^\dagger (1 - c_k^\dagger c_k) c_j = -\frac{1}{2} c_k^\dagger c_j$$

$$c_k^\dagger c_i^\dagger c_k c_k - \frac{1}{2}\{c_i^\dagger c_k, c_k^\dagger c_k\} = c_k^\dagger c_i^\dagger c_k c_k - \frac{1}{2} c_i^\dagger (1 - c_k^\dagger c_k) c_k - \frac{1}{2} c_k^\dagger c_i^\dagger c_k c_k = -\frac{1}{2} c_i^\dagger c_k$$

$$c_k^\dagger c_k^\dagger c_k c_k - \frac{1}{2}\{c_k^\dagger c_k, c_k^\dagger c_k\} = c_k^\dagger c_k^\dagger c_k c_k - \frac{1}{2} c_k^\dagger (1 - c_k^\dagger c_k) c_k - \frac{1}{2} c_k^\dagger (1 - c_k^\dagger) c_k c_k = -c_k^\dagger c_k$$

$$c_k c_k^\dagger c_j c_k^\dagger - \frac{1}{2}\{c_k^\dagger c_j, c_k c_k^\dagger\} = c_k c_k^\dagger c_j c_k^\dagger + \frac{1}{2}(1 - c_k c_k^\dagger) c_j c_k^\dagger - \frac{1}{2} c_k c_k^\dagger c_j c_k^\dagger = -\frac{1}{2} c_k^\dagger c_j$$

$$c_k c_i^\dagger c_k c_k^\dagger - \frac{1}{2}\{c_i^\dagger c_k, c_k c_k^\dagger\} = c_k c_i^\dagger c_k c_k^\dagger - \frac{1}{2} c_k c_i^\dagger c_k c_k^\dagger + \frac{1}{2} c_k c_i^\dagger (1 - c_k^\dagger c_k) = -\frac{1}{2} c_i^\dagger c_k$$

$$c_k c_k^\dagger c_k c_k^\dagger - \frac{1}{2}\{c_k^\dagger c_k, c_k c_k^\dagger\} = c_k c_k^\dagger c_k c_k^\dagger + \frac{1}{2}(1 - c_k) c_k^\dagger c_k c_k^\dagger + \frac{1}{2} c_k c_k^\dagger (1 - c_k c_k^\dagger) = 1 - c_k^\dagger c_k$$

$$(52)$$

Using eqs. (52) the following algorithm for the creation of the desired coefficient matrix can be obtained:

$$
\frac{\mathrm{d}\left\langle c_{ij}^\dagger c_{lk} \right\rangle}{\mathrm{d}t} = \left\langle L c_{ij}^\dagger c_{lk} \right\rangle = \Bigg\langle
\begin{cases} \text{if}(i,j) = (l,k) & : 0 \\ \text{else} & : i\varepsilon_{ij}(t) c_{ij}^\dagger c_{lk} \end{cases}
+ \begin{cases} \text{if}(i,j) = (l,k) & : 0 \\ \text{else} & : i\varepsilon_{lk}(t) c_{ij}^\dagger c_{lk} \end{cases}
$$

$$
+ \begin{cases} \text{if } (i,j) = (l+1,k) & : -it_{l,k,l+1,k}(c_{l,k}^\dagger c_{l,k} - c_{l+1,k}^\dagger c_{l+1,k}) \\ \text{else} & : -it_{l,k,l+1,k} c_{ij}^\dagger c_{l+1,k} + it_{i-1,j,i,j} c_{i-1,j}^\dagger c_{lk} \end{cases}
$$

$$
+ \begin{cases} \text{if } (i,j) = (l-1,k) & : -it_{l,k,l-1,k}(c_{l,k}^\dagger c_{l,k} - c_{l-1,k}^\dagger c_{l-1,k}) \\ \text{else} & : -it_{l,k,l-1,k} c_{ij}^\dagger c_{l-1,k} + it_{i+1,j,i,j} c_{i+1,j}^\dagger c_{lk} \end{cases}
$$

$$
+ \begin{cases} \text{if } (i,j) = (l,k+1) & : -it_{l,k,l,k+1}(c_{l,k}^\dagger c_{l,k} - c_{l,k+1}^\dagger c_{l,k+1}) \\ \text{else} & : -it_{l,k,l,k+1} c_{ij}^\dagger c_{l,k+1} + it_{i,j-1,i,j} c_{i,j-1}^\dagger c_{lk} \end{cases}
$$

$$
+ \begin{cases} \text{if } (i,j) = (l,k-1) & : -it_{l,k,l,k-1}(c_{l,k}^\dagger c_{l,k} - c_{l,k-1}^\dagger c_{l,k-1}) \\ \text{else} & : -it_{l,k,l,k-1} c_{ij}^\dagger c_{l,k-1} + it_{i,j+1,i,j} c_{i,j+1}^\dagger c_{lk} \end{cases}
$$

$$
+ \begin{cases} \text{if } i = \text{start/end} \ \& \ l \neq \text{start/end} & : -\frac{1}{2}(\Gamma_1^{(1)} + \Gamma_1^{(2)}) c_{\text{start/end},j}^\dagger c_{lk} \\ \text{if } l = \text{start/end} \ \& \ i \neq \text{start/end} & : -\frac{1}{2}(\Gamma_1^{(1)} + \Gamma_1^{(2)}) c_{ij}^\dagger c_{\text{start/end},k} \\ \text{if } (i,l) = (\text{start}, \text{start}) & : -(\Gamma_1^{(1)} + \Gamma_1^{(2)}) c_{\text{start},j}^\dagger c_{\text{start},k} + \Gamma_1^{(2)} \\ \text{if } (i,l) = (\text{end}, \text{end}) & : (\Gamma_1^{(1)} + \Gamma_1^{(2)}) c_{\text{end},j}^\dagger c_{\text{end},k} + \Gamma_1^{(1)} \\ \text{else} & : 0 \end{cases}
\Bigg\rangle .
$$

$$(53)$$

Importantly, in the last line, in which we have five conditions, the first two can be true simultaneously!

5 Code verification and testing

Interpreting the results of our simulations makes only sense if they work as intended. To ensure this to a reasonable degree, we must perform some tests, which will be done in this chapter. All energies are given in terms of the hopping values of the leads, termed t, except if specified differently. Furthermore, since we take $\hbar = 1$, we also represent frequencies in this way, and since band gaps are of the magnitude of eV, we choose $t = 1eV$.

5.1 Exact Diagonalization of the many body density-matrix - without periodic driving

To perform a verification of the ED code, we compare Green's functions. On the one hand we can calculate them using the Lehmann representation, on the other hand they can be calculated completely independently for the non-interacting case[19]. Therefore, when setting the interaction to zero, both formula must give the same result.

For comparison we will use a system of size 3, as depicted in figure 3[1], and the following parameters:

$$
\begin{aligned}
t &= 1.0, \\
e &= 0.0, \\
U &= 0.0, \\
\Gamma_1 &= \begin{pmatrix} 0.8 & -0.02 - 0.01i & 0.1 \\ -0.02 + 0.01i & 0.45 & -0.04 + 0.01i \\ 0.1 & -0.04 - 0.01i & 0.2 \end{pmatrix}, \\
\Gamma_2 &= \begin{pmatrix} 0.2 & 0.013 & 0.053 \\ 0.013 & 0.55 & -0.043 - 0.02i \\ 0.053 & -0.043 + 0.02i & 0.8 \end{pmatrix}
\end{aligned}
\tag{54}
$$
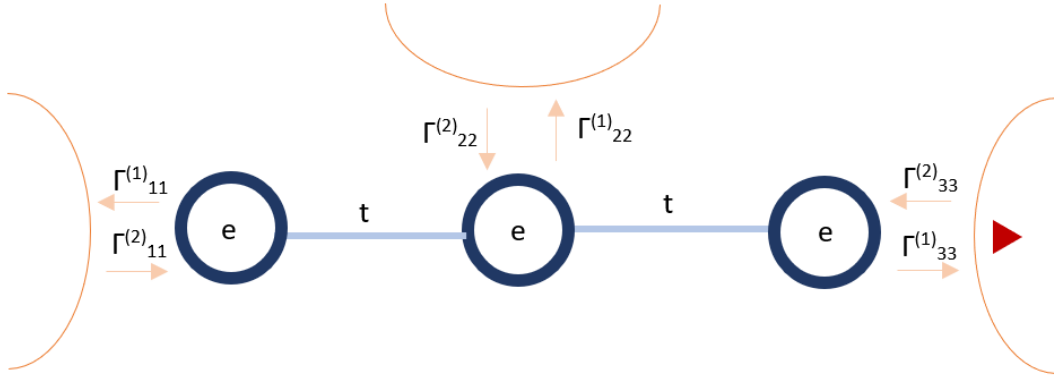
Figure 3: Setup for three sites.

Where t is the hopping parameter, e the on-site energy, U the interaction strength, and Γ the parameters defining the rate at which electrons are added or removed on each site. Figures 4, 5, 6 and 7 show the results. The first two images show the component $(1,1)$, and the last two $(1,3)$, where in both cases the first picture shows the Keldysh, and the second the retarded Green's function. An off diagonal component has been plotted, since an additional phase has to be taken into account there, and we thereby ensure that this is taken into account properly. For the right part of figure 5 it should be mentioned, that the magnitude is 10^{-17}! The actual value is zero, but the fluctuations we can see on this level are purely caused by numerical errors. In all other plots the small absolute error is about sixteen orders of magnitude smaller than the peak, and therefore, the two curves

---

[1]It is difficult to visualizing the off diagonal elements. However, one may imagine that in the picture we use a basis in which the Gamma matrices are diagonal.

completely overlap. These results imply, that the creation of the Lindbladian, and all subsequent steps to get this result, are performed correctly.
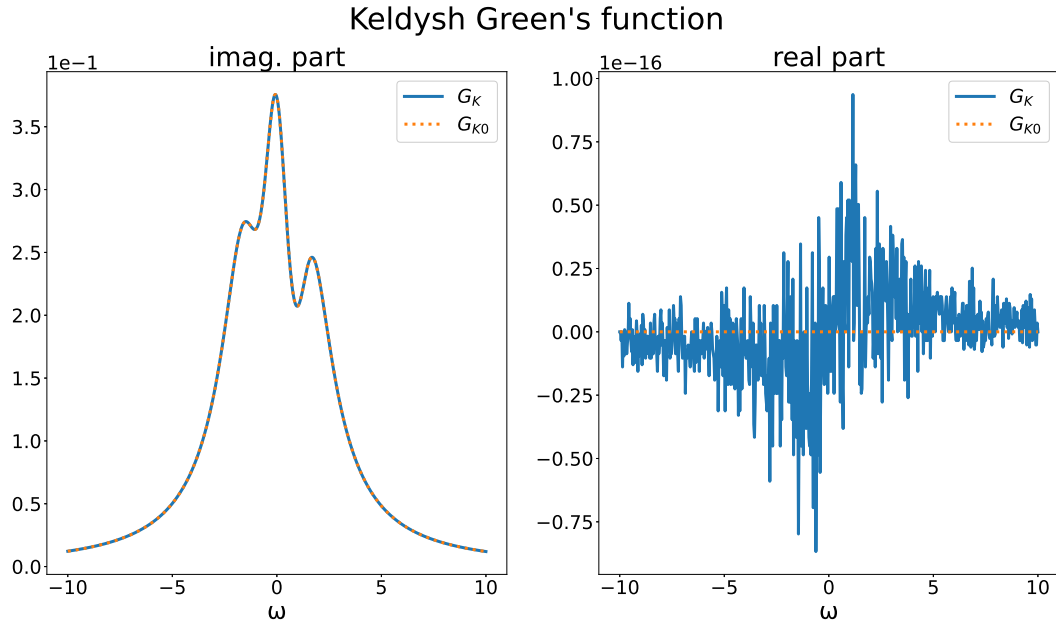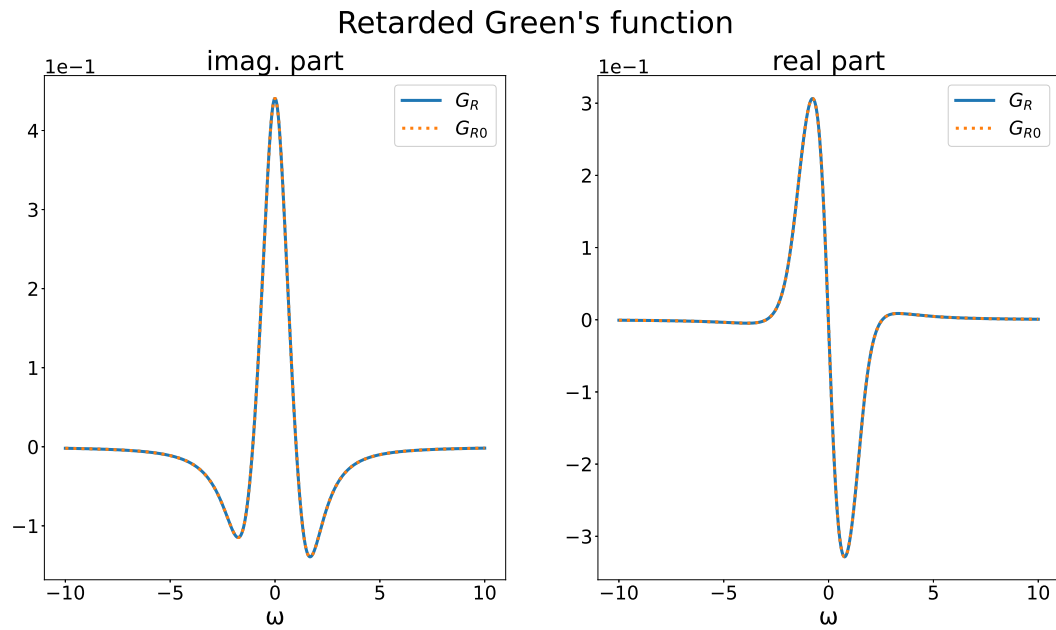

Figure 4: The imaginary and real part of the $(1,1)$ component of the Keldysh Green's function obtained by two different methods. In the imaginary part there is perfect overlap.

Figure 5: The imaginary and real part of the $(1,1)$ component of the Retarded Green's function obtained by two different methods. In both cases there is perfect overlap.
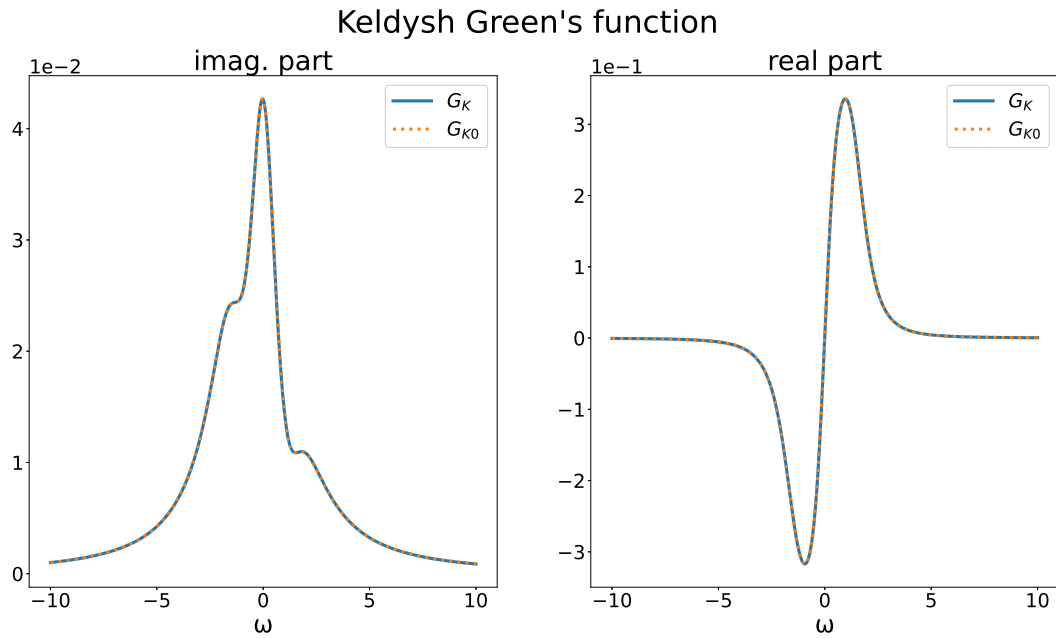
Figure 6: The imaginary and real part of the $(1, 3)$ component of the Keldysh Green's function obtained by two different methods. In both cases there is perfect overlap.

Figure 7: The imaginary and real part of the $(1, 3)$ component of the Retarded Green's function obtained by two different methods. In both cases there is perfect overlap.

5.2 Equations of motion - without periodic driving

Again we use the non-interacting Green's function's for comparison, however this time indirectly. With the Keldysh component, we can calculate the steady state current using [21]:

$$j_{kl} = -\frac{t}{2\pi} \int_{-\infty}^{\infty} d\omega \text{Re} \left\{ G_{kl}^{K}(\omega) \right\}. \tag{55}$$

On the other hand, for the equation of motion case we can use the current operator (eq. (44)) $J_{lk} = -it_{lk}(a_{k}^{\dagger}a_{l} - a_{l}^{\dagger}a_{k})$. The configuration we use is the one for which we are going to create and evaluate results in section 6.2. Its setup is depicted in figure 29. The parameters for the comparison have been chosen arbitrarily:

$structure = 5 - 10 - 5, t = t_a = 1.0, t_b = 0.5, t' = 0.1, \varepsilon_{left} = -1.0, \varepsilon_{central} = 0.0, \varepsilon_{right} = 1.0, \Gamma_1^{(1)} = 0, \Gamma_1^{(1)} = 0.8$
$\rightarrow I_{\text{Green}} = 1.314139 \cdot 10^{-2}, I_{\text{eom}} = 1.314123 \cdot 10^{-2},$

$structure = 3 - 12 - 3, t = t_a = 1.0, t_b = 0.25, t' = 0.05, \varepsilon_{left} = -1.0, \varepsilon_{central} = 0.0, \varepsilon_{right} = 1.0, \Gamma_1^{(1)} = 0, \Gamma_1^{(1)} = 0.8$
$\rightarrow I_{\text{Green}} = 6.179610 \cdot 10^{-5}, I_{\text{eom}} = 6.176938 \cdot 10^{-5},$

$structure = 4 - 8 - 4, t = t_a = 1.0, t_b = 0.5, t' = 0.15, \varepsilon_{left} = -1.0, \varepsilon_{central} = 0.0, \varepsilon_{right} = 1.0, \Gamma_1^{(1)} = 0, \Gamma_1^{(1)} = 0.8$
$\rightarrow I_{\text{Green}} = 5.963727 \cdot 10^{-3}, I_{\text{eom}} = 5.963727 \cdot 10^{-3}.$

$$\tag{56}$$

Where *structure* describes the configuration as $lead_{left} - central - lead_{right}$, t_a, and t_b are the alternating hopping values of the central system, t is the coupling between lead sites, t' the coupling of the leads to the central part, and all other parameters are the same as before. As can be easily seen by comparing the currents obtained via the Green's function and the equation of motion, the results coincide very well. The difference in accuracy arises, because a smaller t' leads to sharper G_K peaks. I.e. if we had always used sufficiently small integration steps we could have obtained agreement up to an arbitrary digit. It is, however, assumed, that the chosen time step proofs the point we wanted to make well enough.

5.3 Equations of motion and Exact Diagonalization of the many body density-matrix - inclusion of periodic driving

Up to now we have shown that both approaches agree with an independent method, for the steady state case. Now we proceed to perform a check in the case of periodic driving. An obvious choice for this is to just compare the results of the two simulations with one another. For both, we know possible errors can only arise from the time periodic part, and it would be an extraordinary coincidence, if both were to be wrong but equivalent. Therefore, we assume that if they match for two different sets of parameters, which again have been chosen arbitrarily, both simulations are working correctly.

Parameter set one:	Parameter set two:
$structure = 1 - 1 - 1,$	$structure = 1 - 1 - 1,$
$driving = 0 - 1 - 0,$	$driving = 0 - 1 - 1,$
$t_a = t_b = t' = 1.0,$	$t_a = t_b = t' = 0.3,$
$\varepsilon_{left} = -1.0,$	$\varepsilon_{left} = -1.3,$
$\varepsilon_{central} = 0.0,$	$\varepsilon_{central} = 0.34,$
$\varepsilon_{right} = 1.0,$	$\varepsilon_{right} = 0.13,$
$\Gamma_1^{(1)} = 0.0,$	$\Gamma_1^{(1)} = 0.7,$
$\Gamma_1^{(2)} = 0.8,$	$\Gamma_1^{(2)} = 0.3,$
$\alpha = 1.0,$	$\alpha = 1.1,$
$\omega = 1.0.$	$\omega = 1.43.$

The parameters have the same meaning as in section *5.2.*

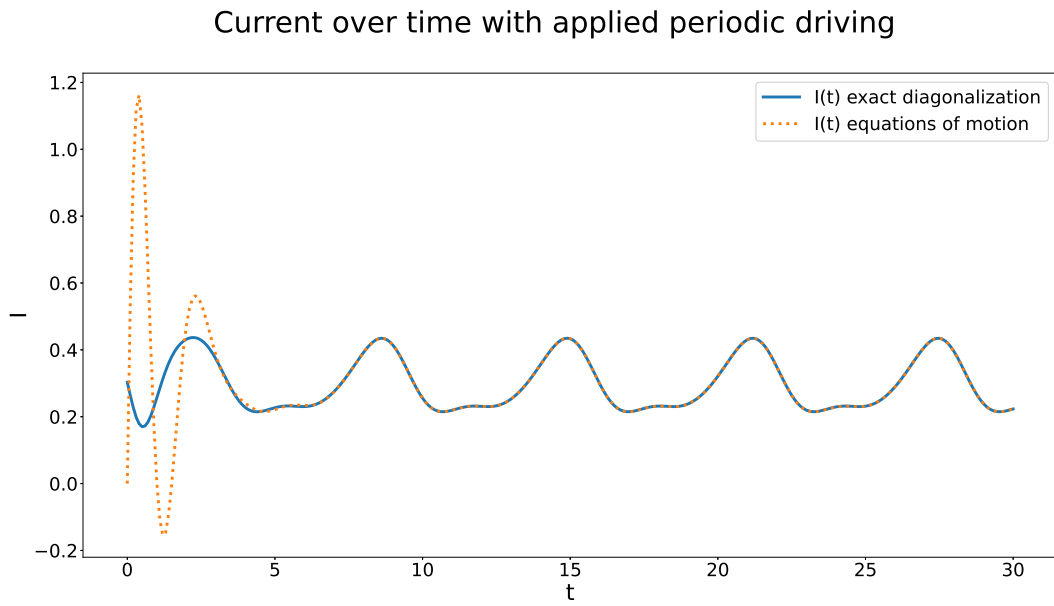Current over time with applied periodic driving

Figure 8: Current due to applied periodic driving, calculated by the equations of motion method, and by exact diagonalization of the many body density-matrix, using parameter set one.
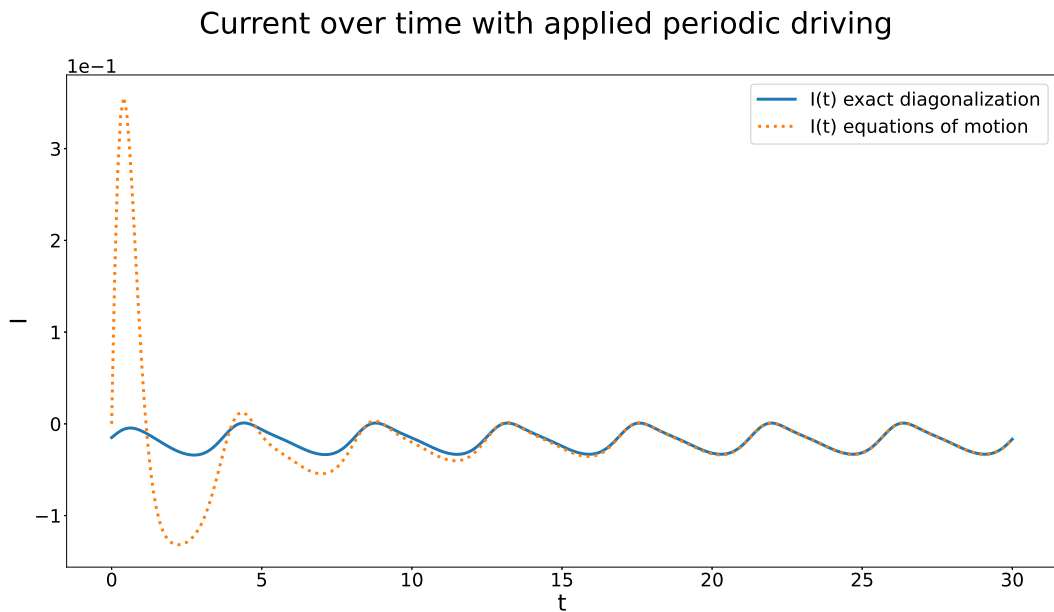
Current over time with applied periodic driving

Figure 9: Current due to applied periodic driving, calculated by the equations of motion method, and by exact diagonalization of the many body density-matrix, using parameter set two.

The two solutions give the same long time behaviour, by which accuracy of the simulations has been shown to a reasonable degree. One would also expect the transient of both methods to coincide, which is not the case, because different initial conditions have been used.

6 Results and Discussion

After thoroughly testing the functionality of our simulations, we can begin to use them. As discussed in the introduction, we will simulate three different systems. In two of those the electron-electron interaction is turned off. These are the one with a ladder structure as the central system, and the one with alternating hopping values in central part. The third one is a smaller system, which has three or five sites, where electron-electron interaction is turned on in the central site/s. In all those cases there is a gap, and we will investigate the average current as a function of the frequency of the applied driving.

6.1 Ladder structure

Figure *10* depicts the structure of the first configuration we will consider. The left and right leads are connected to the central part via the coupling t', which must be taken to be small compared to $t_\parallel$, and $t_\perp$. On their other side, these leads are connected with the environment, and they are an extension of the surroundings, which can be imagine as a metal.
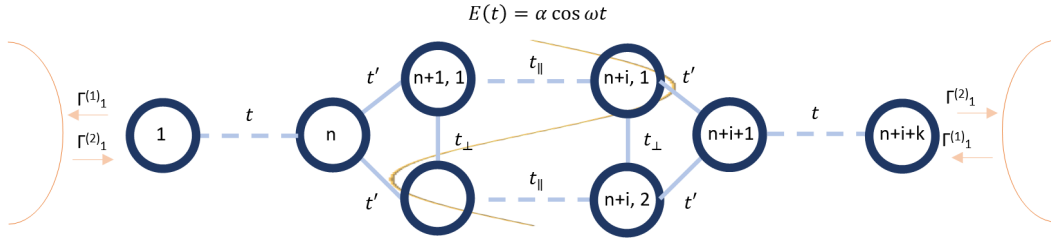
Figure 10: Setup of the simulated system.

To get an approximation for how the band structure of our real system looks like, we create a very long chain with a ladder structure, and then plot the eigenvalues vs. the momentum. To do this, we need to know the Hamiltonian of this large configuration, which is given by:

$$H = \sum_{j=1}^{2} \sum_{i=1}^{N-1} (a_{ij}^\dagger a_{(i+1)j} + a_{(i+1)j}^\dagger a_{ij}) t_\parallel + \sum_{i=1}^{N} (a_{i1}^\dagger a_{i2} + a_{i2}^\dagger a_{i1}) t_\perp, \tag{57}$$

where $t_\parallel$ and $t_\perp$ are the hopping values in and normal to the direction of chain extension respectively, and the all other symbols have the same meaning as explained in section *4.2.4*. The resulting band structure is shown in figure *12*. This is an idealized setup, which still give us an idea about the behaviour of the average current as a function of ω. We have an indirect band gap[2] starting from $\omega = 1.0$, and a direct one[3] only at exactly $\omega = 2.0$. Therefore, we expect a maximum at $\omega = 2.0$, but since in our real system no state corresponds to a precise momentum, we also expect a smooth increase/decrease before/afterwards.
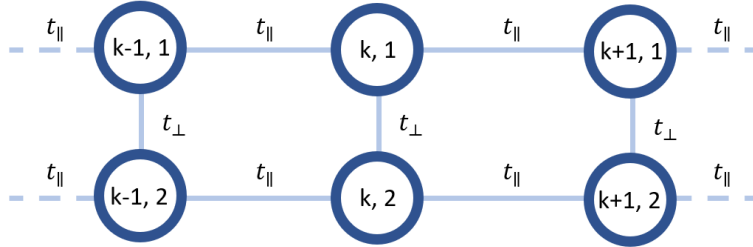
Figure 11: Infinite ladder system, with potentially different hopping values parallel and perpendicular to chain expansion.

---

[2]That means the periodic driving is strong enough to excite an electron from the lower to the higher band gap, but additionally some momentum has to be given/taken to/from the electron.
[3]In this case the initial and final state have the same momentum.
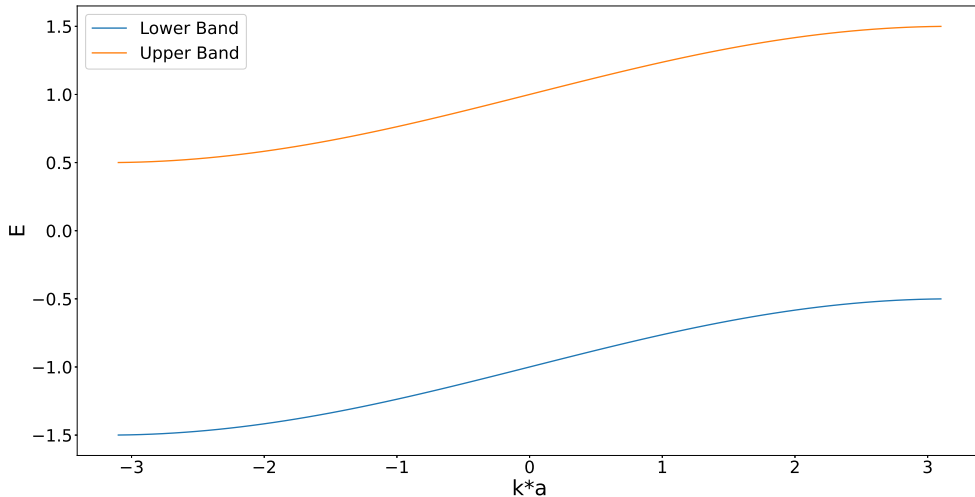
Figure 12: Band structure of the infinite ladder structure, as depicted in figure *11*.

If not specified otherwise, the following parameters are always being used:

$$
\begin{aligned}
\varepsilon_{left} &= -1.0, \\
\varepsilon_{right} &= 1.0, \\
\varepsilon_{central} &= 0.0, \\
t_{\parallel} &= 0.25, \\
t = t_{\perp} &= 1.0, \\
t' &= 0.1, \\
\alpha &= 1.0, \\
structure &= 5 - 10 - 5, \\
solver &= Tsit5[22]^4 \\
\Gamma_1^{(1)} &= 0, \\
\Gamma_1^{(2)} &= 0.8, \\
U &= 0.0.
\end{aligned}
\tag{58}
$$

Where ε gives (dependent on index) the on-site energy of the left lead, the system, and the right lead, *structure* gives the structure of our setup as $[length\text{-}of\text{-}left\text{-}lead - length\text{-}of\text{-}system - length\text{-}of\text{-}right\text{-}lead]$, t' describes the coupling between the leads and the system, α is the amplitude, and ω the frequency of the periodic driving, U the electron-electron interaction, $\Gamma_1^{(1)}$ and $\Gamma_1^{(2)}$ described the rate of removal and insertion of particles on the right- and leftmost site of the chain respectively, and $t_{\parallel}$ and $t_{\perp}$ are the hopping parameters parallel, and normal to the chain expansion respectively. These last two parameters define the band structure of the system.

To get reasonable results for the average current as a function of ω, it is necessary to get proper results for the current as a function of time. We assume for the output to be a periodic function, but we will have a transient, and for our calculation of the average current curves, we must only use parts of the current that are beyond its influential zone. Since the average value of a periodic function stays constant over an integer number of periods, we use a moving average to get a better idea about how much the average value changes locally, which, according to our expectation, should be not much if we include sufficiently much periods in the moving average. If we do get a periodic function of time, where the lowest appearing frequency is sufficiently small compared to the number

---

[4]Tsitouras 5/4 Runge-Kutta method

of time units we use for the moving average, then we expect a connection between the degree of relative fluctuation of the moving average, and the fluctuation of the average current as a function of ω. At least close to the chosen ω value. Now we must choose some parameter sets, from which we can derive representative data. It seems reasonable to make a comparison between the results used in figures _16_, _19_, and _21_ which have parameters $\alpha = 5.0$, $\alpha = 1.0$, and $structure = 2 - 4 - 2$ respectively, with all other parameters as given in eq. (_58_). These three represent three different "stages". The first one shows a maxima at $\omega = 2.0$, which is what we expect, and the curve is very smooth. The second one also shows a maxima at $\omega = 2.0$, but there are significant fluctuations, and in the last one, we can see no structure at all, and fluctuations are strong. We chose $\omega = 1.45$ as our representative value, because it is a value of the middle. In each case we created one subplot on the left hand side showing the transient, where we also included an exponential fit to show its influential range, and another one on the right hand side, in which we zoomed in to get a better look at the periodic behaviour, where a moving average over twenty time units is included. The plots are shown in figures _13_ to _15_.
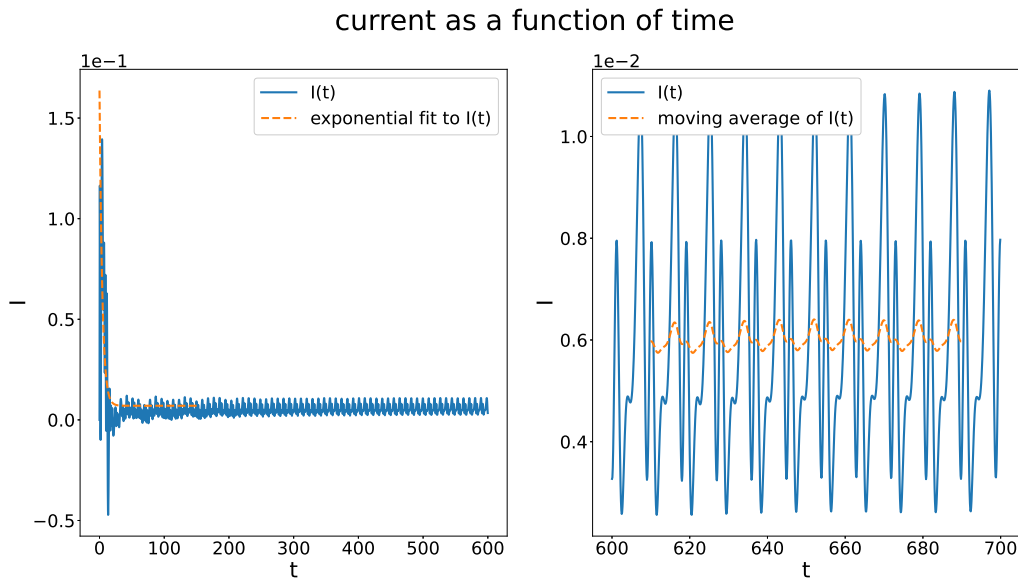
Figure 13: Current as a function of time for $\alpha = 1.0$, and $structure = 2-4-2$. All other parameters are given in eq. (_58_).

current as a function of time
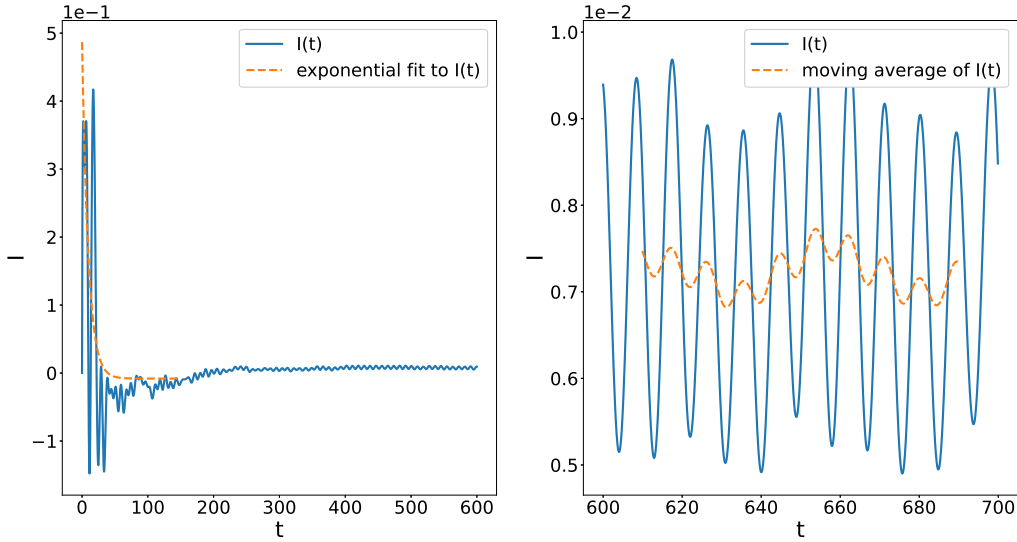
Figure 14: Current as a function of time for $\alpha = 1.0$, and $structure = 5-10-5$. All other parameters are given in eq. (58).

current as a function of time
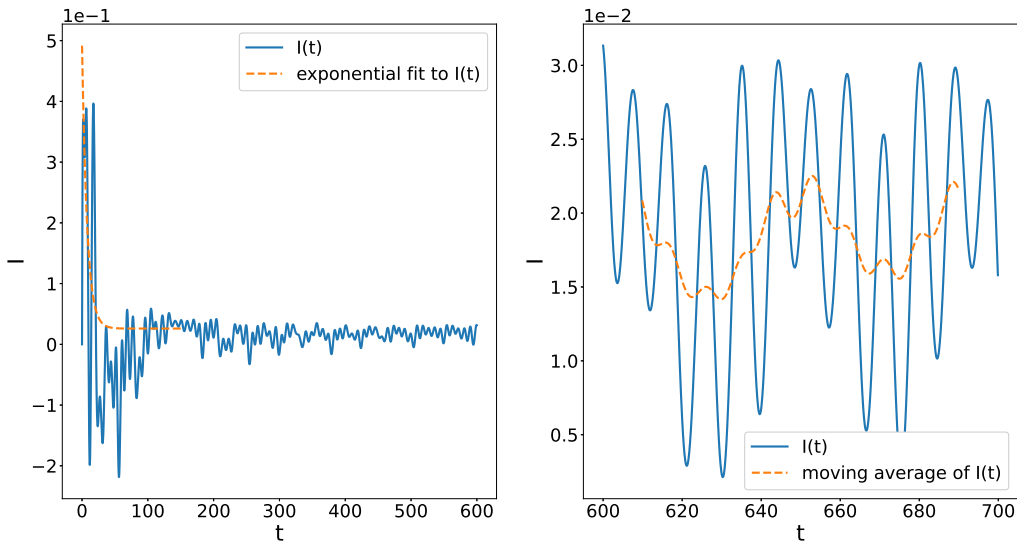
Figure 15: Current as a function of time for $\alpha = 5.0$, and $structure = 5-10-5$. All other parameters are given in eq. (58).

We reach times far beyond the influential part of the transient. For figure 13, we can see on the left hand side, that we have a small overall change, which happens continuously, but the relative fluctuations of the moving average is tiny. For figure 14 the relative fluctuations are visibly stronger, and for figure 15 the relative fluctuations are clearly the worst. These results imply that the numerical solving process of the differential equations, or components with frequencies so low, that we could not properly capture them on the presented time scale, have the main responsibility for fluctuations, and deviations from our expected behaviour, i.e. a maximum at $\omega = 2.0$, in the average current plots.

Let us now come to the plots of the average current as a function of ω. Many of them show a fluctuating graph instead of a continuous line. Therefore, a moving average, combined with interpolation, has been added as a dashed line, to get a smoother result.

We now show results for the structures: $2-4-2, 3-6-3, 4-8-4$, and $5-10-5$.
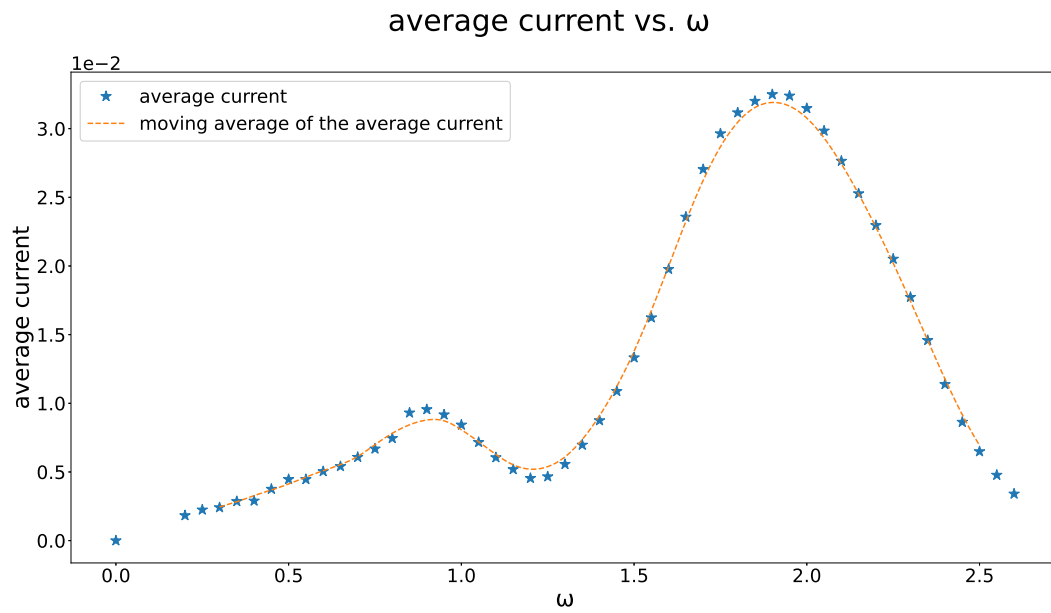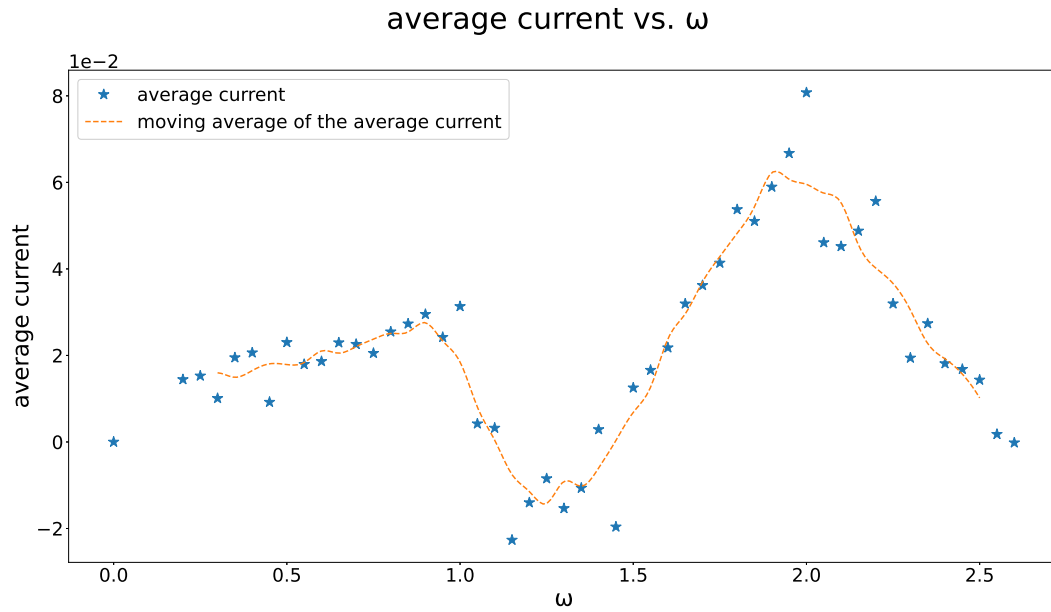

Figure 16: Average current as a function of ω for a 2-4-2 system. All other parameters are given in eq. (58).
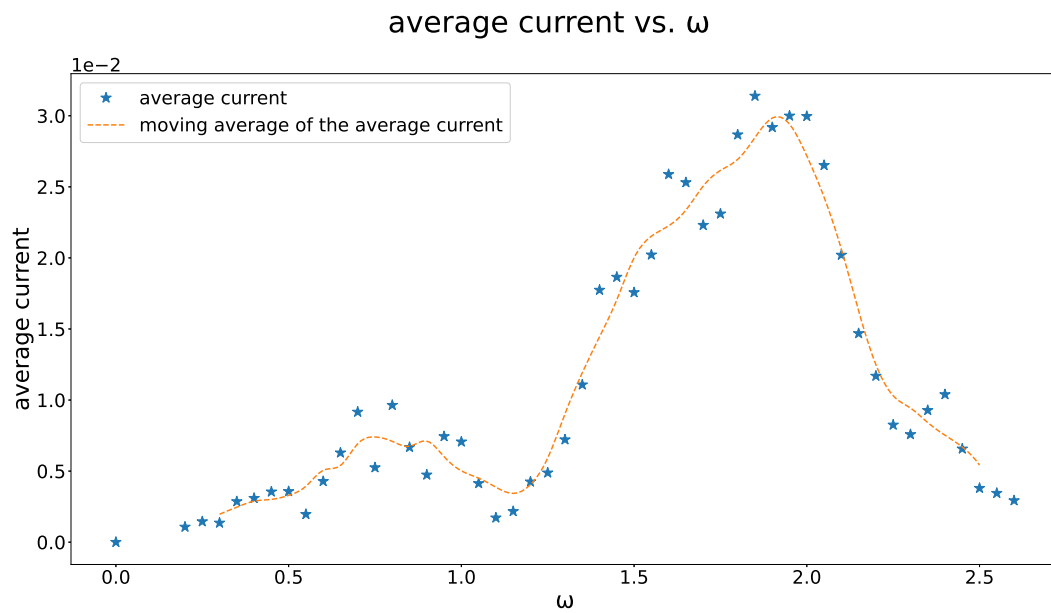
Figure 17: Average current as a function of ω for a 3-6-3 system. All other parameters are given in eq. (58).
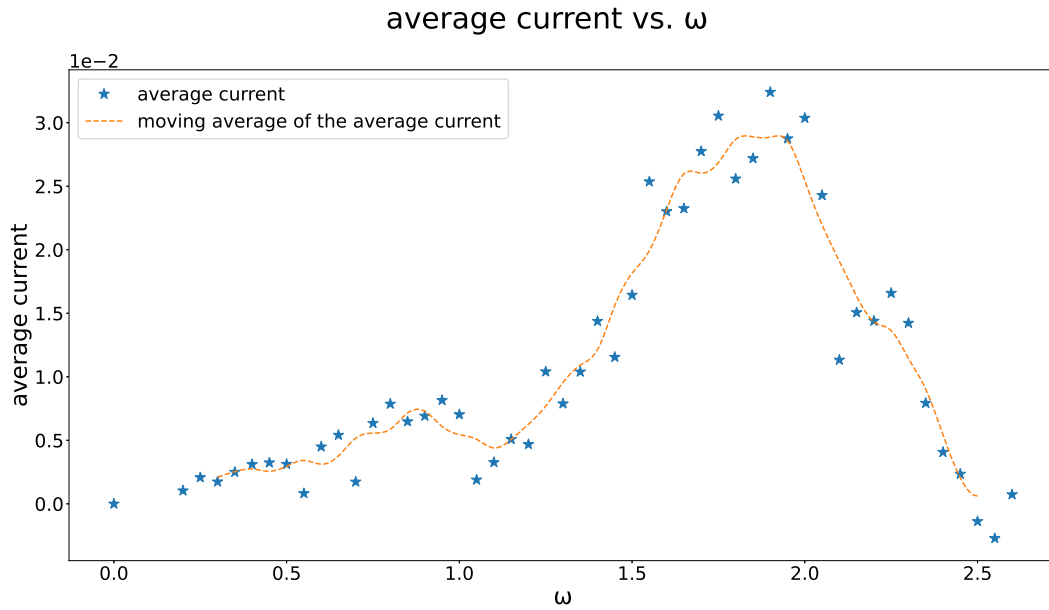
Figure 18: Average current as a function of ω for a 4-8-4 system. All other parameters are given in eq. (*58*).
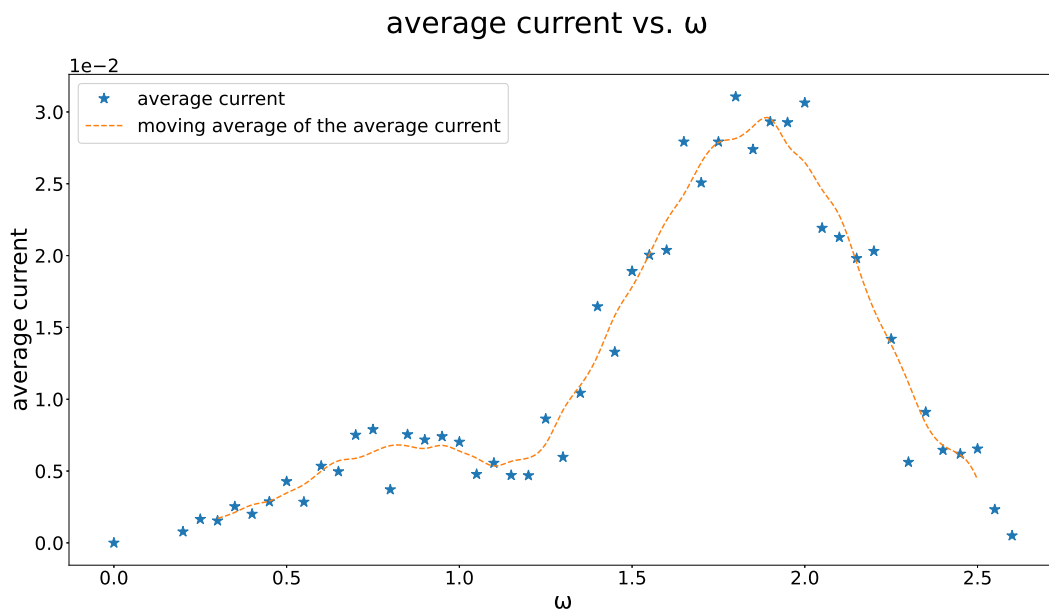
Figure 19: Average current as a function of ω for a 5-10-5 system. All other parameters are given in eq. (*58*).

The figures *16* to *19* show the influence of different system sizes. The $2-4-2$ configuration is the only one with a continuous line, all others have small, and equally appearing fluctuations. This is partially surprising, since on the one hand we see that more differential equations cause more fluctuations of the average current plots, as one may expect, but on the other hand, for all setups larger than $2-4-2$, there seems to be no additional increase.

We now show results for the values $\alpha = 3.0, 5.0$. The result for $\alpha = 1.0$ has already been presented in figure *19*.

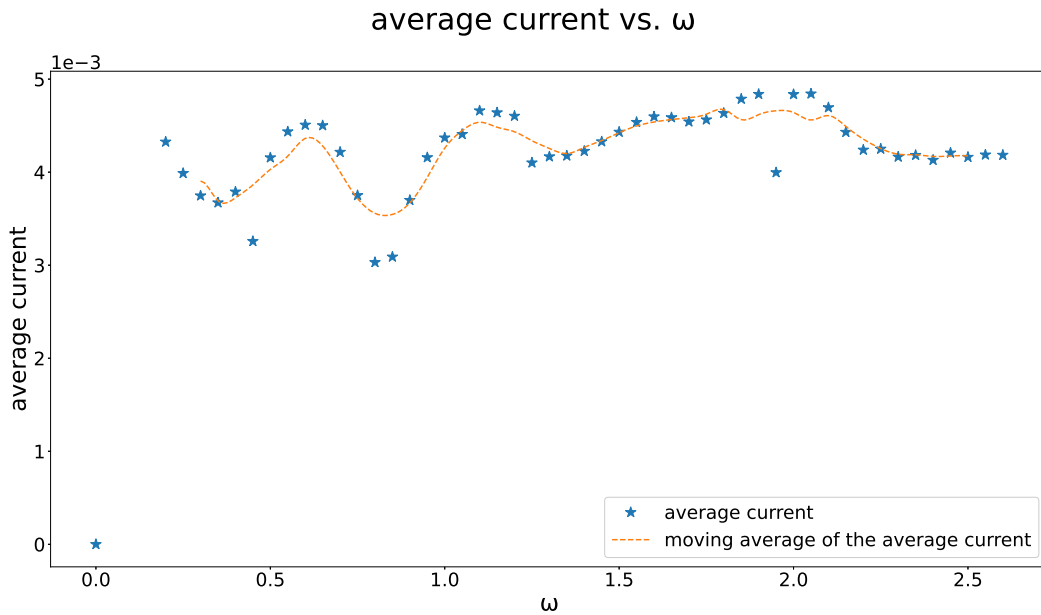Figure 20: Average current as a function of ω for $\alpha = 3.0$. All other parameters are given in eq. (*58*).
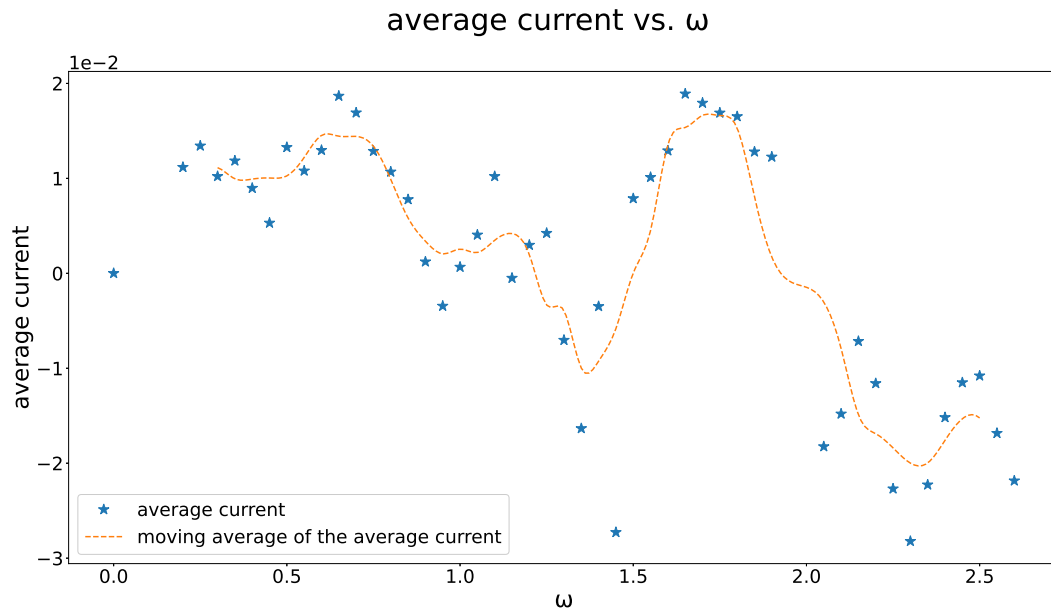
Figure 21: Average current as a function of ω for $\alpha = 5.0$. All other parameters are given in eq. (*58*).

Figures *19*, *20*, and *21* show that an increase in α leads to a stronger scattering, and it eventually destroys the overall curve shape, and we even get nonsensical negative values. The latter result seems to indicate, that this problem is based on numerics. What we would expect from an increase in α, which corresponds to the intensity of the light, is an increase of the current. Comparing figures *19*, and *20*, we can indeed see such an effect, since the peak is at around $3 \cdot 10^{-2}$ in the former, and at around $8 \cdot 10^{-2}$ in the latter case.

We now show results for the values $t' = 0.02, 0.3$. The result for $t' = 0.1$ has already been presented in figure *19*.
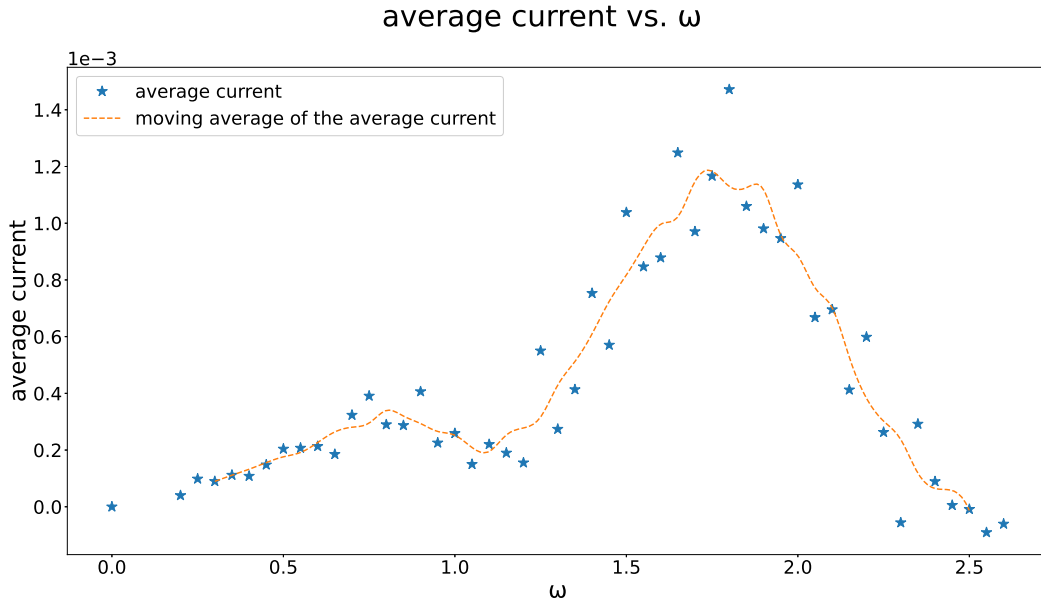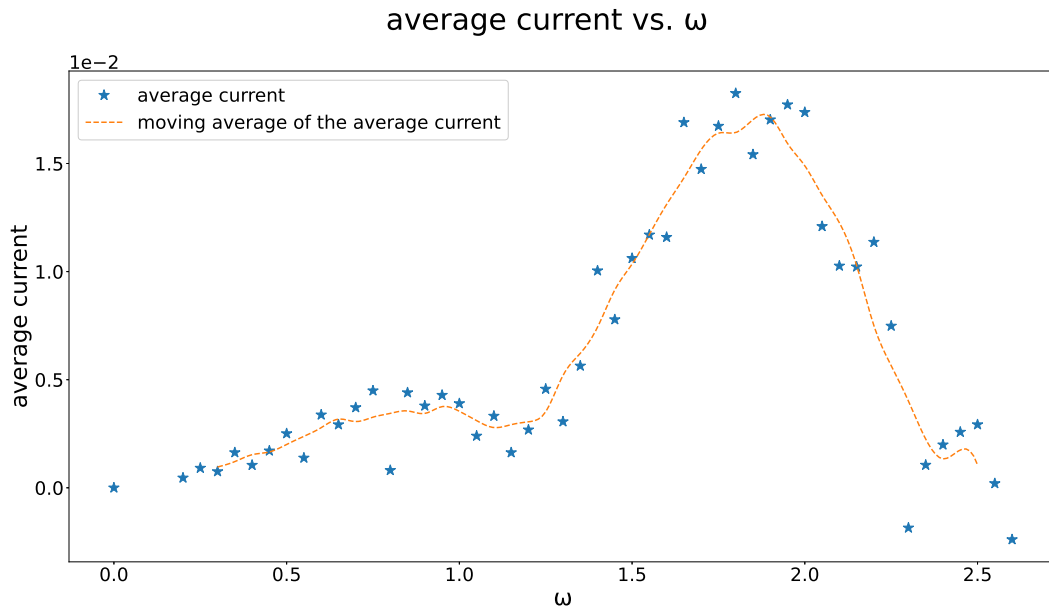

Figure 22: Average current as a function of ω for $t' = 0.02$. All other parameters are given in eq. (*58*).
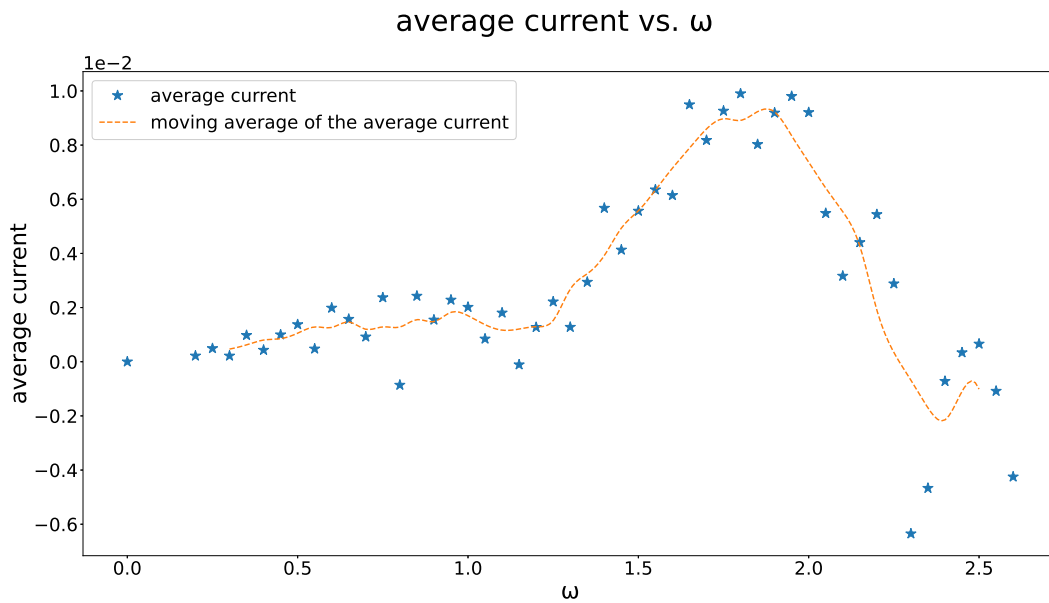

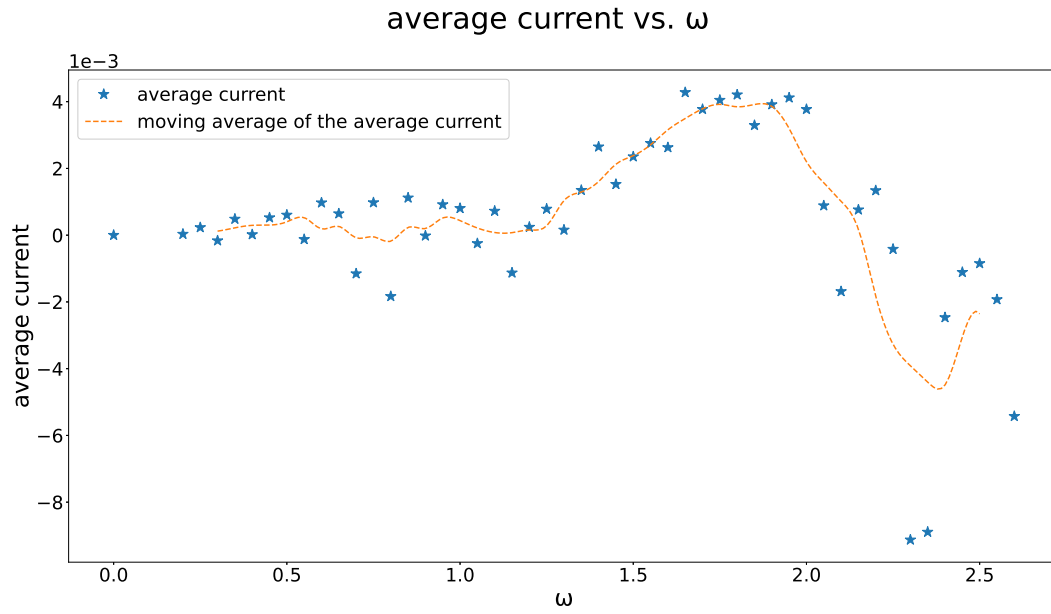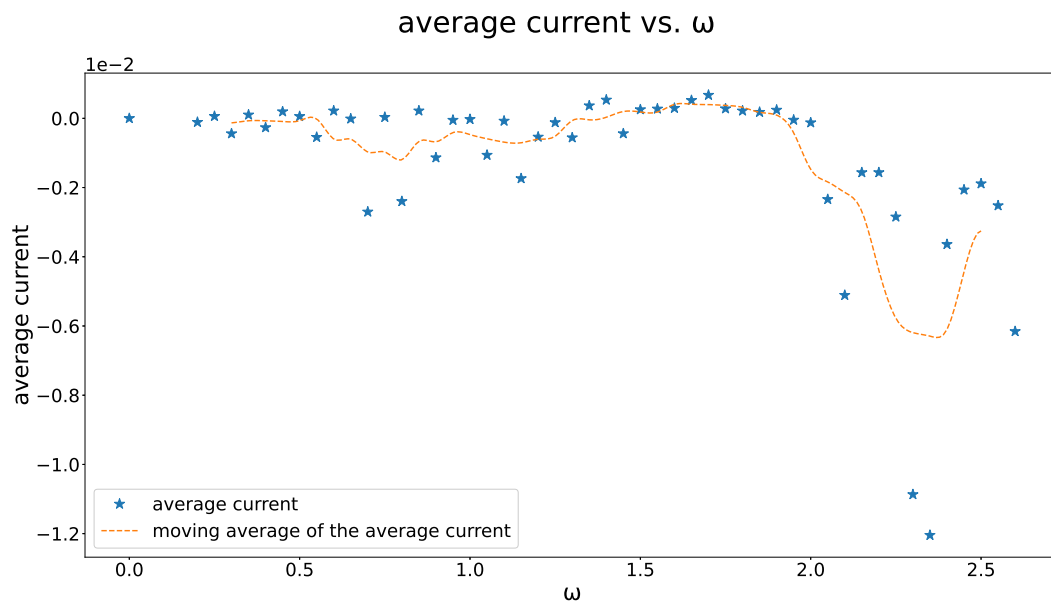Figure 23: Average current as a function of ω for $t' = 0.3$. All other parameters are given in eq. (*58*).

For $t' = 0.02$, as shown in figure *22*, the current is smaller than for larger t', since a smaller hopping parameter means a smaller probability for an electron transfer. The overall form of the curve is not influenced, but scattering seems increased. When using $t' = 0.3$, as shown in figure *23*, on the other hand, the curve shape deviates from the expected one. We want the central part of the chain relatively decoupled from the leads, but this is not the case here, since $t_{\parallel} = 0.25 < t' = 0.3$. This seems to be the most likely cause, for the disappearance of any structure in the respective average current plot.

Up to now we purely inserted particles on the left hand side, and removed them on the right hand side. Here we use non-zero values for the parameter responsible for the removal of particles on the left, and insertion of particles on the right hand side, i.e. $\Gamma_1^{(1)}$. We now show results for the values $\Gamma_1^{(1)} = 0.2, 0.4, 0.6, 0.8$. The result for $\Gamma_1^{(1)} = 0.0$ has already been presented in figure 19.

Figure 24: Average current as a function of ω for $\Gamma_1^{(1)} = 0.2$. All other parameters are given in eq. (58).

Figure 25: Average current as a function of ω for $\Gamma_1^{(1)} = 0.4$. All other parameters are given in eq. (58).

Figure 26: Average current as a function of ω for $\Gamma_1^{(1)} = 0.6$. All other parameters are given in eq. (58).

Figure 27: Average current as a function of ω for $\Gamma_1^{(1)} = 0.8$. All other parameters are given in eq. (58).

In order to see the dependence on $\Gamma_1^{(1)}$ we plot all the results in a single graph, and, furthermore, smooth out the curves. This is shown in figure *28*.
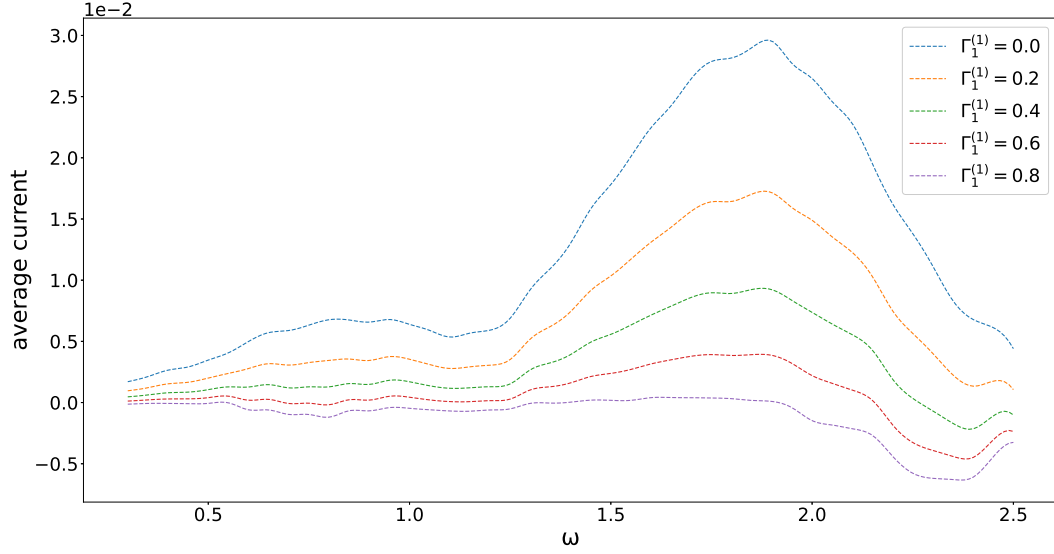
Figure 28: Comparison of all the average currents for different $\Gamma_1^{(1)}$ values.

Turning on $\Gamma_1^{(1)}$ leads to a decrease of the average current. This seems intuitive, since some of the particles that are inserted in the left lead are being removed again, resulting in fewer entering the central system. Therefore, there are less particles that can get excited by the external periodic field.

There are also some overall results that should be discussed. For one, we can see that the maximum always appears at around $\omega = 2.0$, as we expected, judging from the large idealized system. What we can also see, is another small maximum appearing close to $\omega = 1.0$. Since this one is much smaller, it could have the physical interpretation of the less likely case that two photons simultaneously excite an electron to the upper band.

6.2 Alternating hopping values

In the second configuration we consider, the band gap is produced by an alternation of the hopping in the central region. Figure *29* shows the setup, where we have left and right leads that connect the system to the environment. The idea is the same one as before, with the difference that the band structure is a another one.
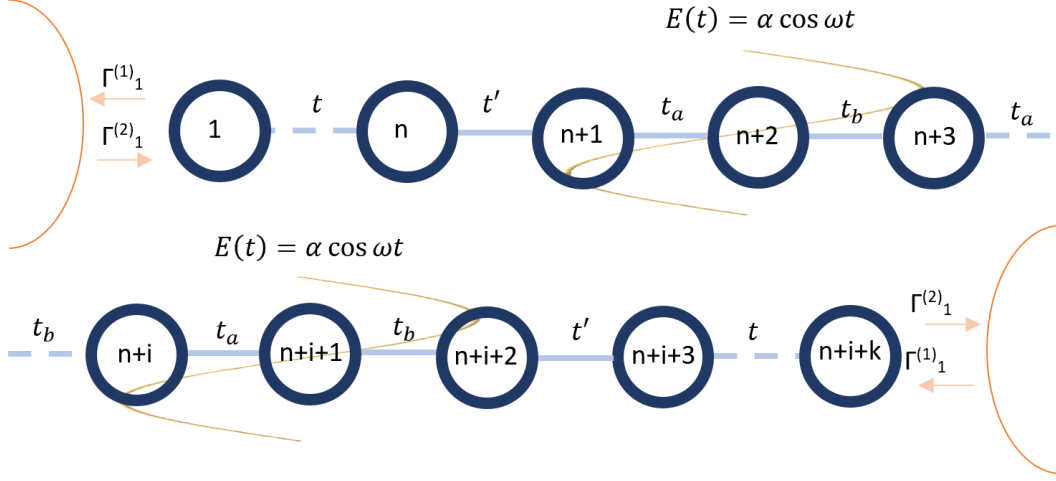

Figure 29: Setup for the case of alternating hopping parameter.

The Hamiltonian of the central system in this case is given by:

$$H = \sum_{i=1}^{\frac{N-1}{2}} (a_{2i}^{\dagger} a_{2i-1} + a_{2i-1}^{\dagger} a_{2i}) t_a + (a_{2i+1}^{\dagger} a_{2i} + a_{2i}^{\dagger} a_{2i+1}) t_b. \tag{59}$$

where t_a, and t_b are the alternating hopping values of the central system, and the other symbols have the same meaning as the ones in eq. (*57*). Figure *30* gives a graphical representation of this setup, and figure *31* shows its band structure for large N. We can see that for $1.5 < \omega < 3.0$ the electrons get enough energy to get from the lower to the upper band, and for each ω value in this range, there exists a direct band gap. Therefore, purely judging from this idealized system, we would expect an increase of the current starting at $\omega = 1.5$, and not much change afterwards. Since we do not have this idealized system, we expect to find a smooth transition, and not a step function.
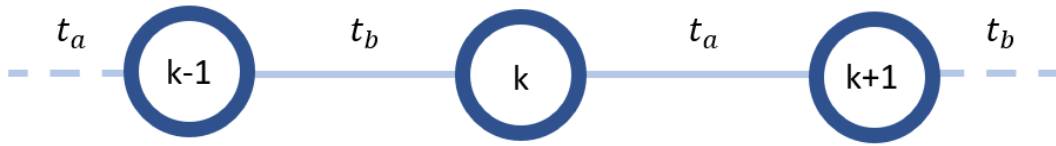

Figure 30: System of infinite sites with alternating hopping parameter.
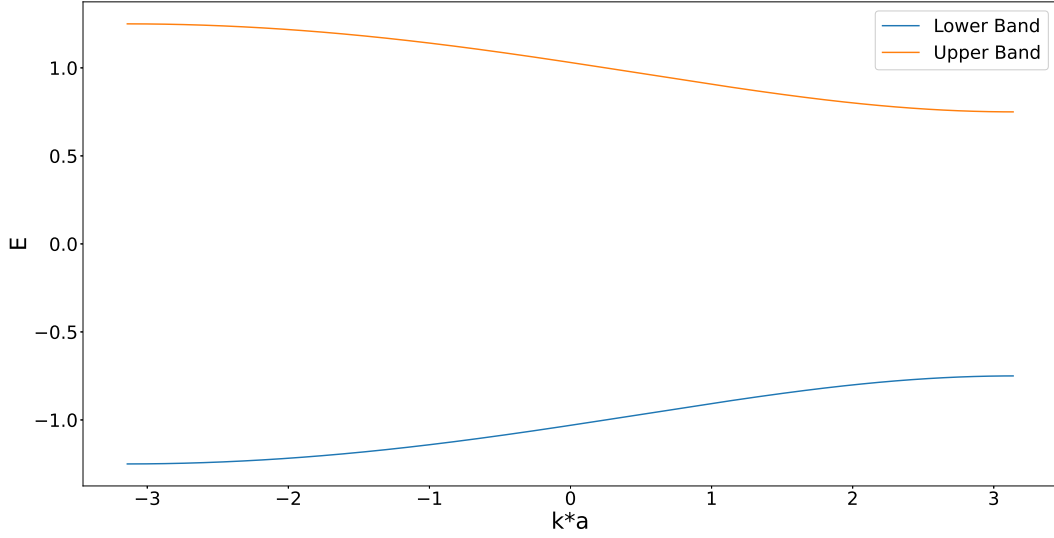
Figure 31: System of infinite sites with alternating hopping parameter.

If not specified otherwise, the following parameters are being used:

$$
\begin{aligned}
\varepsilon_{left} &= -1.0, \\
\varepsilon_{right} &= 1.0, \\
\varepsilon_{central} &= 0.0, \\
structure &= 3 - 12 - 3, \\
t' &= 0.1, \\
\alpha &= 1.0, \\
solver &= Tsit5, \\
\Gamma_1^{(1)} &= 0, \\
\Gamma_1^{(2)} &= 0.8, \\
t_a = t &= 1.0, \\
t_b &= 0.25, \\
U &= 0.0.
\end{aligned}
\tag{60}
$$

All already mentioned parameters have the same meaning as before, and t_a, and t_b, are the hopping parameters, which are alternated along the central part of the chain. For this configuration, there are some additional choices one may make. For one, we can decide to either use an even or odd number of hopping parameters, and if we choose an odd number of central sites, we can use either the larger or smaller t at the two bonds at the boundary of the chain. Trying these different configurations showed, that the results mostly coinciding with our expectations are obtained when using an odd number of central sites, and the smaller t as the boundary hopping value. However, we will also show some results for the case in which the boundary hopping value is the larger t.

34

Again, we will initially look into the current as a function of time, and similarly as for the ladder structure, we included a moving average, which has a range of ten time units here. We choose the results used in figures *38*, *42*, and *39*, which have parameters $structure = 4 - 14 - 4$, $structure = 3 - 8 - 3$, and $structure = 3 - 8 - 3$ respectively, with all other parameters as give in eq. (*66*), where for all except for the last one, the boundary hopping value is the smaller t. The first figure shows good agreement with our expectations, i.e. an increase of the average current up to $\omega = 1.5$, and not much change afterwards, but the other two do not. Surprisingly, using the larger instead of the smaller hopping value at the boundaries of the central part for the $3-8-3$ structure, happens to give unexpected results. Furthermore, we can see that the fluctuations in all figures showing the average current as a function of ω, are strongest in the range $\omega = 0.2 - 1.0$, and mostly stable afterwards. Since we assume fluctuations in the average current plots to be caused by numerics, or components with low frequencies, this gives us a good opportunity for testing this assumption. Therefore, we will not only compare the results of these different configurations, but also for different ω values. We will take one ω value from the strongly fluctuating area, which we choose to be $\omega = 0.7$, and another one from the more stable range, for which we take $\omega = 2.0$.
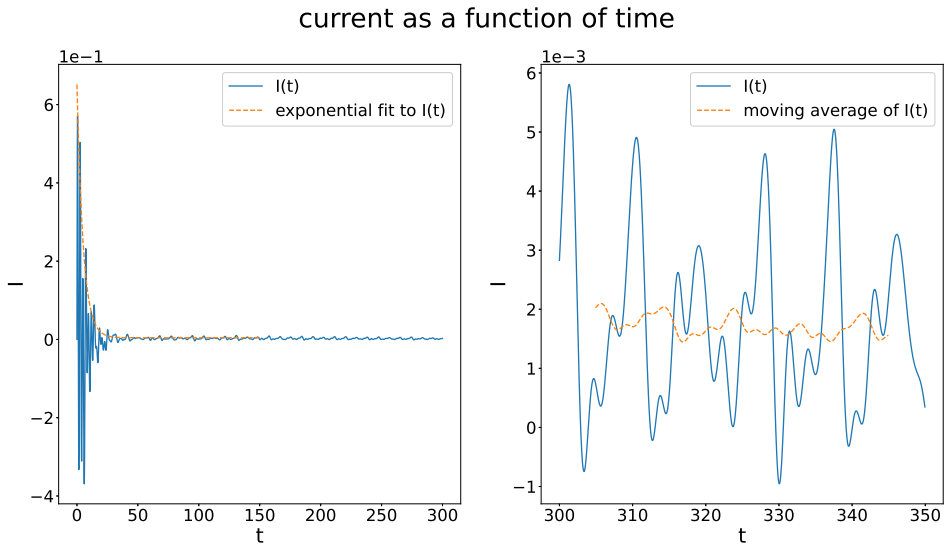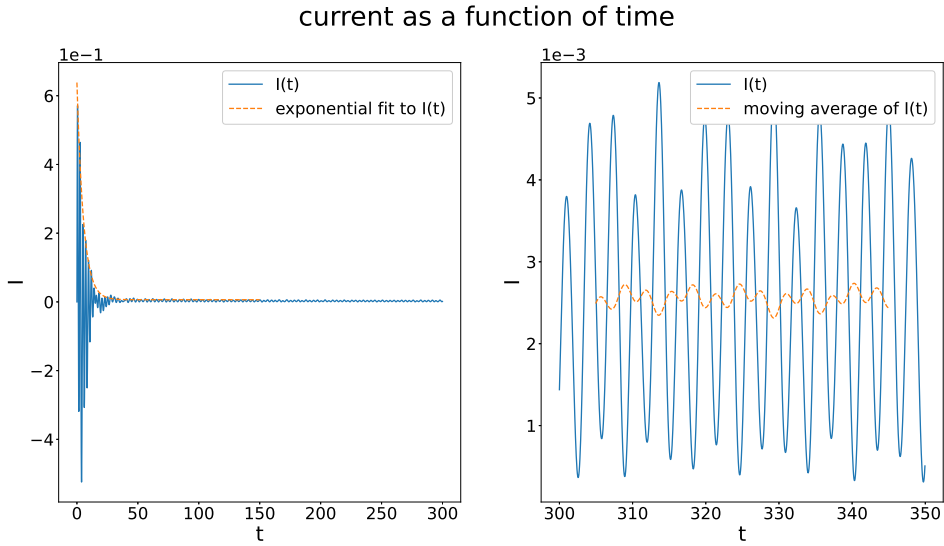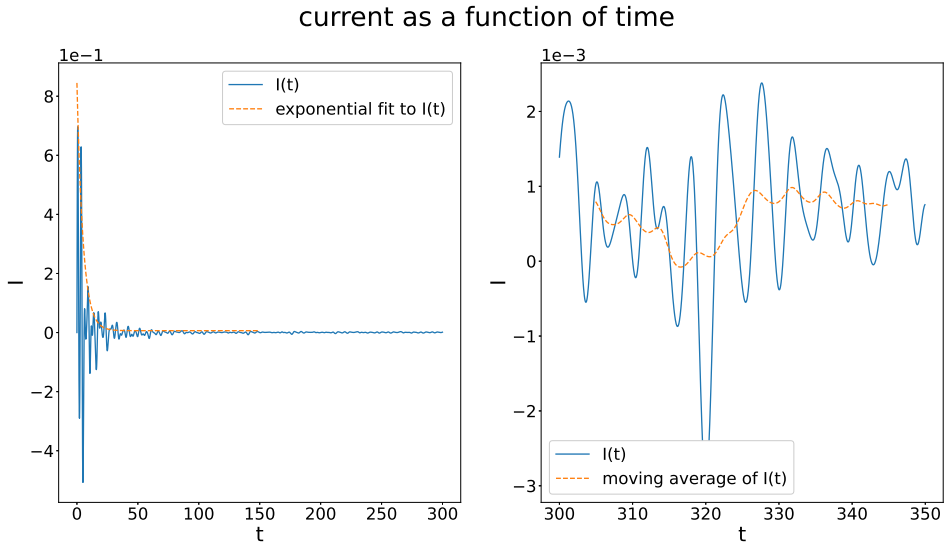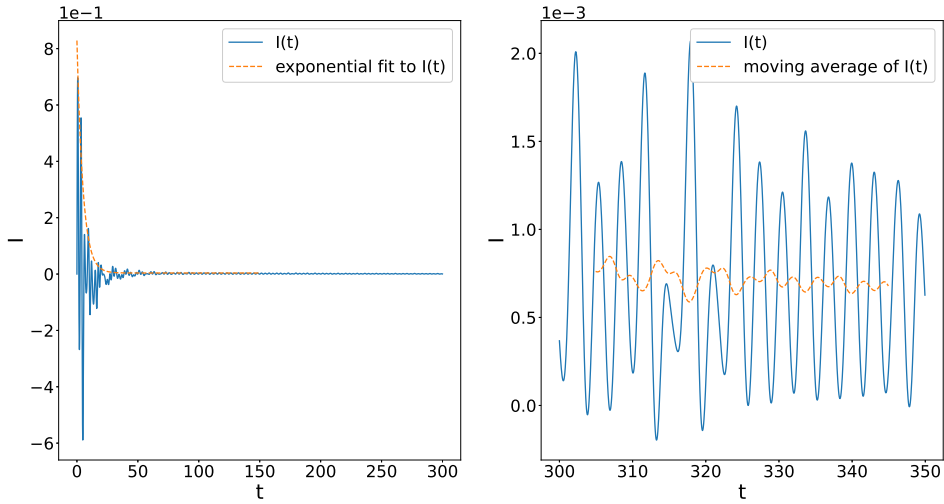

Figure 32: Current as a function of time for $\alpha = 1.0$, and $structure = 3 - 8 - 3$, for $\omega = 0.7$. All other parameters are given in eq. (*60*). Here t_b is the boundary hopping value of the system.

Figure 33: Current as a function of time for $\alpha = 1.0$, and $structure = 3 - 8 - 3$, for $\omega = 2.0$. All other parameters are given in eq. (60). Here t_b is the boundary hopping value of the system.
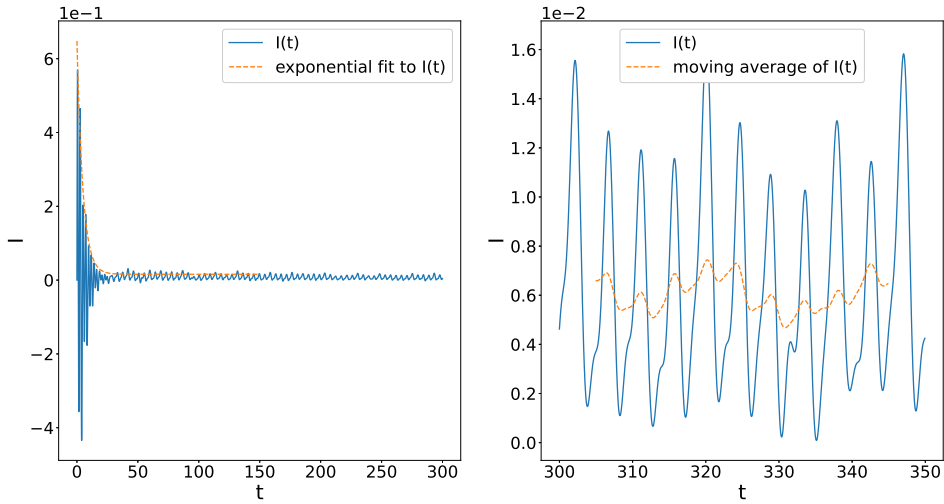

Figure 34: Current as a function of time for $\alpha = 1.0$, and $structure = 4 - 14 - 4$, for $\omega = 0.7$. All other parameters are given in eq. (60). Here t_b is the boundary hopping value of the system.

current as a function of time

Figure 35: Current as a function of time for $\alpha = 1.0$, and $structure = 4 - 14 - 4$, for $\omega = 2.0$. All other parameters are given in eq. (60). Here t_b is the boundary hopping value of the system.
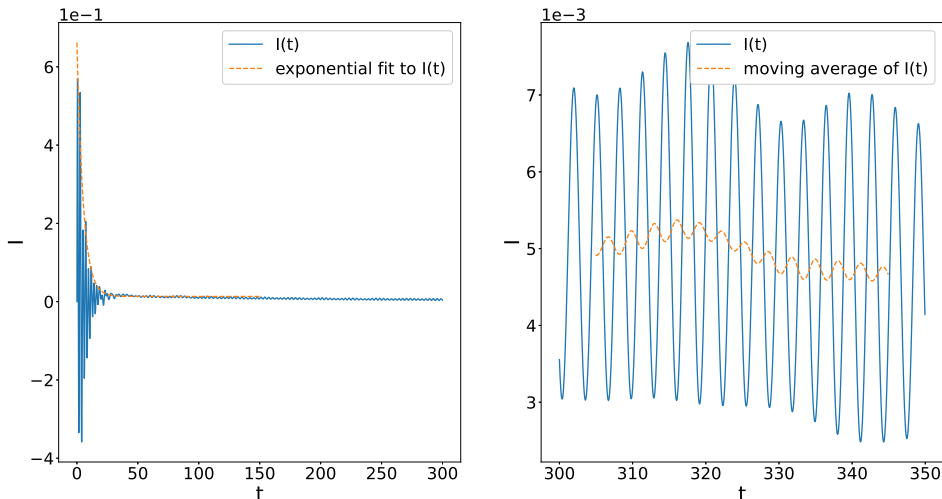

current as a function of time

Figure 36: Current as a function of time for $\alpha = 1.0$, and $structure = 3 - 8 - 3$, for $\omega = 0.7$. All other parameters are given in eq. (60). Here t_a is the boundary hopping value of the system.

Figure 37: Current as a function of time for $\alpha = 1.0$, and $structure = 3 - 8 - 3$, for $\omega = 2.0$. All other parameters are given in eq. (60). Here t_a is the boundary hopping value of the system.

Again we reach times far beyond the influential part of the transient. Comparing the results for $\omega = 0.7$, and $\omega = 2.0$, clearly shows in all cases, that the relative fluctuation of the moving average is much stronger for $\omega = 0.7$. When comparing figures 32, and 34, we get the impression, that for the structure $4 - 14 - 4$ numerics or low frequencies are to blame for the unexpected behaviour of its average current plot, as shown in figure 42. This seems to support our idea, that larger structures give worse results. However, when comparing figures 36 and 32 the relative fluctuations of the moving average seem rather equal, which we interpret such, that we cannot blame numerics for the odd behaviour we see when using the larger hopping value at the boundaries of the central system, instead of the smaller one.

Let us also try to guess why the numerical solution of the system of differential equations we get in the case of the ladder structure seem much more stable than the one we get for the system with alternating hopping values in the central part. In the former case, each site has a neighbour perpendicular to chain extension. This perhaps has a two sided advantage. For one, we need only a shorter chain length to get a certain amount of states, compared with the 1D case, and we do want as much states in the central part as possible to approach the infinite system in behaviour. Furthermore, intuitively this may numerically also stabilize the system, since every site is coupled to three, instead of two other sites.

We simulated the configurations: 3-8-3, 3-12-3, 4-14-4, and 4-16-4. We show the results for the case of the boundary hopping value being t_a, as well as for the case in which it is t_b.
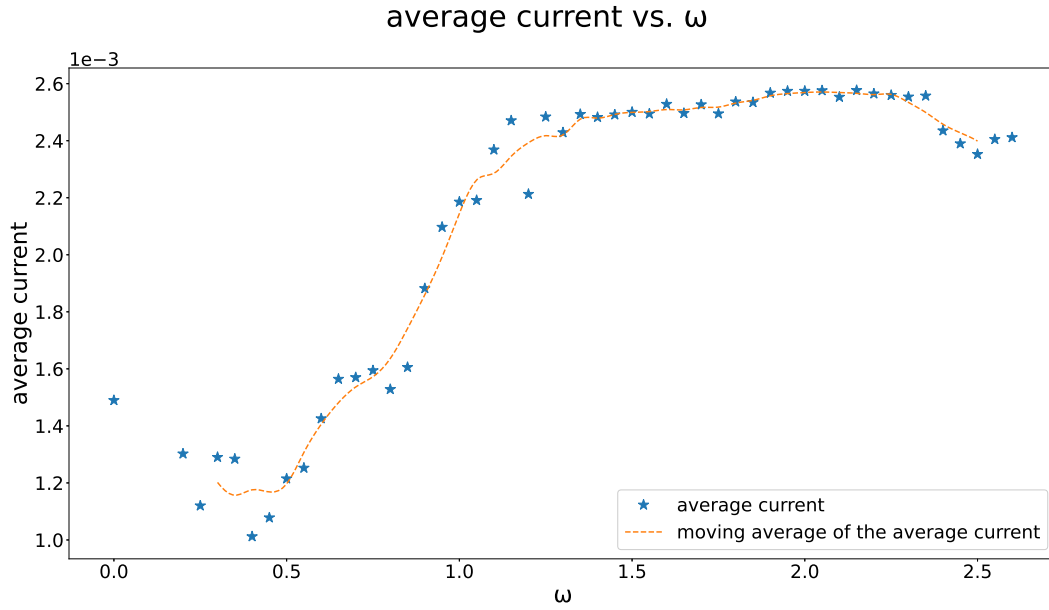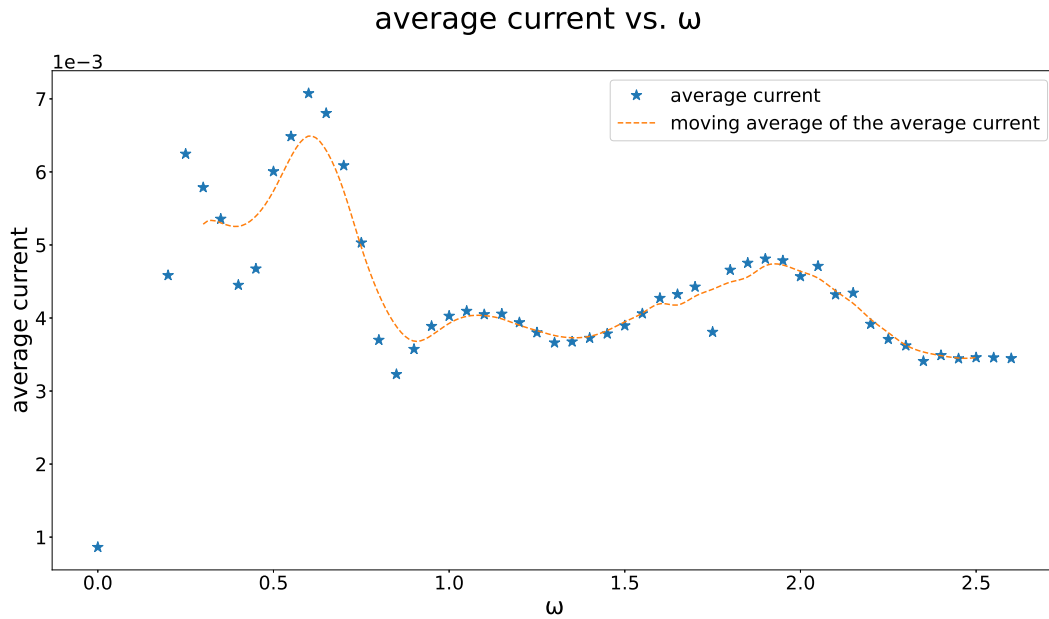

Figure 38: Average current as a function of ω for $structure = 3 - 8 - 3$. All other parameters are given in eq. (60). The boundary bond of the central region is t_b.

Figure 39: Average current as a function of ω for $structure = 3 - 8 - 3$. All other parameters are given in eq. (60). The boundary bond of the central region is t_a.
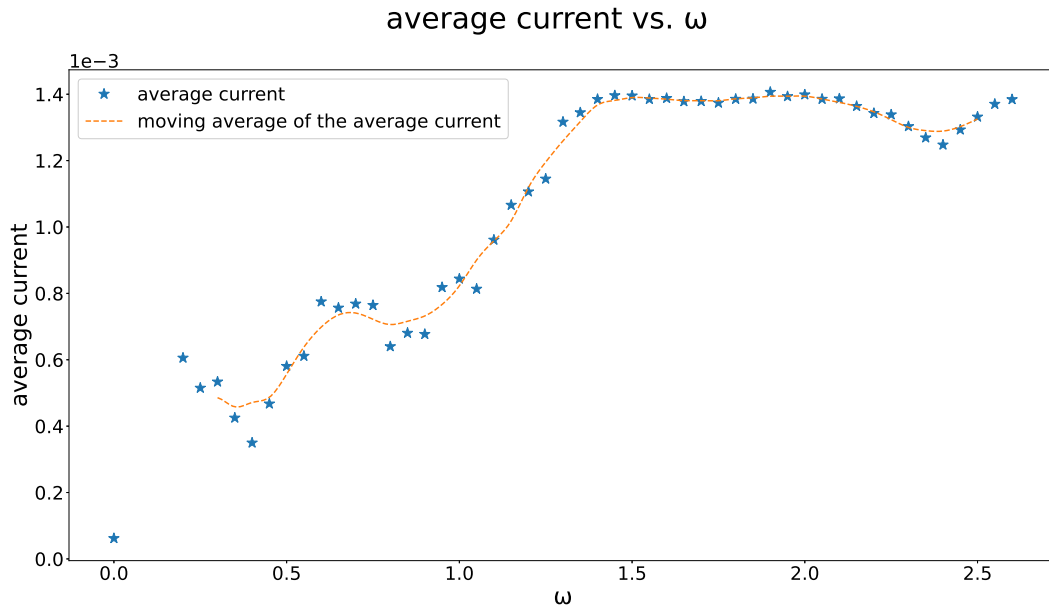
Figure 40: Average current as a function of ω for $structure = 3 - 12 - 3$. All other parameters are given in eq. (60). The boundary bond of the central region is t_b.
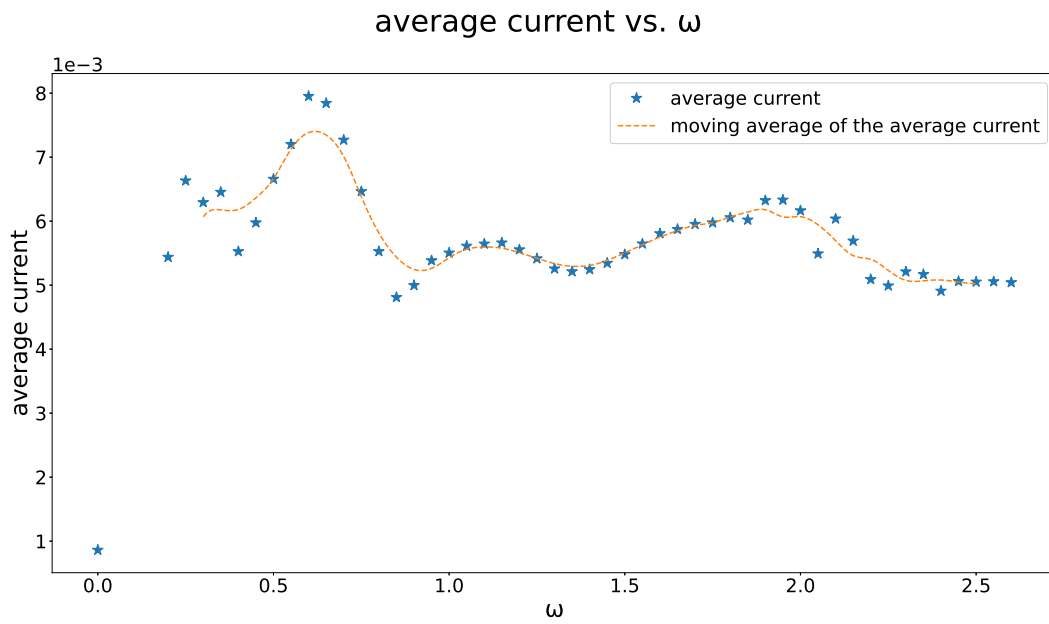

Figure 41: Average current as a function of ω for $structure = 3 - 12 - 3$. All other parameters are given in eq. (60). The boundary bond of the central region is t_a

Figure 42: Average current as a function of ω for $structure = 4 - 14 - 4$. All other parameters are given in eq. (60). The boundary bond of the central region is t_b.
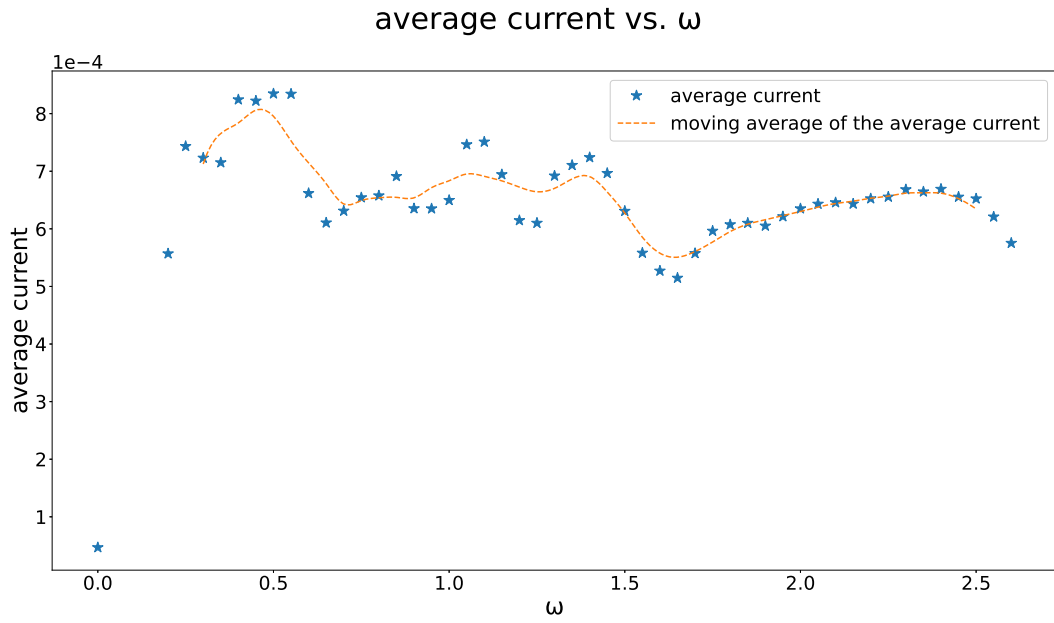

Figure 43: Average current as a function of ω for $structure = 4 - 14 - 4$. All other parameters are given in eq. (60). The boundary bond of the central region is t_a

Figure 44: Average current as a function of ω for $structure = 4 - 16 - 4$. All other parameters are given in eq. (60). The boundary bond of the central region is t_b.
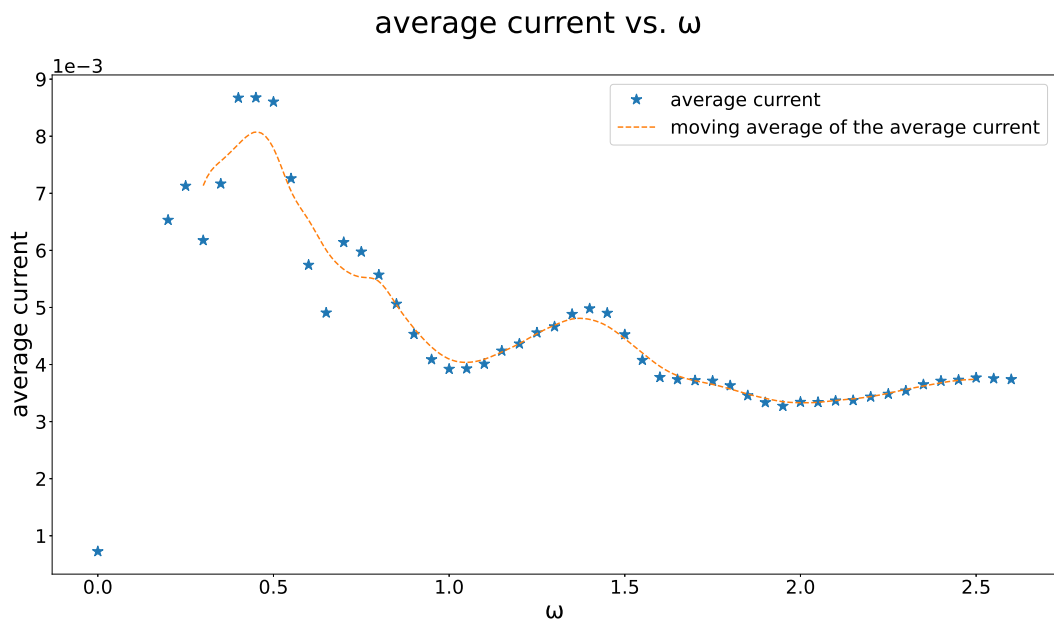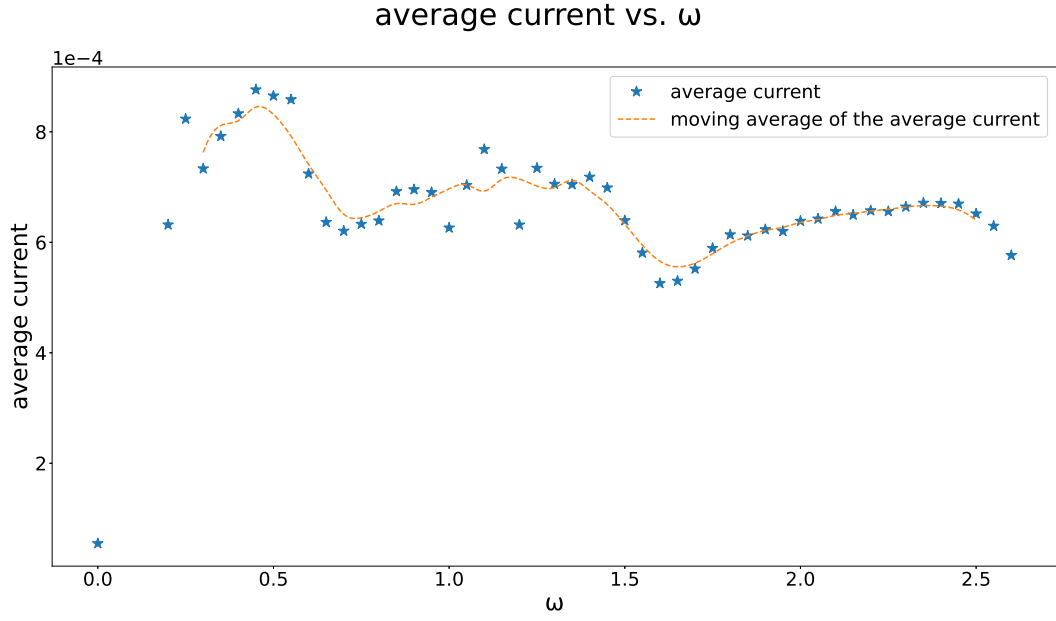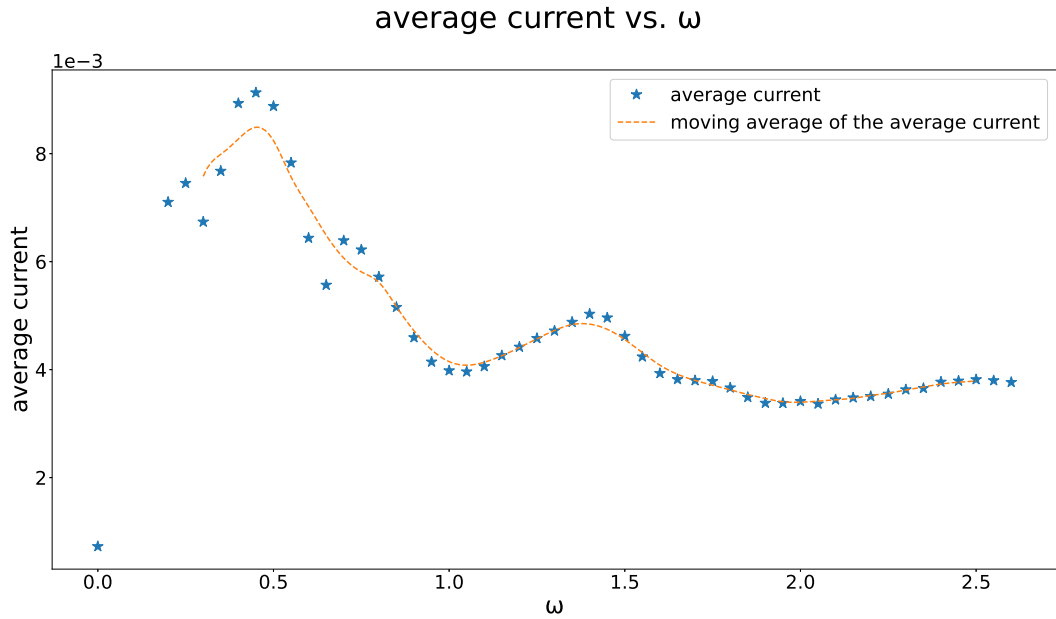

Figure 45: Average current as a function of ω for $structure = 4 - 16 - 4$. All other parameters are given in eq. (60). The boundary bond of the central region is t_a

We can see that whenever we use t_a as the boundary hopping value of the central region, the results do not coincide with what we expected. Quite the opposite, the average current is in many cases even larger before reaching $\omega = 1.5$. In case of t_b being the boundary hopping value of the central system, the configurations $3-8-3$, and $3-12-3$, shown in figures 38, and 40, show the expected behaviour, i.e. an increase up to $\omega = 1.5$, and not much change afterwards. Our results from investigating the current as a function of time imply, that numerics, or lower frequencies, could cause the unpredicted behaviour observed in the results of larger structures. However, we found no answer regarding the odd behaviour when using a larger hopping value at the boundary of the central system.

We simulated for the values: 0.02, and 0.3 The result for $t' = 0.1$ has already been shown in figure *40*. The boundary bond of the central region is always t_b.
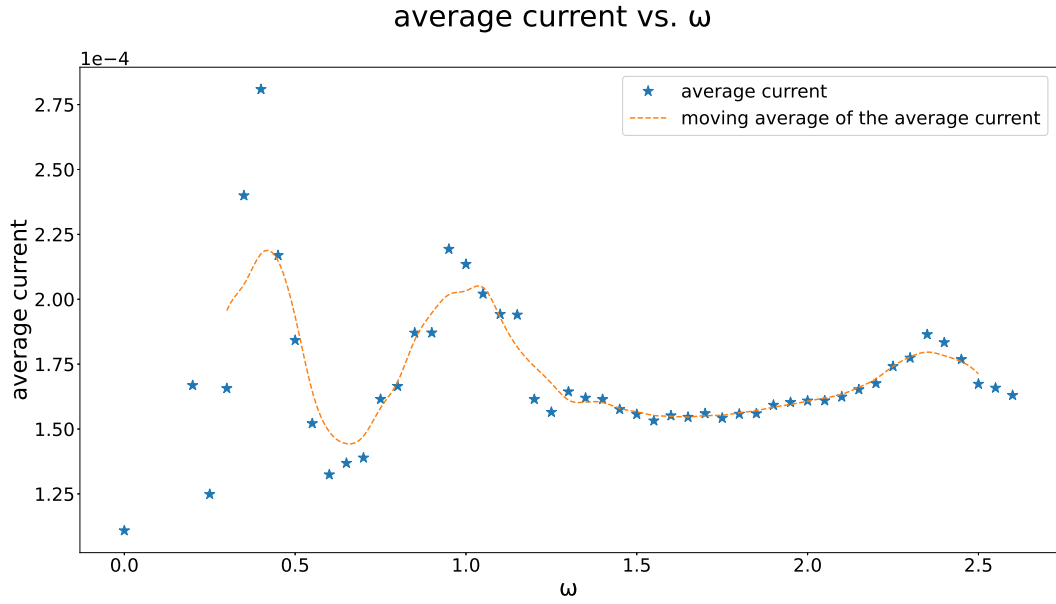

Figure 46: Average current as a function of ω for $t' = 0.02$. All other parameters are given in eq. (*60*). The boundary bond of the central region is t_b.
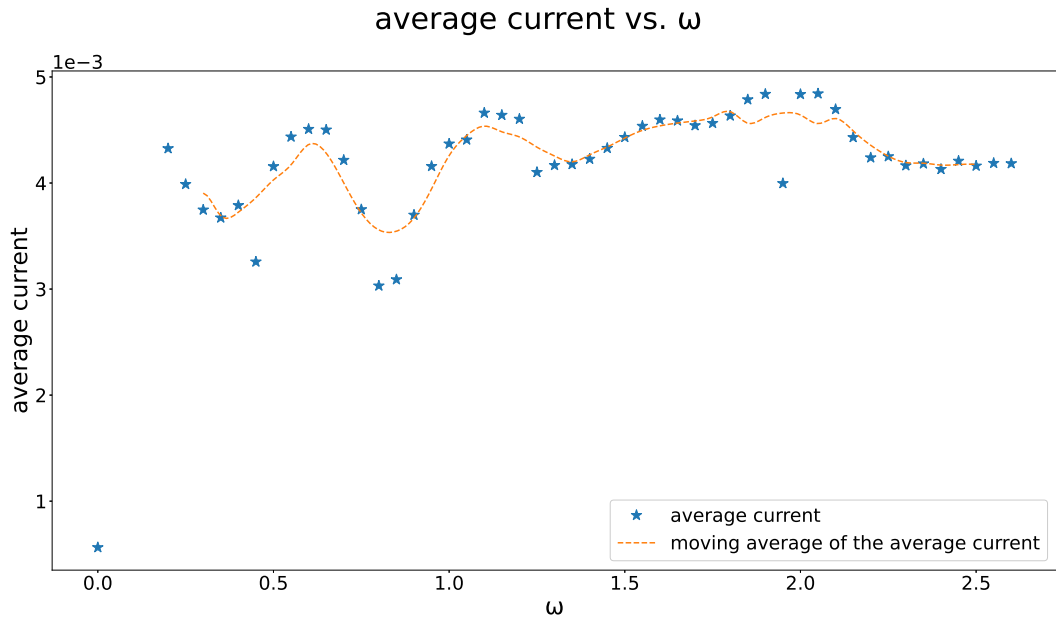
Figure 47: Average current as a function of ω for $t' = 0.3$. All other parameters are given in eq. (*60*). The boundary bond of the central region is t_b.

The change of t' destroys the overall form of the plots, but presumably for two different reasons. For $t' = 0.02$, shown in figure *46*, we can see severe scattering of the average current curve, which we interpret as numerical issues, or the influence of lower frequencies. When using $t' = 0.3$, as presented in figure *47*, we assume the reason to be the insufficient decoupling of the central system, since $t' = 0.3 > t_b = 0.25$.

Up to now we purely inserted particles on the left hand side, and removed them on the right hand side. Here we use non-zero values for the parameter responsible for the removal of particles on the left, and insertion of particles on the right hand side, i.e. $\Gamma_1^{(1)}$. We now show results for the values $\Gamma_1^{(1)} = 0.8, 1.0$. The result for $\Gamma_1^{(1)} = 0.0$ has already been shown in figure 40. The boundary bond of the central region is always t_b.

Figure 48: Average current as a function of ω for $\Gamma_1^{(1)} = 0.8$. All other parameters are given in eq. (60). The boundary bond of the central region is t_b.
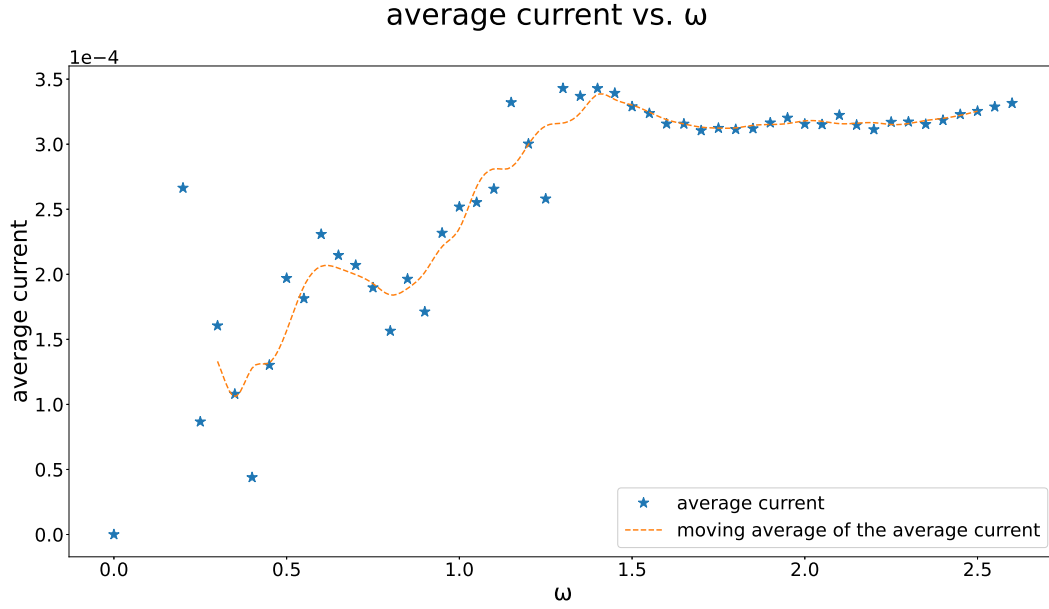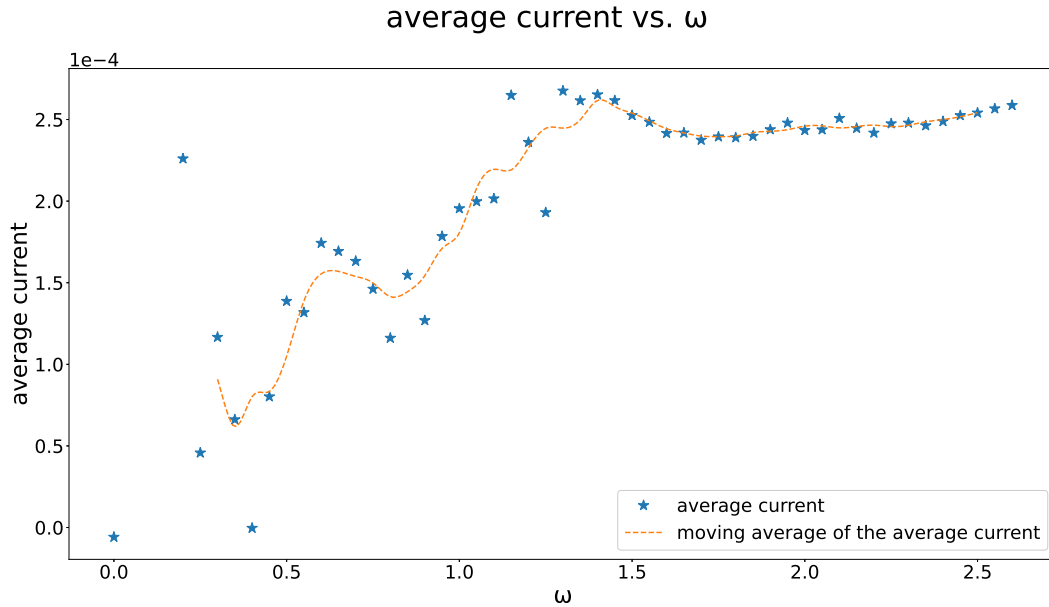

Figure 49: Average current as a function of ω for $\Gamma_1^{(1)} = 1.0$. All other parameters are given in eq. (60). The boundary bond of the central region is t_b.

In order to see the dependence on $\Gamma_1^{(1)}$, we plot all the results in a single graph, and, furthermore, smooth out the curves. This is shown in figure *50*.
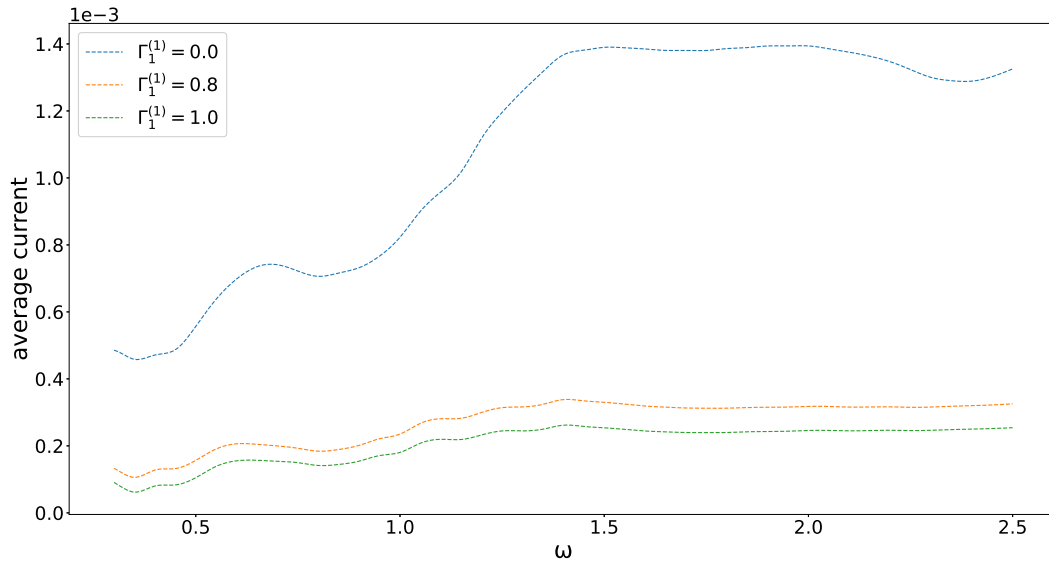
Figure 50: Comparison of all the average currents for different $\Gamma_1^{(1)}$ values.

There is a detail here, which is more distinct than in figure *28*. When the parameters responsible for inserting, and removing particles are equal on both ends of the chain, the current is still positive. Therefore, here we even simulated a case for which $\Gamma_1^{(1)} > \Gamma_1^{(2)}$, and also in this case we get a positive average current, when turning on the light source. One may imagine this to be caused by an increase in particle density in the higher energy levels, and a decrease in the lower ones, due to the external driving. So for the leftmost site, which has low energy, the particle number is decreased, and for the rightmost, which has high energy, it is increased. This overpowers the Γ parameters, which give a negative current (i.e. from the right to the left lead) in the steady state.

When taking a closer look at the results for high $\Gamma_1^{(1)}$ values, as presented in figure *51*, we can see an interesting feature.
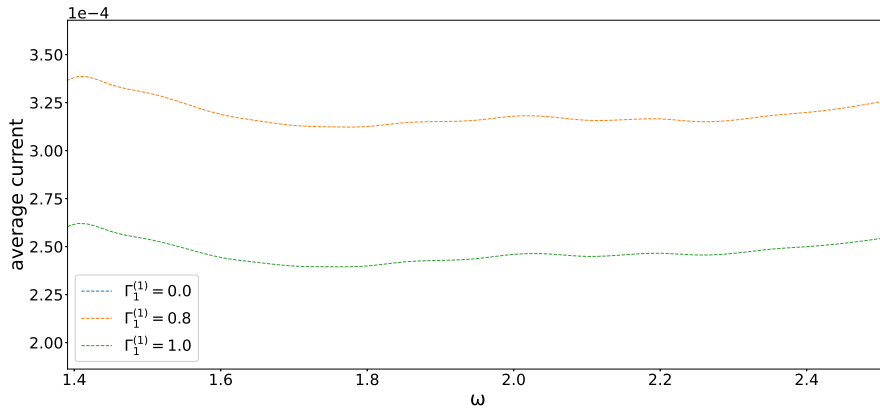
Figure 51: Detail view for large $\Gamma_1^{(1)}$ values.

There is a minimum between $\omega \approx 1.4$, and $\omega \approx 2.5$. When looking at figure *31*, we can see that the density of states decreases between these values. Therefore, the shape shown in figure *51* is interpreted as a result of this state over energy distribution.

Let us make a final global remark. We see that we can use parameters which give us the expected behaviour for the average current as a function of ω, i.e. an increase for $\omega < 1.5$, and not much change afterwards, but the curve shape is very fragile. Small changes can already lead to results we cannot interpret. We could also see very clearly, that the setup with a central ladder structure gives results that are much more stable.

6.3 Results for the case with electron-electron interaction

We will investigate an interacting site, which is connected to a left and a right non-interacting site, that are connected to reservoirs. The interaction in the central site is what leads to the gap. Again we want to look into the dependency of the average current on the driving frequency ω. Compared to the previous method, the system size is very limited here. We will start by showing results for the case of three sites, which is easily simulated. After those we will also present some results for the case of five sites. We will not analyse this latter configuration as detailed as the other one however, since obtaining results is computationally expensive due to the large matrix size.

Figure *52* shows the setup of our system. First we may want to look at the spectral function, given as [*3*, eq. 11]:

$$A(\omega) = -\frac{1}{\pi} \operatorname{Im}\{G_R(\omega)\}. \tag{61}$$

The DOS curve for the central site is depicted in figure *54*. We also showed that an increase of t' leads to a broadening of the peaks. Furthermore, we can see that the gap between the two DOS peaks corresponds to the interaction strength. Therefore, we generally assume the gap to be proportional to U, where U is the interaction strength.
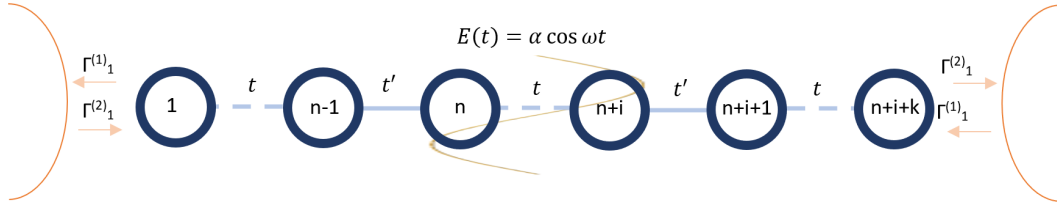
Figure 52: General structure of our system, where interaction is turned on in the central site/s.
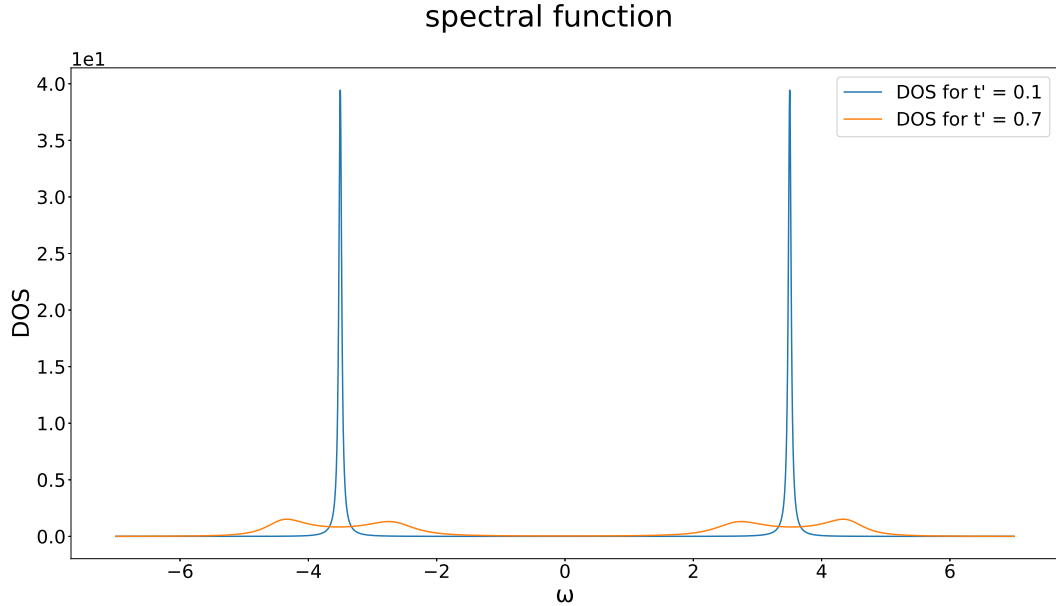
Figure 53: DOS for: $sites = 3, t'$ as given in the legend, $U = 7.0, \varepsilon_{left} = -U/2, \varepsilon_{central} = -U/2, \varepsilon_{right} = U/2$

47

If not specified otherwise, the following parameters are being used:

$$U = 7.0$$
$$\varepsilon_{left} = \varepsilon_{central} = -U/2$$
$$\varepsilon_{right} = U/2$$
$$t' = 0.1 \tag{62}$$
$$solver = Tsit5,$$
$$\alpha = 1.0$$
$$structure = 1 - 1 - 1$$

Looking at the average current as a function of ω, we can see that all our plots look very smooth. Therefore, we will only show a single plot of the current as a function of time for the case of three sites, using the highest frequency, and amplitude of the driving field, i.e. $\omega = 14.0$, and $\alpha = 5.0$, with all other parameters as given in eq. (62).
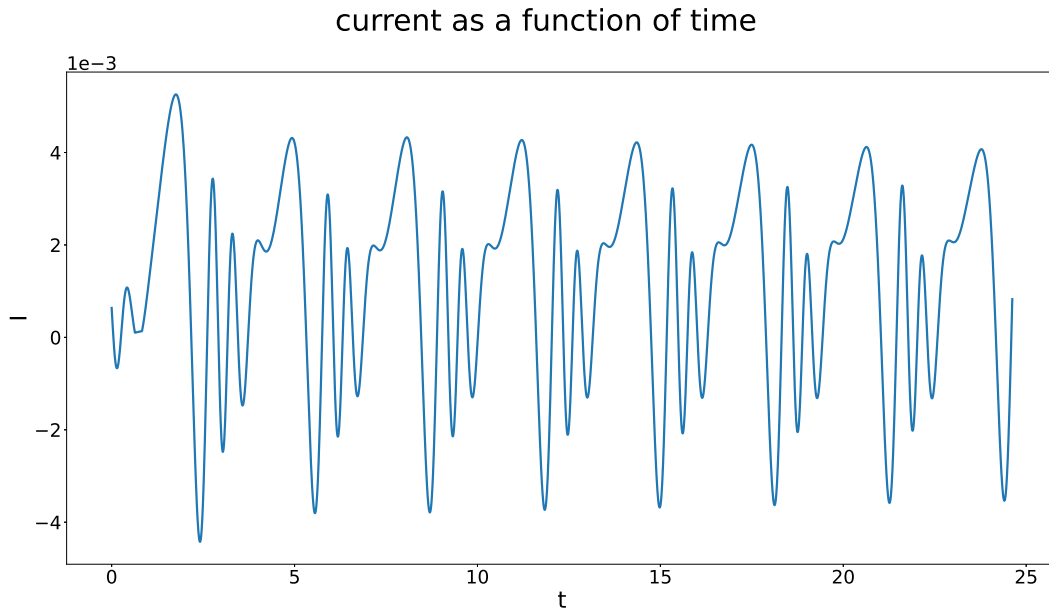
Figure 54: Current as a function of time for $\omega = 14.0$, and $\alpha = 5.0$.

We can see that a periodic behaviour is reached already in the second period we are showing here, as expected.

We now show results for the values $U = 5.0, 7.0, 9.0$.

average current vs. omega

Figure 55: Average current as a function of ω for $U = 5.0$. All other parameters are given in eq. (*62*).

average current vs. omega
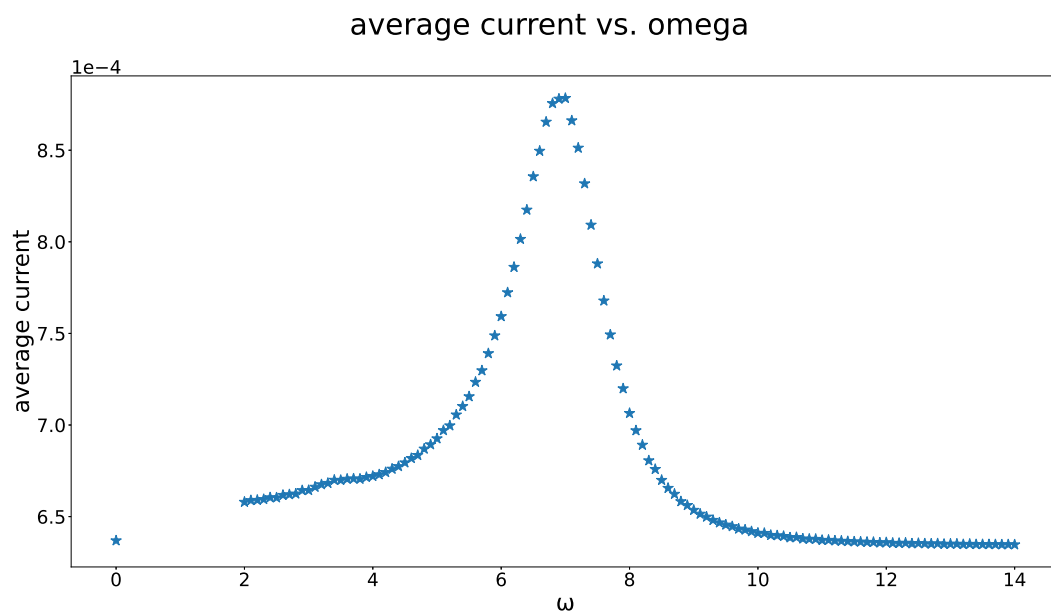
Figure 56: Average current as a function of ω for $U = 7.0$. All other parameters are given in eq. (*62*).
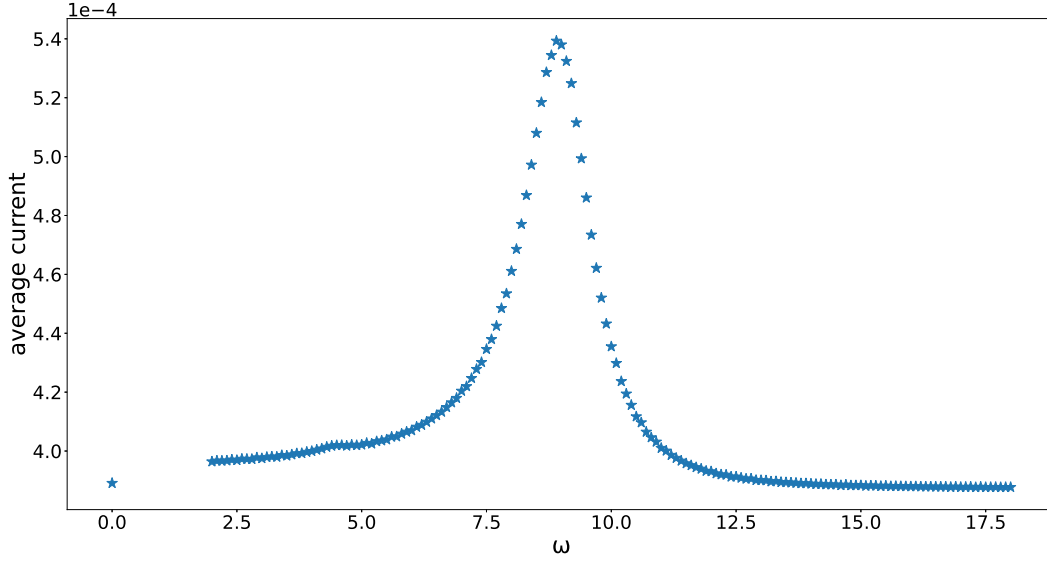
Figure 57: Average current as a function of ω for $U = 9.0$. All other parameters are given in eq. (*62*).

We can see that the peaks are at the position of the gap. Looking at the plots one may get the impression that the peaks are becoming thinner as U increases, but the range on the y-axis is also increasing. To get a better view on this, let us normalize the plots, and put the peaks on top of each other.
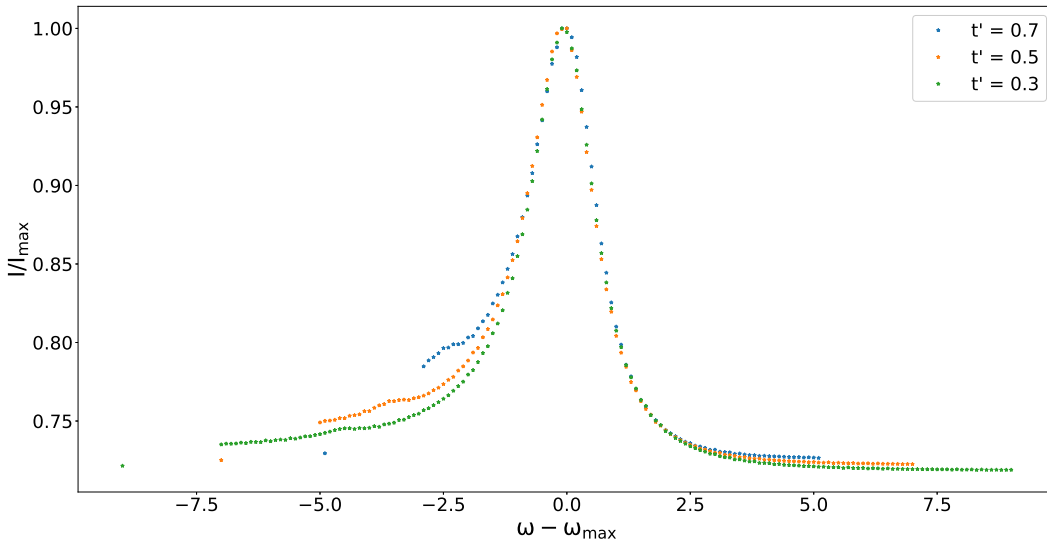
Figure 58: Normalized, and shifted plots for $U = 5.0, 7.0, 9.0$

We can see that the peaks coincide almost perfectly. Also the normalized steady state currents differ only slightly, but since they decrease in absolute value as the gap increases, this means the absolute peak value decreases as well. This later result can also be seen quite well in figures *55* to *58* directly. Considering that $I \propto \alpha^2$, $I \propto n_1$ and $I = \frac{E}{Ft} = \frac{\hbar \omega_1 n_1}{Ft} = \frac{\hbar \omega_2 n_2}{Ft} \rightarrow J_1 = J_2 \frac{\omega_2}{\omega_1}$, where n is the particle number, I the intensity, J the current, and F the area, we can see that the higher the individual photon energy, the fewer photons exist, at equal intensity. This in turn means a smaller peak current, the larger the gap. So qualitatively a decrease in absolute current value coincides with what we expect.

50

We now show results for the values $\alpha = 1.0, 3.0, 5.0$. The result for $\alpha = 1.0$ has already been shown in figure *56*.
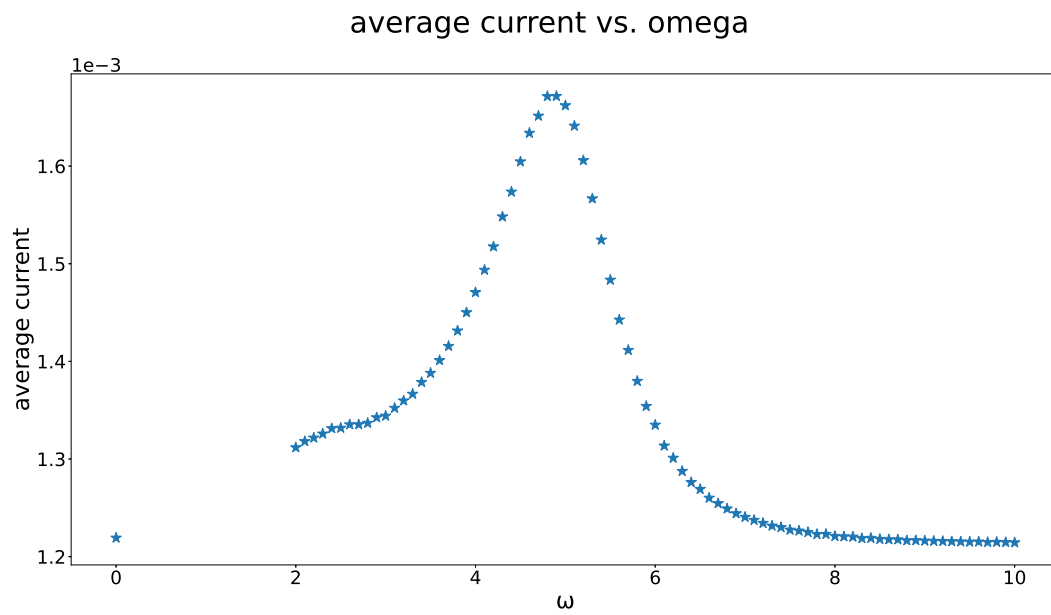

Figure 59: Average current as a function of ω for $\alpha = 3.0$. All other parameters are given in eq. (*62*).

Figure 60: Average current as a function of ω for $\alpha = 5.0$. All other parameters are given in eq. (*62*).

Using $\alpha = 1.0$, as is done in all other plots, the peak is about $1.2 - 1.3$ times the value of the steady state current. With $\alpha = 5.0$, as shown in figure *60*, the factor is increased to almost 10. Since $I \propto \alpha^2$, a higher value leads to more electron excitations, which then results in a higher average current, as expected. We can also see a second, and even a third peak. The second peak also shows in other plots, but very weakly. A similar effect has already been discussed for the ladder structure, and here we consider the same reason to be the cause, i.e. two, or in case of the third (weakest)

51

peak three, photons excite one electron. For this, the peaks should be at values $\omega = 2.33, 3.5$, since those correspond to $U/2$ and $U/3$, and reading off the peak frequencies, we indeed get $\omega = 2.3, 3.5$.

We now show results for the values $t' = 0.1, 0.3, 0.5, 0.7$. The result for $t' = 0.1$ has already been shown in figure *56*.
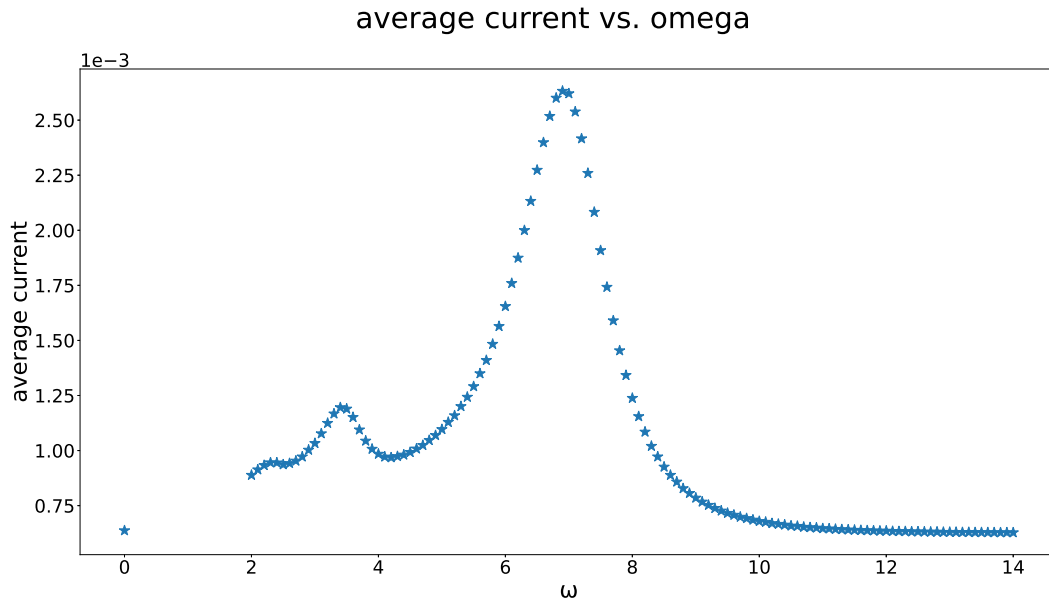

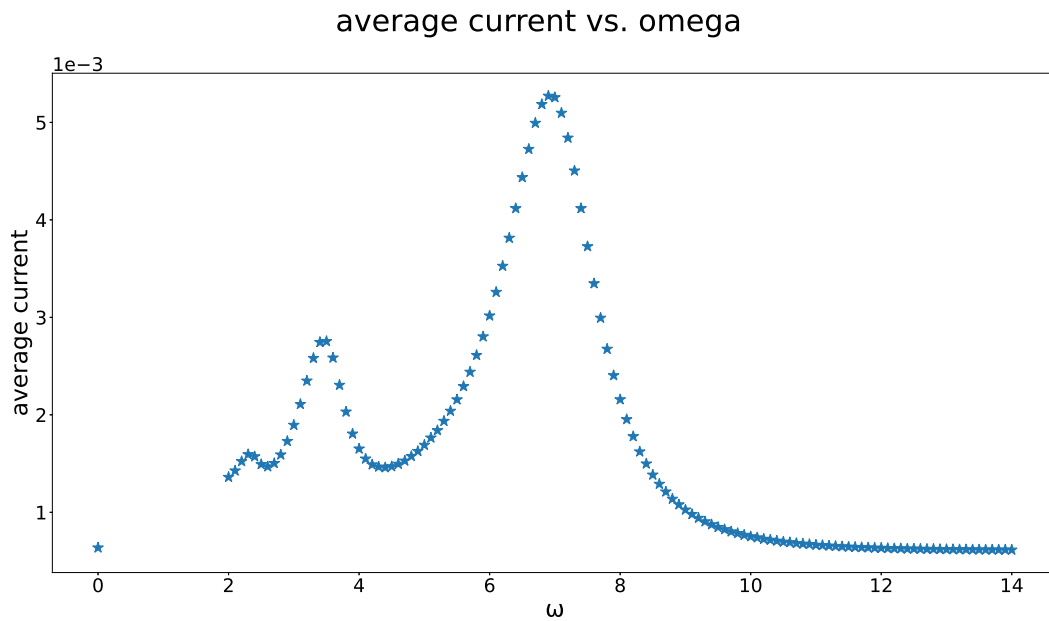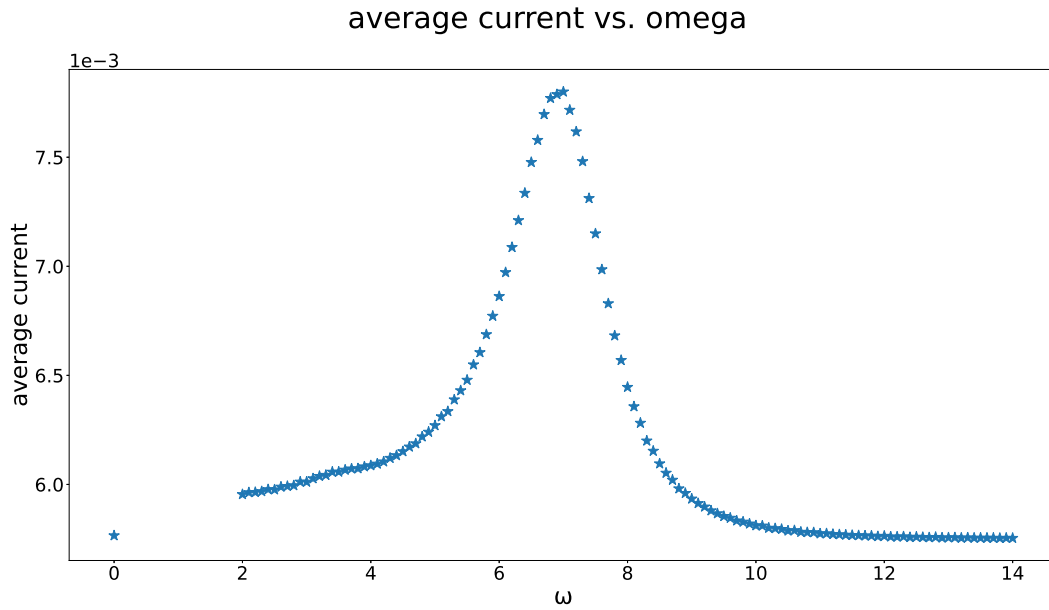Figure 61: Average current as a function of ω for $t' = 0.3$. All other parameters are given in eq. (*62*).
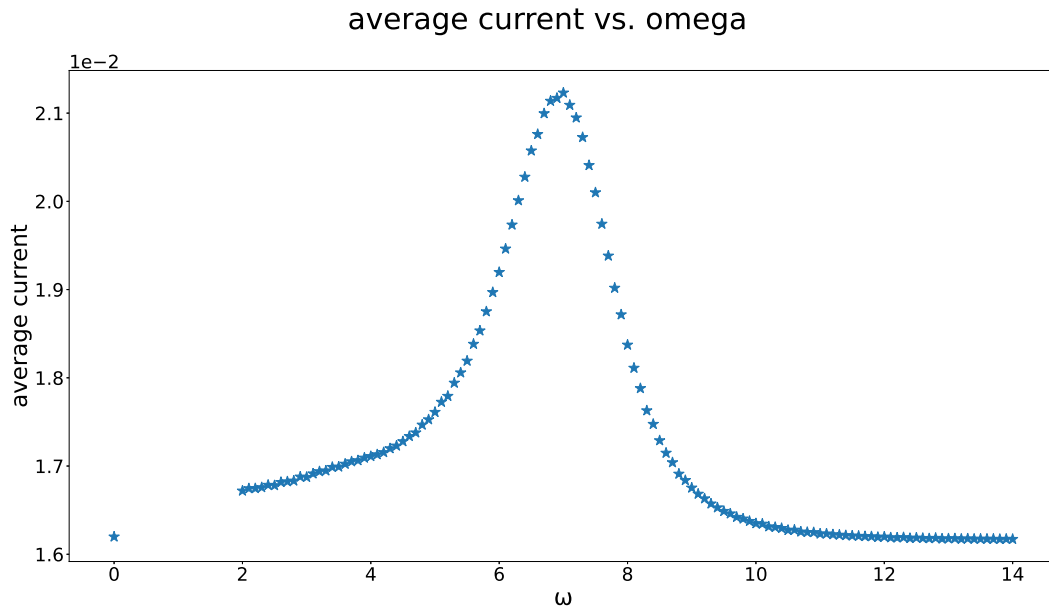
Figure 62: Average current as a function of ω for $t' = 0.5$. All other parameters are given in eq. (*62*).
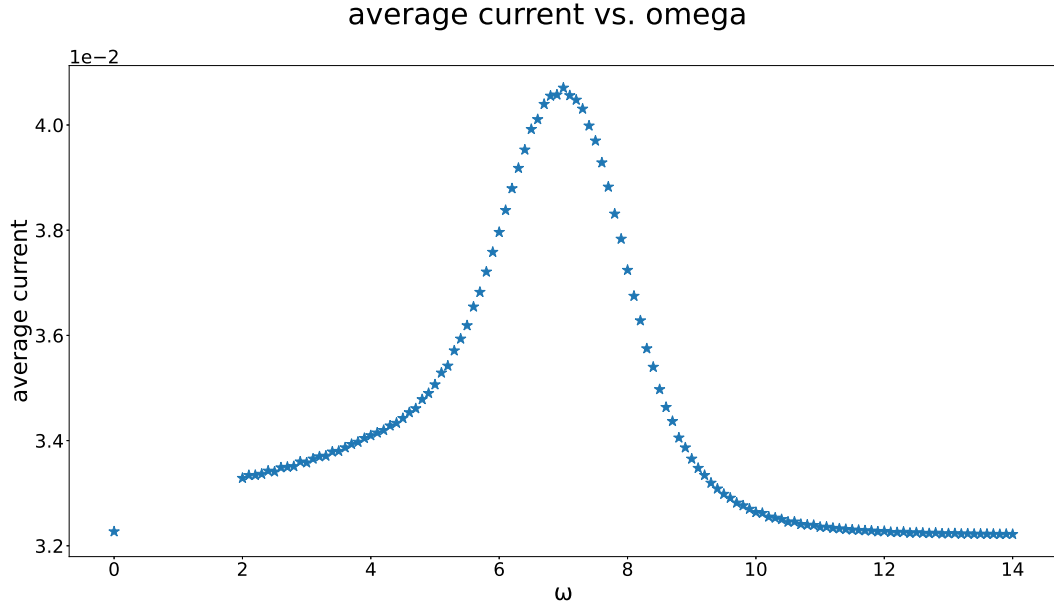
Figure 63: Average current as a function of ω for $t' = 0.7$. All other parameters are given in eq. (62).

In figure 54, we already showed that an increase of t' broadens the peaks of the spectral function. Hence, electrons from a wider energy range can be excited by the driving electric field. Therefore, this should also broaden the average current peak. To visualize this, we normalized and combined the plots for the different t' values in figure 64.
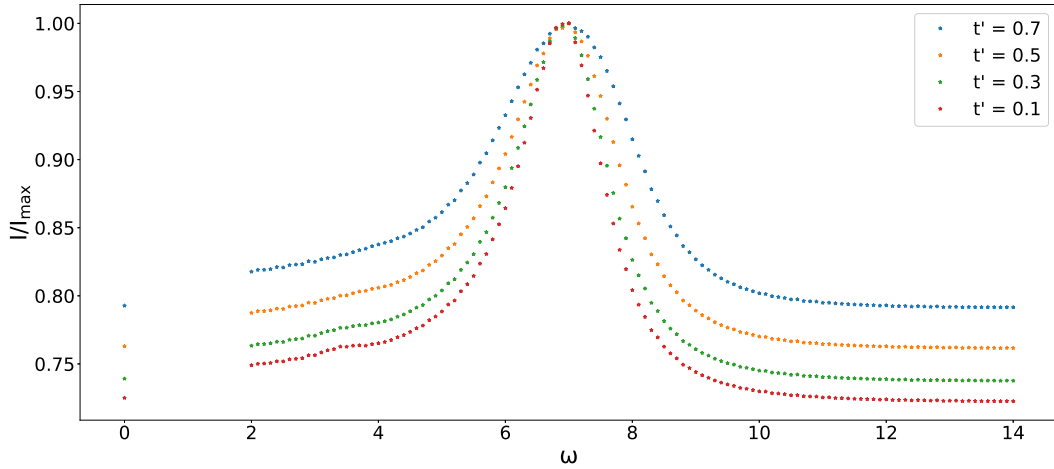
Figure 64: Comparison of all the average currents for different t' values.

We can see precisely the result we predicted. Additionally, the peaks become smaller compared to the respective steady state current, as t' increases. For small t' and $\omega = U$ we transfer electrons in a low energy state with high DOS value, to a high energy state with high DOS value. The more ω differs from U, the stronger the difference between the respective DOS values. For large t' this is similar as in the previous case, except that the largest absolute DOS values are smaller, and the DOS peaks are broader. This is interpreted such, that the more similar the DOS values of the initial, and the excited state of an electron are, the higher the average current, and the larger the highest absolute DOS values in case of $\omega = U$, the larger the peak current compared to the steady state.

53

Up to now we purely inserted particles on the left side, and removed them on the right side. Here we use non-zero values for the parameter responsible for the removal of particles on the left, and adding of particles on the right side, i.e. $\Gamma_1^{(1)}$. We now show results for the values $\Gamma_1^{(1)} = 0.0, 0.2, 0.4, 0.6, 0.8$. The result for $\Gamma_1^{(1)} = 0.0$ has already been shown in figure *56*.
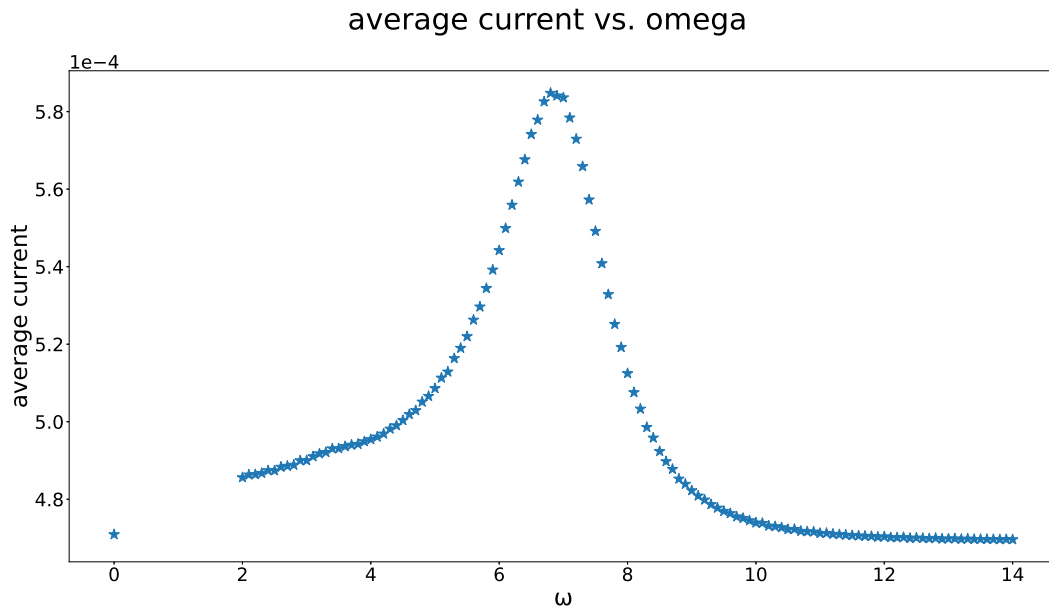
Figure 65: Average current as a function of ω for $\Gamma_1^{(1)} = 0.2$. All other parameters are given in eq. (*62*).
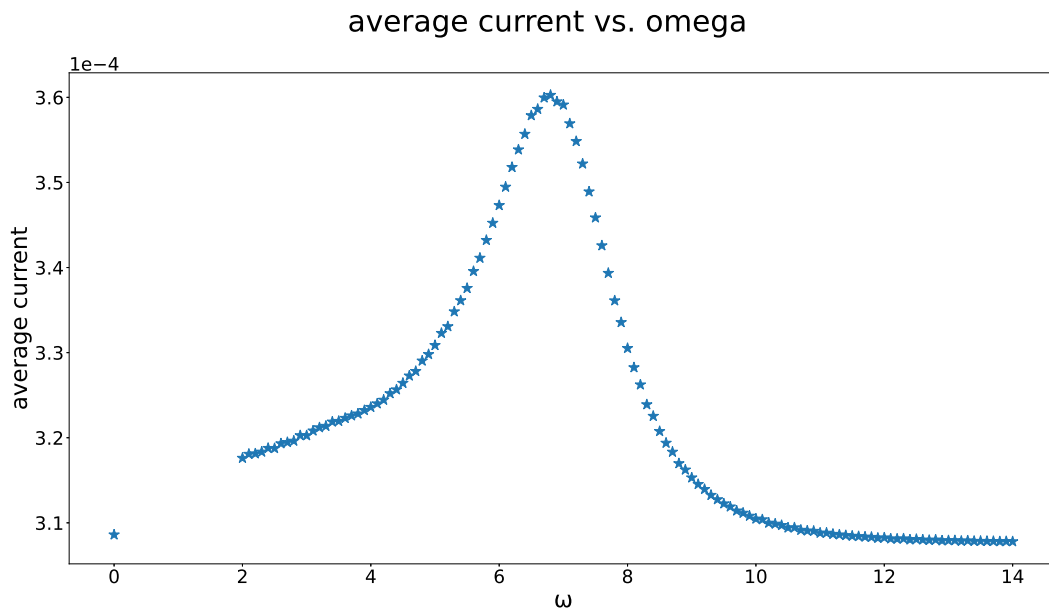
Figure 66: Average current as a function of ω for $\Gamma_1^{(1)} = 0.4$. All other parameters are given in eq. (*62*).
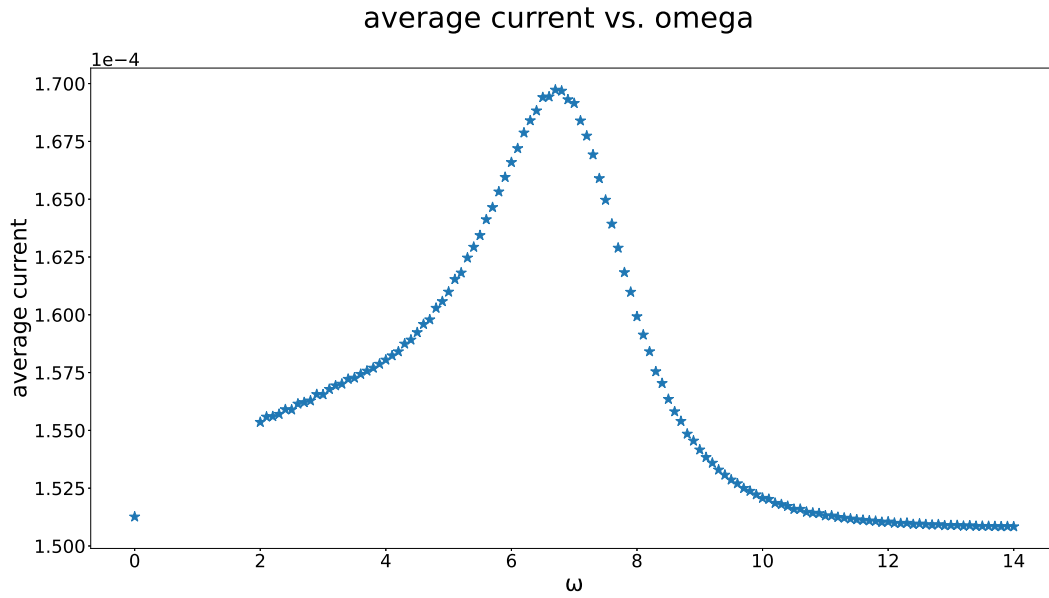
Figure 67: Average current as a function of ω for $\Gamma_1^{(1)} = 0.6$. All other parameters are given in eq. (62).
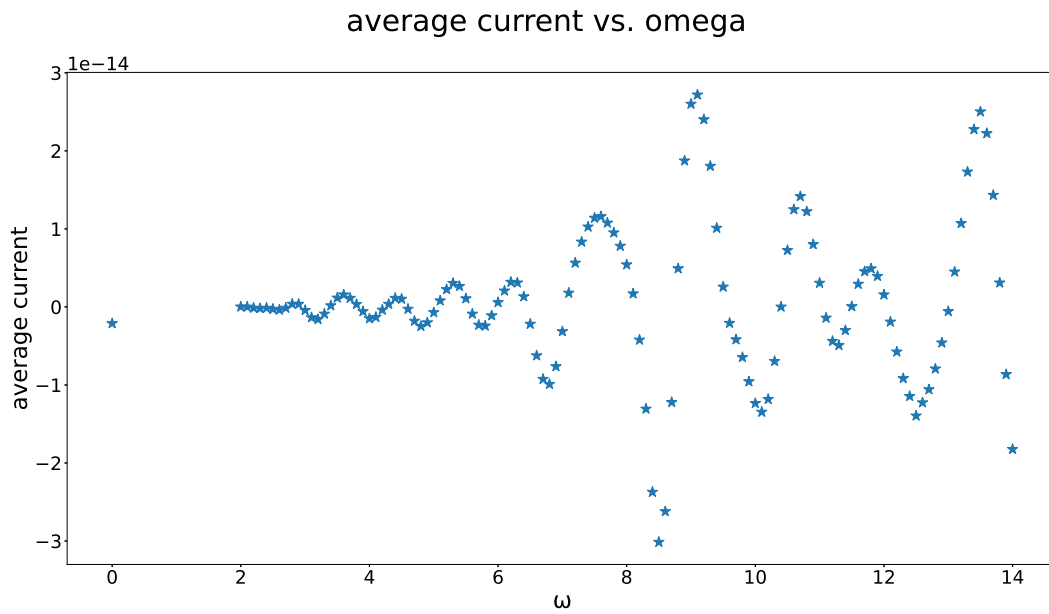
Figure 68: Average current as a function of ω for $\Gamma_1^{(1)} = 0.8$. All other parameters are given in eq. (62).

In order to see the dependence on $\Gamma_1^{(1)}$, we plot all the results in a single graph, as shown in 69. The steady state current, as well as the peak value, decrease, as $\Gamma_1^{(1)}$ increases, and at $\Gamma_1^{(1)} = 0.8$ the average current becomes zero, up to numerical fluctuations.

However, when looking more closely, which we can do by normalizing the plots, as is done in figure 70, we can see that the peaks decrease relatively stronger than the steady state currents.
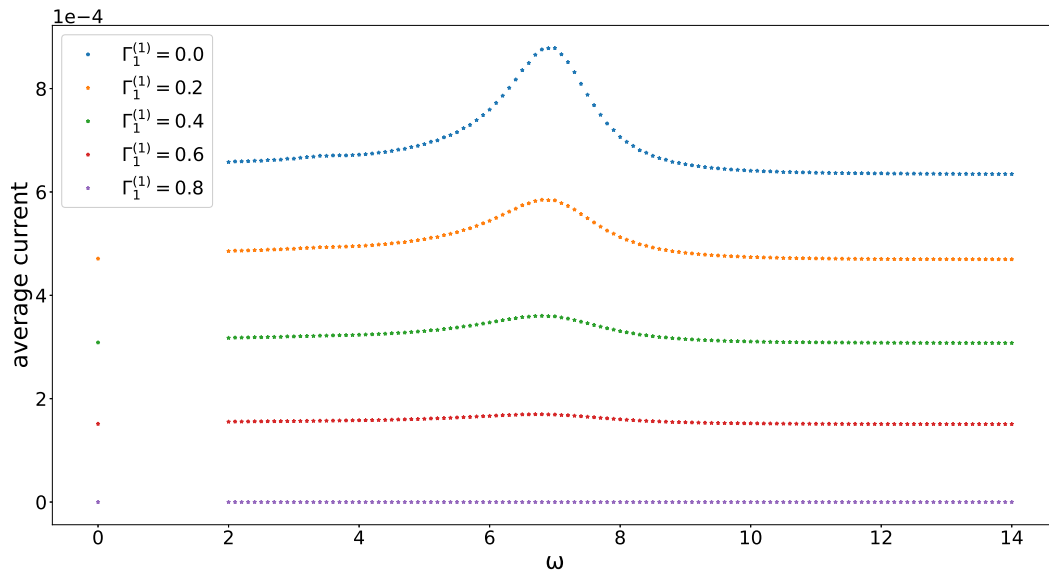
Figure 69: Comparison of all the average currents for different $\Gamma_1^{(1)}$ values.
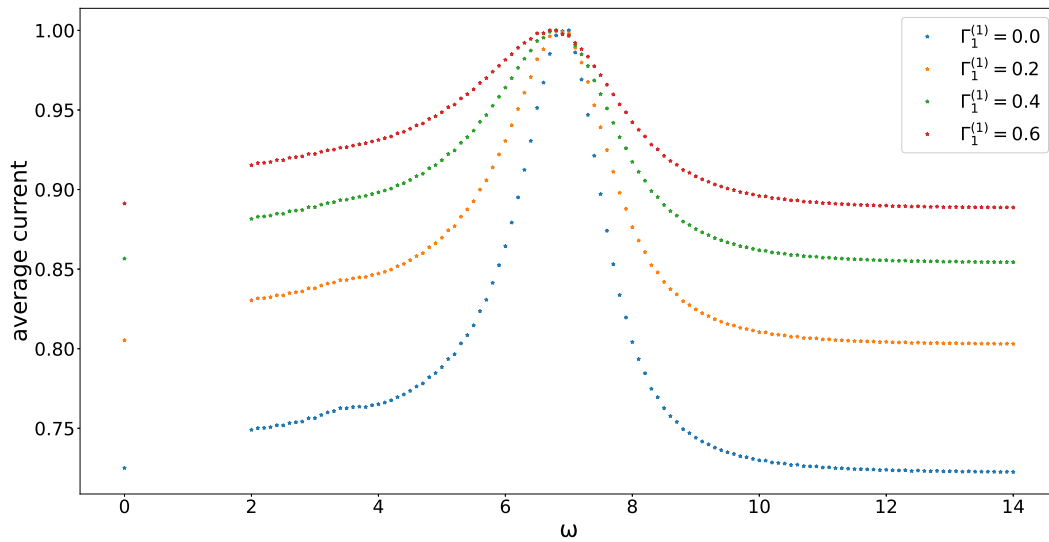
Figure 70: Normalized comparison of the results for all $\Gamma_1^{(1)}$ values.

Following a first intuition, we may want to look at the spectral functions for the cases of $\Gamma_1^{(1)} = 0.0$, and $\Gamma_1^{(1)} = 0.6$ [5], depicted in figure *71*.
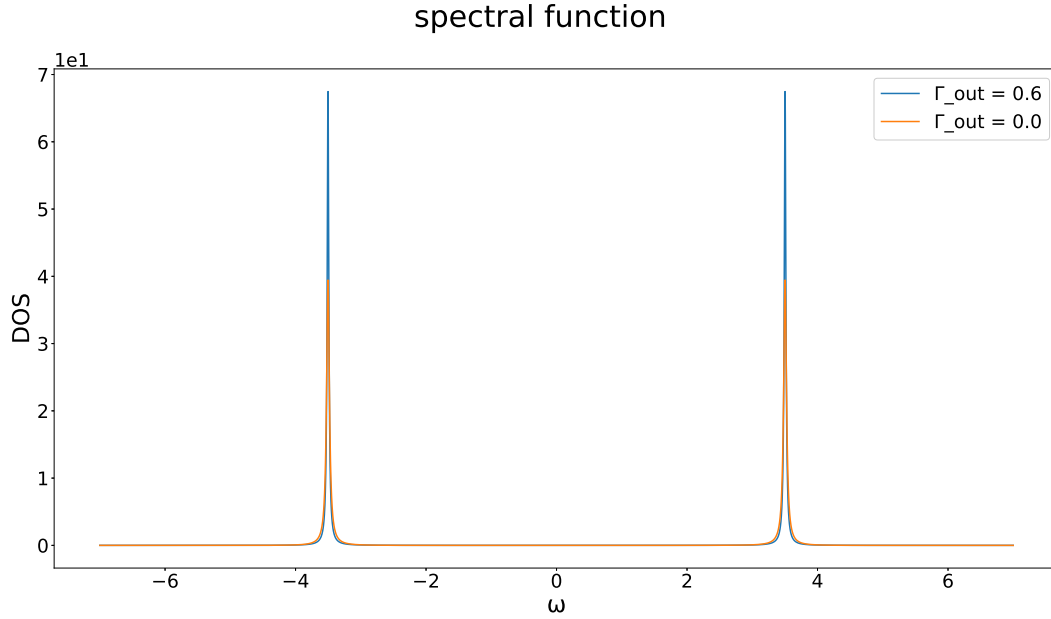
Figure 71: Spectral functions for $\Gamma_1^{(1)} = 0.0$, and $\Gamma_1^{(1)} = 0.6$.

Oddly, however, these would suggest the reverse behaviour, since the peaks become sharper as $\Gamma_1^{(1)}$ increases. Perhaps we can interpret this such, that the highest current we can get by optimal excitation frequency, is affected overproportionally by reducing the electrons introduced from the left lead. However, there is yet another interesting behaviour in figure *70*. For the setup with a central ladder structure, and the one with alternating hopping values in the center, we had a current flow even if there were equilibrium conditions at the environment connections. Here, on the other hand, we get zero for this setting, apart from numerical deviations. It would seem most straightforward, to blame this on the small size of our setup. To see if this is true, let us look at the result for a ladder chain[6], for which we depicted the general setup in figure *10*, with $structure = 1 - 1 - 1$, and $\Gamma_1^{(1)} = 0.0, 0.8$, and all other parameters as given in eq. (*58*). The result is depicted in figures *72*, and *73*.

---

[5]Since the current is zero for $\Gamma_1^{(1)} = 0.8$

[6]Which is in truth not really ladder like, since it only contains a single "rung".
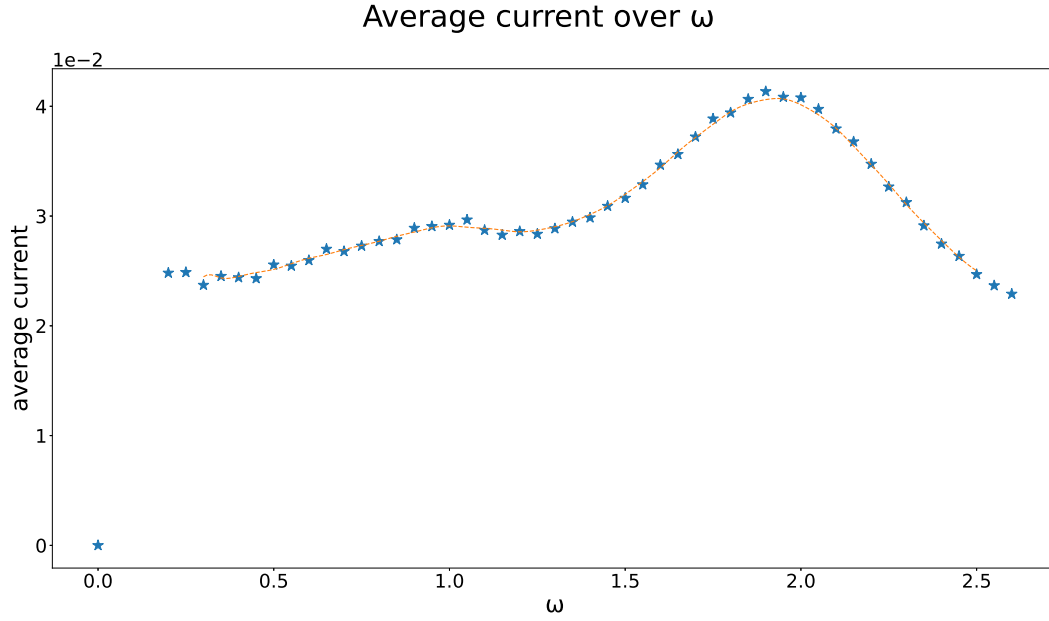
Figure 72: Average current as a function of ω for $structure = 1 - 1 - 1$, with $\Gamma_1^{(1)} = 0.0$. All other parameters are given in eq. (58).
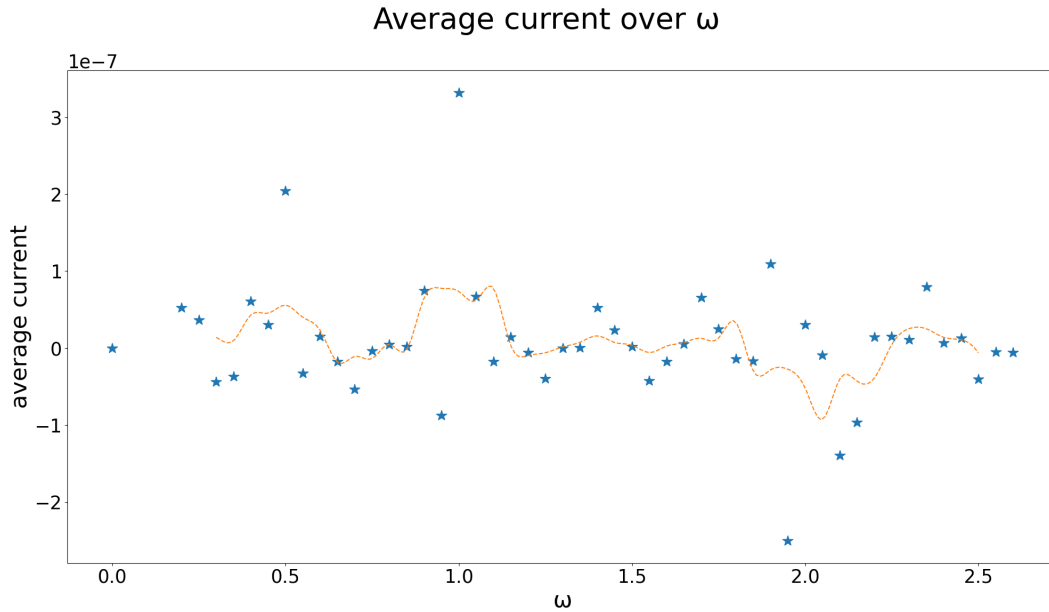
Figure 73: Average current as a function of ω for $structure = 1 - 1 - 1$, with $\Gamma_1^{(1)} = 0.8$. All other parameters are given in eq. (58).

We can see that the average current for $\Gamma_1^{(1)} = 0.8$, as shown in figure 73, is of an order that we interpret as numerically zero. This is the same result we got for the case with one interacting central site, for $\Gamma_1^{(1)} = 0.8$. This supports our initial idea, which makes the system size responsible. However, there are some additional questions we may ask. Is it the fault of the short leads or the short central part? What is the underlying reason in either case? To answer the first question, let us look at the average current plots for a system with a ladder structure in the center, with parameters $1 - 6 - 1$, and $4 - 1 - 4$, where all others are given in eq. (58). The results are shown in figures 74, and 76 respectively. The result for $1 - 6 - 1$ gives us negative values, which we cannot interpret in a sensible way. This tempts us to consider the reason to be non-physical. For the average current

of the $4-1-4$ system, however, we get results that are small enough that we can interpret them as zero. Therefore, this may have physical reasons related to the small size of the central part.
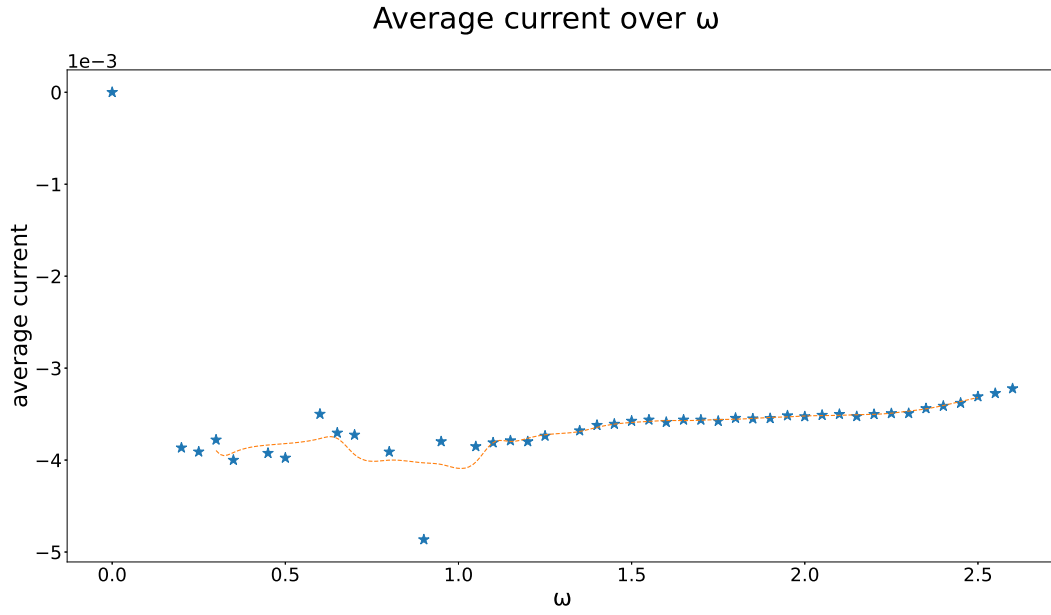
Figure 74: Average current as a function of ω for $structure = 1 - 6 - 1$. All other parameters are given in eq. (58).
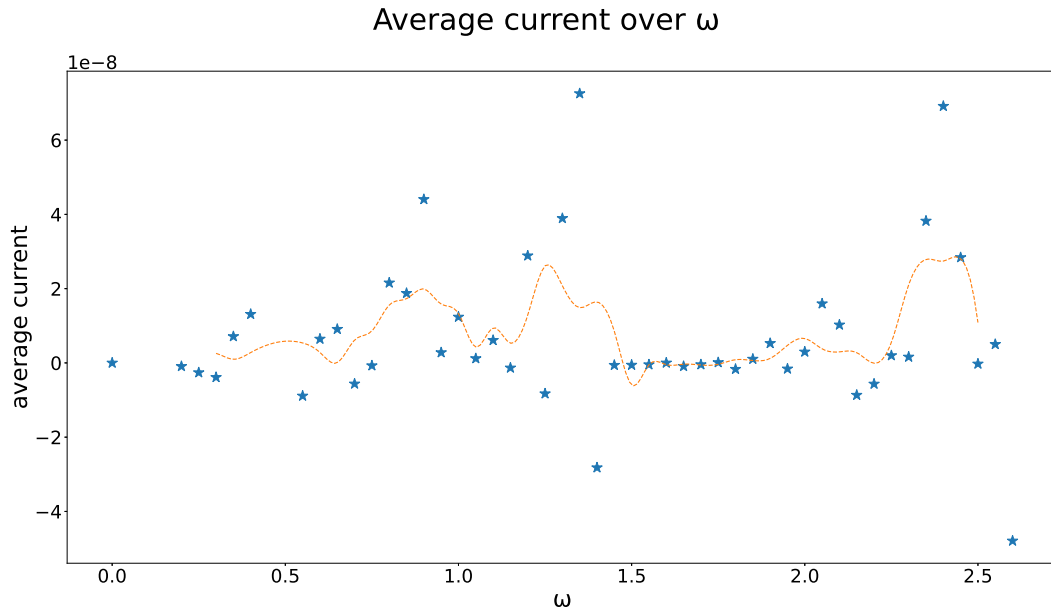
Figure 75: Average current as a function of ω for $structure = 4 - 1 - 4$. All other parameters are given in eq. (58).

Here, we will present some results for structures with five sites, but first we will look into the behaviour of the current as a function of time. Judging from the smoothness of the average current as a function of ω, we would again predict a small relative fluctuation of the moving average. Let us look into a setup with three interacting sites in the central system, with $\omega = 11.0$, and all other parameters as given in eq. (62).
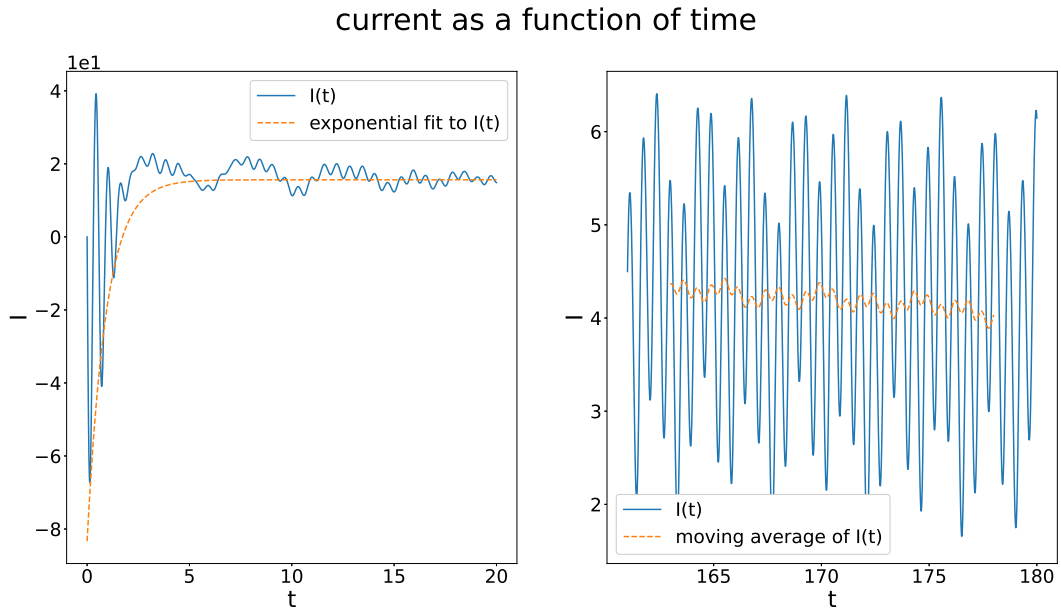
Figure 76: Current as a function of time for $structure = 1-3-1$, and $\omega = 11.0$. All other parameters are given in eq. (62).

Again we reach times far beyond the influential part of the transient, and the moving average shows the result we expected. It should be mentioned, that here we are not starting from a normalized state, therefore, we get an additional factor for our currents. This means we cannot compare the value of the currents with previous results.

The following setups have been simulated: $\{structure = 2 - 1 - 2, U = 5.0\}$, $\{structure = 2 - 1 - 2, U = 7.0\}$, $\{structure = 2 - 1 - 2, U = 7.0, \alpha = 3.0\}$, $\{structure = 2 - 1 - 2, U = 7.0, \alpha = 3.0, t' = 0.02\}$, $\{structure = 2 - 1 - 2, U = 9.0\}$, $\{structure = 1 - 3 - 1, U = 11.0\}$, $\{structure = 1 - 3 - 1, U = 11.0, \alpha = 3.0\}$.
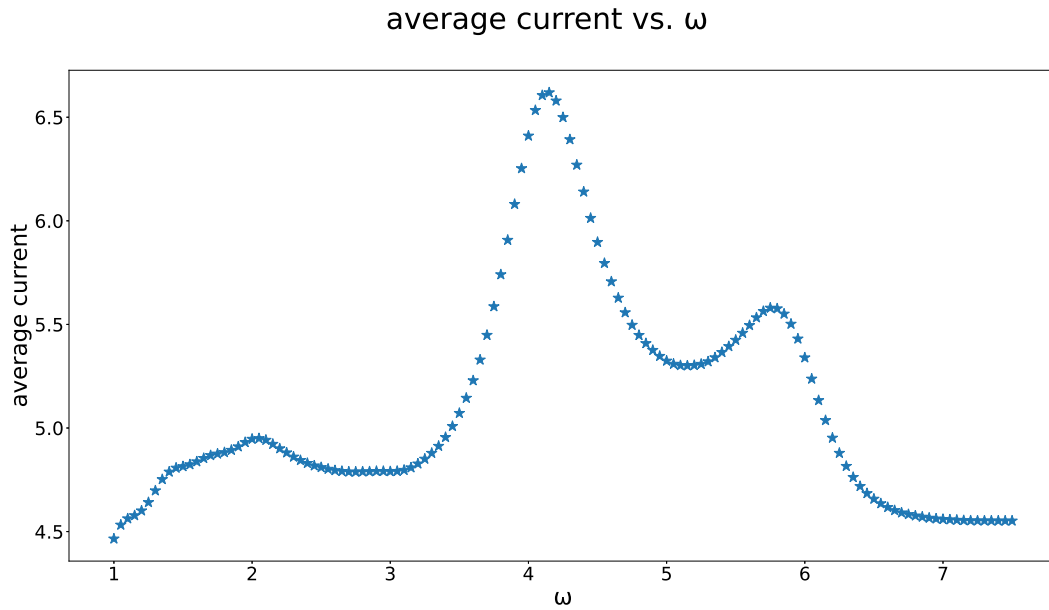
Figure 77: Average current as a function of ω for $structure = 2-1-2, U = 5.0$. All other parameters are given in eq. (62).
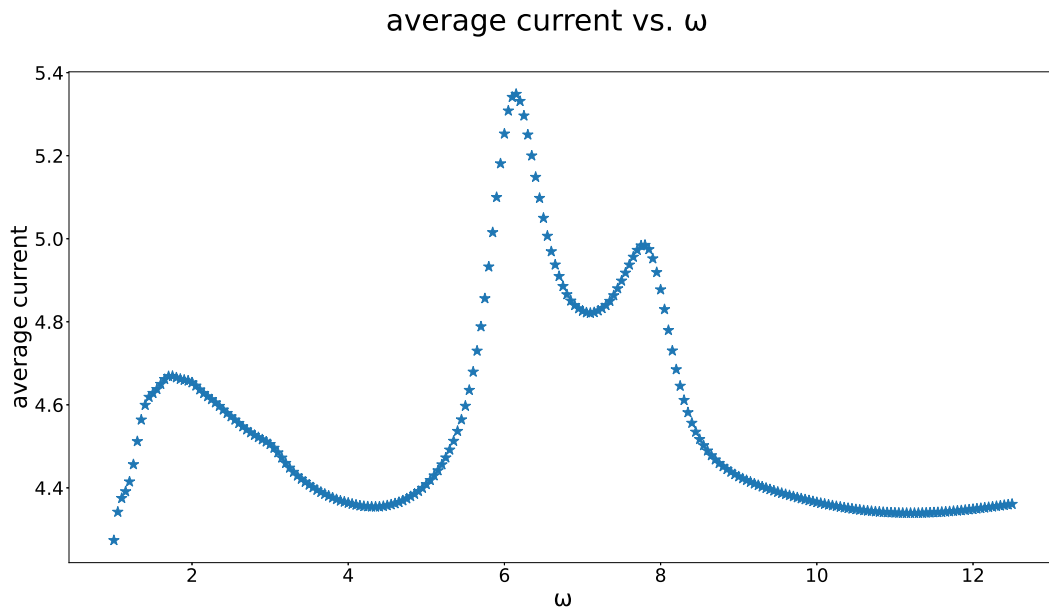
Figure 78: Average current as a function of ω for $structure = 2-1-2, U = 7.0$. All other parameters are given in eq. (62).
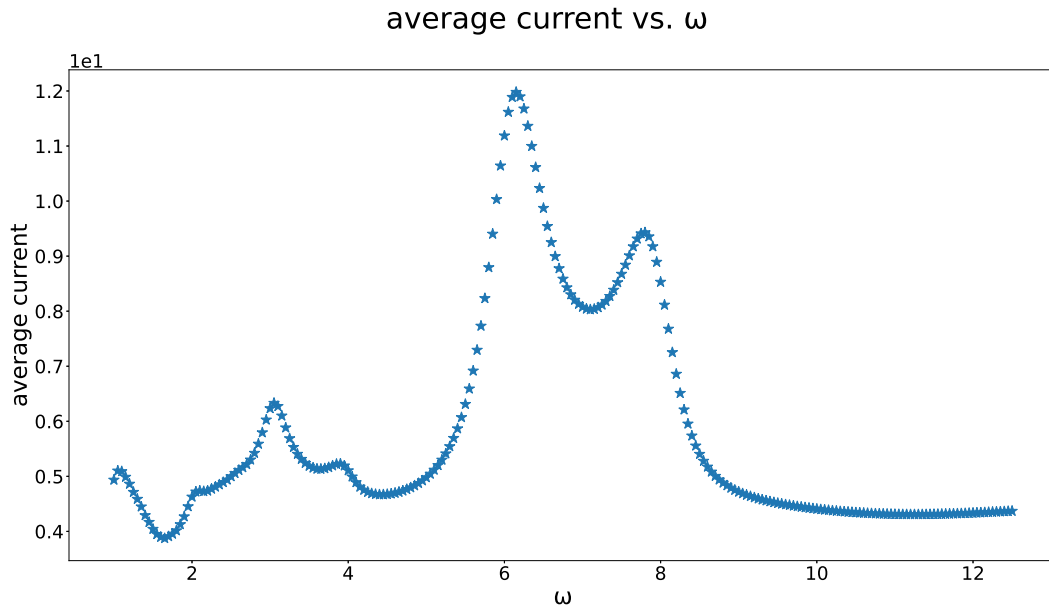
Figure 79: Average current as a function of ω for $structure = 2-1-2, U = 7.0, \alpha = 3.0$. All other parameters are given in eq. (62).
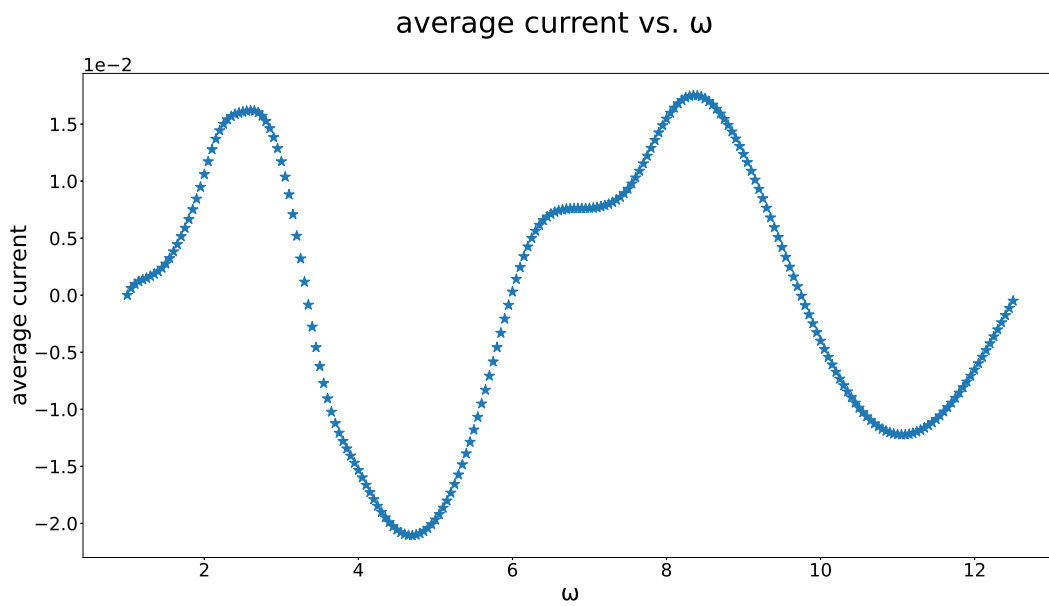
Figure 80: Average current as a function of ω for $structure = 2-1-2, U = 7.0, \alpha = 3.0, t' = 0.02$. All other parameters are given in eq. (62).

average current vs. ω
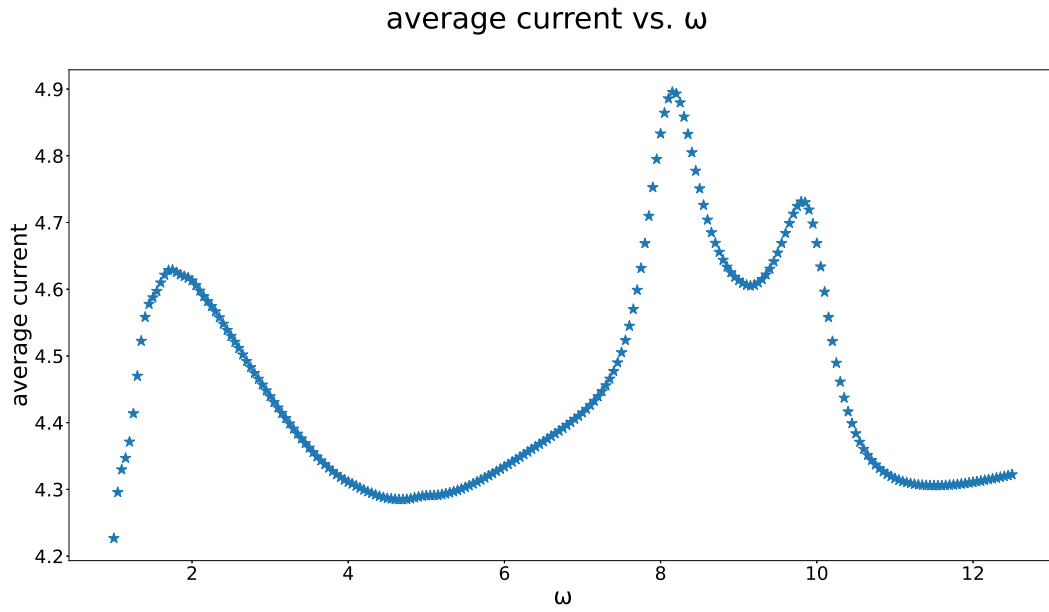
Figure 81: Average current as a function of ω for $structure = 2-1-2, U = 9.0$. All other parameters are given in eq. (62).

average current vs. ω
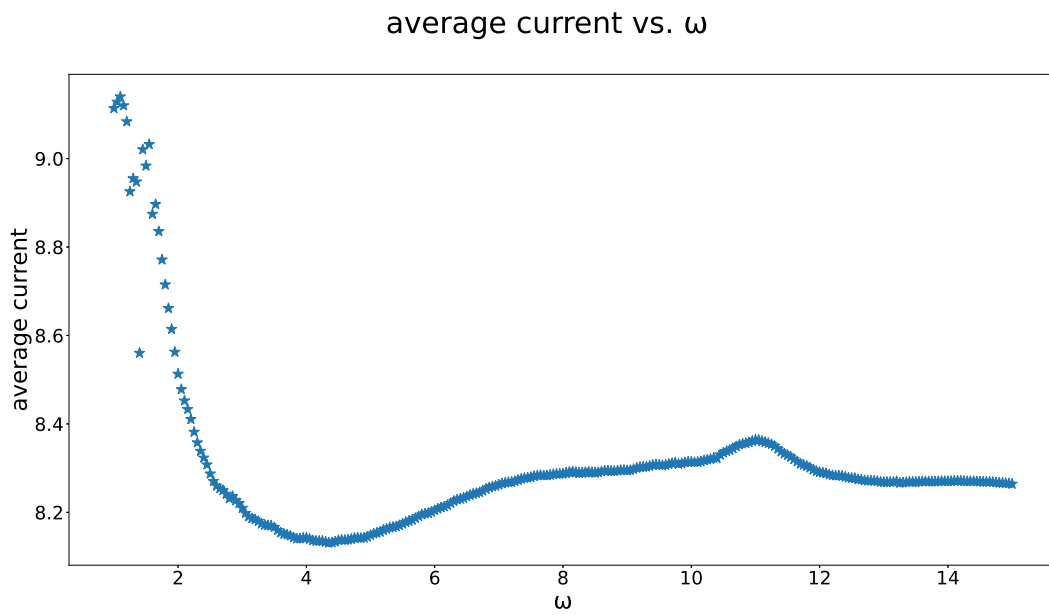
Figure 82: Average current as a function of ω for $structure = 1 - 3 - 1, U = 11.0$. All other parameters are given in eq. (62).
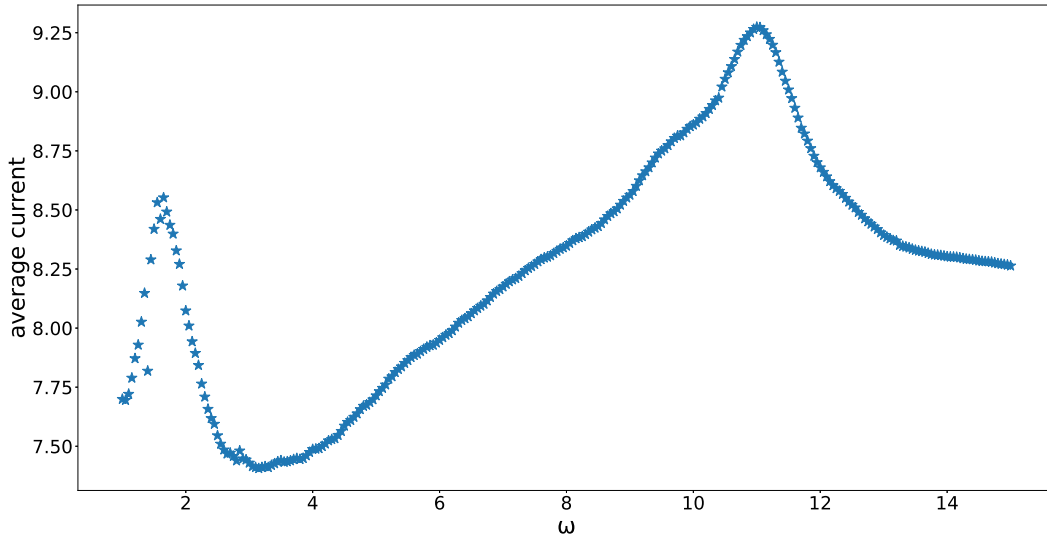
Figure 83: Average current as a function of ω for $structure = 1 - 3 - 1, U = 11.0, \alpha = 3.0$. All other parameters are given in eq. (62).

We can see that in all cases, in which we have two leads on each site, we get a double peak, with the first one more distinct than the second, and the minimum between the two precisely where we would expect the maximum in the three sites case. We could not find a way to obtain the spectral function here, because it would require calculating all the eigenvectors of matrices similarly large as the Lindbladian matrix, where we even failed to obtain the steady state eigenvector of that one. Therefore, we cannot use it to obtain more insight.

In figure 80 we showed the result for $t' = 0.02$, which gives a result with partially negative values, which does not make sense to us. The overall curve shape, however, is similar as in other $2 - 1 - 2$ structure plots, and we can also see that it looks more like having a single maxima rather than two. Perhaps this split into two peaks in the other $2 - 1 - 2$ structures comes from a split of the spectral function peaks, which is reduced by a smaller t' value.

For figures 82, and 83, in which we have three sites in the central part with interaction turned on, we have the peak at $\omega = 11.0$, as we would expect for a three-sites system. However, it is less symmetric than in the three-sites case, and also sharper on the very top.

An odd behaviour is the peak arising at $\omega = 2.0$, which shows up in almost all plots, for which no explanation has been found. It does not seem to be significantly influenced by intensity, as a comparison of figures 82, and 83 shows, and in case of figure 79 it seems to be completely gone.

In figure 79 we can, furthermore, see a smaller double peak at $\omega = 3.5$, which we again interpret as a double photon effect.

7   Conclusion

In this thesis we created two simulations for open quantum systems, which are based on the Lindblad equation. In chapter 5, we showed to a reasonable degree, that they can give accurate results within this framework. Also the results we got from the setups we simulated, implied that the simulations are working correctly.

For the ladder structure, the results always coincided with the rough expectations we obtained from the infinitely large system, which is a maximum at $\omega = 2.0 \cdot t$. For the structure in which we used alternating hopping values in the central part we got some results where we could see an increase up to $\omega = 1.5 \cdot t$, and a rather constant average current afterwards, as we anticipated. However, there were also many examples that showed clear deviation from this behaviour. Our investigations of the current as a function of time suggested that numerical artifacts are one of the possible reasons. We are solving huge systems of differential equations, and since this is done numerically, errors are expected to occur, therefore this did not come as a surprise. We, however, also saw that this was likely not the only reason. The latter remark especially refers to the setups in which we used the larger hopping value on the boundary of the central system.

In the last part of the thesis we studied systems with electron-electron interaction, which are the most interesting and challenging ones. In this case we always obtained a very smooth plot of the average current vs. frequency. All of them showed a peak, or in the case of five sites a minimum in between a double-peak, at a frequency of the order of the interaction U. where we had $\omega = U$. At least for the case of three sites, this is what is expected from the spectral function.

These observations again show that the simulation is working correctly. Let us discuss some of the more intriguing outcomes of our calculation. One of these are the maxima we could see at smaller ω values in the ladder structure, and much more clearly for the structure with three sites, in which we had interacting electrons. They appeared at precisely the half, or a third of the main maximum, and, furthermore, increased with the intensity of the light. These observations suggest the existence of two, or three photon effects. I.e. several photons are transferring their energy to an electron simultaneously, giving it enough energy to become excited into the upper band, even at frequencies far below the band gap. It should be mentioned, that this effect is only expected to occur, if the interaction of the photons with the electrons is very strong.

Another interesting result we could obtain for the behaviour of the current for the case of five sites, with interaction in the three or single central site/s. In this case however, we observe a double peak instead of a single one, when we used two sites as leads, instead of one, which attribute to a split in the spectral function. This is, however, only a speculation.

In one configuration for the structure with alternating hopping values in the central sites, we could show that we can also obtain a an average current from the left to the right lead due to electron excitations, if we use Γ values that lead to a reverse current in the steady state case. Furthermore, we could see a small indication of a decline of the average current in this same structure between $\omega = 1.5 \cdot t$, and $\omega = 2.5 \cdot t$, which we interpreted as the result of a decline of the state density.

To summarize, we obtained some interesting results we could interpret, but there are still open questions, and further things that should be analysed more in detail.

A   Code description

The code has been written in the programming language Julia. It should be mentioned, however, that this was not the first choice. Initially Python has been used, at some point the code has been translated to Julia, and the speed advantage purely from switching was a factor of approximately five. Using multi threading in for-loops, again increased the speed significantly, especially for longer calculations. For the latter case, the gain in speed has not been assessed, but comparing full processor usage to that of a single core gives an estimate.

A.1   Exact Diagonalization of the many body density-matrix

We already discussed the basis we are using in chapter *4.3.1*. Our way of representing these states in the simulation, is in terms of a string. It contains $n_{sites} \cdot 4$ zeros, or ones, where a zero means empty, and a one means occupied.
The first and second entry refer to the first site, third and fourth to the second, and so on. For each such pair the left entry stands for spin up and the right one for spin down. It seemed convenient to, in some sense, separate the normal, and the tilde space, which is why each state consists of two separate strings. Equation (*63*) gives an example for the representation of a state in our program, and figure *1* visualizes this precise state.

$$[[\underbrace{["011001"]}_{\text{normal space}}, \underbrace{["101110"]}_{\text{tilde space}}]] \tag{63}$$

In the code presented, there will be variables containing the name "phase". These just contain the appropriate phase factors for each expression, which come from swapping operators, and from the tilde space. Partially this has been discussed in section *4.2.2*. We have, however, not mentioned in this chapter phase factors obtained from applying two operators with different indices, which we will need here, and, therefore, we will briefly discuss them. Eq. (*64*) shows the mentioned setup:

$$c_i^\dagger c_j \left| 101...\underbrace{1}_{j}...\underbrace{0}_{i}...001 \right\rangle = c_i^\dagger c_j c_1^\dagger c_3^\dagger...c_j^\dagger...c_{\text{end}}^\dagger |0\rangle \tag{64}$$

We have to bring the operators to their appropriate position. Up to position j, both are swapped with the same amount of operators, which means we get a factor of $(-1)^{2n} = 1$, with n an integer. Afterwards, however, we only get contributions from $c_i^\dagger$. This means that we get a factor of $(-1)^m$, where m is just the number of operators between position j, and i. Here we did not explicitly show the case in which one operator is from the normal, and the other from the tilde space, but the procedure is the exact same.

We start with the discussion of the code with the basis states, as shown in listing *1*, since they are the foundation of our program. In lines 4 to 8, we create the basis states of the normal space. The `for` loop runs through all the numbers from one to the total numbers of states in the normal space. These numbers are then converted to their binary representation, and saved in the list `basis_states_s`. In the 10th line a predefined function is used, that gives all permutations of the two lists of strings. In our case, each list of strings corresponds to all the basis states for the normal space. Therefore, what we are doing here is creating the full basis for the normal-plus-tilde space. For all our purposes we are only interested in a subspace in which $n - \tilde{n}$ is conserved. That is the reason why, in the expression starting in line 13, we remove all states for which the condition $n - \tilde{n} =$ `particle_number_d/u` is not fulfilled. `_d` stands for spin down, and `_u` for spin up, and for each spin state this conservation applies individually, since also spin is conserved.

Listing 1: Function to obtain the basis states..

```julia
function get_basis_states(sites, particle_number_d, particle_number_u)
    basis_states = []

    for i in 1:2^(2*sites)
        bin_temp = string(i-1, base=2)
        bin_temp = "0"^(2*sites - length(bin_temp)) * bin_temp[1:end]
        append!(basis_states, [bin_temp])
    end

    temp = Iterators.product(basis_states, basis_states)
    basis_states_s = [i for i in temp]

    basis_states_s = [x for x in basis_states_s if
    sum([parse(Int, y) for y in x[1][1:2:end]]) -
    sum([parse(Int, y) for y in x[2][1:2:end]]) == particle_number_d &&
    sum([parse(Int, y) for y in x[1][2:2:end]]) -
    sum([parse(Int, y) for y in x[2][2:2:end]]) == particle_number_u]

    return basis_states_s
end
```

Since the creation and annihilation operators are essential to get the Lindbladian, we will discuss them next. In line one of listing *2*, we see the two arguments our function needs. For one the position, and for another the state. However, not the whole state, but just either the part in normal or in tilde space. Then in line 7, we get the character at position `position` of the string `state`, convert it to an integer, add one and save this integer on `state_temp_create`. We must, of course, check if by increasing the particle number we already exceed one, which is done in lines 9 to 11. If so, then the state is annihilated, and we return the value `nothing`. Otherwise, we just change the appropriate position of the string to `'1'`, and return this state. We also have to take into account the cases in which we apply two or more operators on a state, and a previous creation operator already annihilated the state. This is done in lines 3 to 5, where we check if the state has the value `nothing`. Since the procedure for the creation operator is a similar one, we will not discuss its code.

Listing 2: Function corresponding to the creation operator..

```julia
function create(position, state)

    if state == nothing
        return nothing
    end

    state_temp_create = parse(Int, state[position]) + 1

    if state_temp_create == 2
        return nothing

    else
        state = collect(state)
        state[position] = '1'
        state = join(state)
    end
    return state
end
```

The creation of the Lindbladian contains several steps, therefore, the respective code has been split into three pieces. All the parts shown are within a loop, running over all the ket basis states. We start with the part that takes into account the on-site energy, and the electron-electron interaction on each site, shown in listing *3*. Here contributions can only occur on the diagonal, which means we do not need to find the position, we only have to calculate the energy value. To do this, we have to sum over all the on-site energies of the sites that are occupied by the respective state. This is done in lines 1 and 3, for the normal and tilde space respectively. The electron-electron interaction is dealt with in lines 6 to 15. Here we only add a contribution, if both spin states of a site are occupied, and we must check this for each site, which is the reason for the `for`-loop. Again, we separately take into account the contribution of the tilde, and normal space. [7]

---

[7]In Julia arrays starts from 1, which is the reason for the 2- 1, which may be counter intuitive coming from other languages.

Listing 3: Lindblad operator 1/3, on-site energy, and interaction of electrons with each other.

```
1   L_s[i,i] += -1im*sum(e[broadcast(x -> parse(Int, x) == 1,
2   [y for y in basis_states_s[i][1]])])
3   L_s[i,i] += 1im*sum(e[broadcast(x -> parse(Int, x) == 1,
4   [y for y in basis_states_s[i][2]])])
5
6   for k in 1:sites
7
8       if create(2*k - 1, ann(2*k - 1, create(2*k, ann(2*k,basis_states_s[i][1]))))
9       != nothing && (U_site == k || U_site == 0)
10          L_s[i,i] += - 1im*U
11      end
12
13      if create(2*k - 1, ann(2*k - 1, create(2*k, ann(2*k,basis_states_s[i][2]))))
14      != nothing && (U_site == k || U_site == 0)
15          L_s[i,i] += + 1im*U
16      end
17  end
```

As a next step, we take into account the hopping between sites, which is presented in listing *4*. The loop runs over the number of sites minus one, since hopping can only occur between neighbouring sites. `L_s` is given to the function `get_L_s_coupling` to add the contributions from hopping between sites.[8]

Listing 4: Lindblad operator 2/3, hopping between sites.

```
1   for k in 1:sites-1
2       get_L_s_coupling(basis_states_s[i][1], basis_states_s[i][2], k, t, L_s, i)
3   end
```

We will now consider the subfunction `get_L_s_coupling`, shown in listing *5*. In lines 3 to 6, we give the possibility to change the coupling constant between the central, and the two outermost sites. In lines 9 to 12, we show an exemplary `if` condition of this function. Since all of them work similarly, it is sufficient to explain a single one. Every possible hopping to a neighbouring site, gives a contribution of `t` or `t_prime`. Each single `if` condition checks this for two neighbouring sites, where `k` determines which those are, for one specific spin, space, and direction. Therefore, the `for` loop in the main code again runs over the number of sites minus one, to take into account all possible contributions. Inside the `if` condition, we have to look for the matrix position of the bra corresponding to the new ket state, which is done by the predefined function `findall`.

Listing 5: Subfunction to include hopping between sites.

```
1   function get_L_s_coupling(state_x, state_x_t, k, t, L_s, i)
2
3       if  k == sites - 1 || k == 1
4           t_temp = t_prime
5       else
6           t_temp = t
7       end
8
9       if (create(2*k+1, ann(2*k-1, state_x)), state_x_t) in basis_states_s
10          L_s[i, findall(x -> x ==  (create(2*k+1, ann(2*k-1, state_x))
11          , state_x_t), basis_states_s)]
12          .+= -1im*t_temp * (-1)^parse(Int, state_x[2*k])
13      end
```

Up to now we dealt with L_H, now we consider the contributions of L_D. This is done in listing *6*. The most general description of the constants that describe the coupling with the environment, is via a matrix which contains $n_{\text{sites}} \cdot n_{\text{sites}}$ entries (for each spin state), the so called Γ matrices, which must also be Hermitian and positive semidefinite[*19*, p.4]. All the `if` conditions appearing in this expression, only serve the purpose of skipping over parts to speed up the code. The individual terms again perform similar tasks, just for different cases. One of those is again the spin, and the other is, if particles are incoming (described by `gam_in_down/up`) or outgoing (described by `gam_out_down/up`). Again we pass `L_s` by reference.

---

[8]In julia, all variables given to a function are called by reference.

Listing 6: Lindblad operator 3/3, interaction with the environment.

```
1   for l in 1:sites
2       for k in 1:sites
3
4           if gam_in_up[k, l] == 0 && gam_in_down[k, l] == 0 && gam_out_up[k, l]
5           == 0 && gam_out_down[k, l] == 0
6               continue
7           end
8
9           if gam_in_up[k, l] != 0
10              get_gam_2(k, l, gam_in_up[k, l],basis_states_s[i][1]
11              , basis_states_s[i][2], phase_up_in, 0, L_inflow, L_s, i)
12          end
13
14          if gam_in_down[k, l] != 0
15              get_gam_2(k, l, gam_in_down[k, l],basis_states_s[i][1]
16              ,  basis_states_s[i][2], phase_down_in, 1,  L_inflow, L_s, i)
17          end
18
19          if gam_out_up[k, l] != 0
20              get_gam_1(k, l, gam_out_up[k, l],basis_states_s[i][1]
21              , basis_states_s[i][2], phase_up_out, 0, L_outflow, L_s, i)
22          end
23
24          if gam_out_down[k, l] != 0
25              get_gam_1(k, l, gam_out_down[k, l],basis_states_s[i][1]
26              , basis_states_s[i][2], phase_down_out, 1, L_outflow, L_s, i)
27          end
28      end
29  end
```

In the next code snippet, listing 7, we exemplary discuss the function `get_gam_2`[9] used in listing 6. From eq. (38), one can see that the dissipative part of our Lindblad operator multiplied by $\Gamma^{(2)}$, has three operator terms. Here this corresponds to the three if-conditions in the lines 3 to 28. In each one, the corresponding creation, or annihilation operators are applied to the normal or tilde (ket) state. Then we have to search for the corresponding bra, i.e. we need to find the appropriate position for the entry in the matrix. The matrix `L_inflow`, is the one we use to obtain the current inflow from the outside, and it is calculated precisely as described in section 4.3.3.

Listing 7: Subfunction for including interaction with the environment..

```
1   function get_gam_2(k, l, gam_in, state_x, state_x_t, phase, spin, L_inflow, L_s, i)
2
3       if (create(2*k  -  spin, state_x), create(2*l  -  spin, state_x_t))
4       in basis_states_s
5           L_s[i, findall(x -> x == (create(2*k  -  spin, state_x),
6           create(2*l  -  spin, state_x_t)), basis_states_s)] .+= -2im*gam_in*phase
7           L_inflow[i, findall(x -> x == (create(2*k  -  spin, state_x),
8           create(2*l  -  spin, state_x_t)), basis_states_s)] .+= -2im*gam_in*phase
9       end
10
11      if (ann(2*l  -  spin, create(2*k  -  spin, state_x)), state_x_t)
12      in basis_states_s
13          L_s[i, findall(x -> x == (ann(2*l  -  spin, create(2*k  -  spin, state_x))
14          , state_x_t), basis_states_s)] .+= -gam_in*off_diag_phase
15          L_inflow[i, findall(x -> x == (ann(2*l  -  spin
16          , create(2*k  -  spin, state_x)), state_x_t), basis_states_s)]
17          .+= -gam_in*off_diag_phase
18      end
19
20      if (state_x, ann(2*k  -  spin, create(2*l  -  spin, state_x_t)))
21      in basis_states_s
22          L_s[i, findall(x -> x == (state_x, ann(2*k  -  spin
23          , create(2*l  -  spin, state_x_t))), basis_states_s)]
24          .+= -gam_in*off_diag_phase_t
25          L_inflow[i, findall(x -> x == (state_x, ann(2*k  -  spin
26          , create(2*l  -  spin, state_x_t))), basis_states_s)]
27          .+= -gam_in*off_diag_phase_t
28      end
29  end
```

---

[9] Which works similar as `get_gam_1`, therefore, we again will only discuss one of them.

Listing *8* shows the current operators, which we need to obtain the current between sites. For each site, we calculate two operators, one for the current to/from the right, and one for the current to/from the left site. Those are saved in the arrays of matrices `I_right`, and `I_left`, which are given to the functions `get_I_left`, and `get_I_right` respectively. These subfunctions work as the one described in listing *5*, therefore, we will not repeat this discussion.

Listing 8: Subfunction to compute the current operators..

```
1  for o in 1:sites-1
2      get_I_left(basis_states_s[i][1], basis_states_s[i][2], o, o+1, t, I_left, i)
3
4      get_I_right(basis_states_s[i][1], basis_states_s[i][2], o, o, t, I_right, i)
5  end
```

Having obtained the Lindblad matrix, it is now possible to calculate the steady state, i.e. the state fulfilling $L \left| \rho_\infty \right\rangle = 0$, as is done in listing *9*. Therefore, what we want is the state with eigenvalue zero. First we have to calculate the eigenvalues, and eigenvectors, but this can be done using the predefined functions in lines 1 and 2. The corresponding eigenvalues and -vectors are saved at the same place in the arrays `eig_val`, and `eig_vect`, i.e. the eigenvector `eig_vect[:,i]` has eigenvalue `eig_val[i]`. This means we have to search for the smallest eigenvalue, in absolute value, as is done in line 6, and then we know the position of the relevant eigenstate. Eventually, in line 10, the steady state is normalized to its corresponding left eigenvector, the left vacuum, where `vac_left' · steady_state` is the inner product of the left vacuum, and the steady state. The variable `stationary` will be relevant in listing *12*.

Listing 9: Function to obtain the normalized steady state.

```
1      eig_val = eigvals(L_s)
2      eig_vect = eigvecs(L_s)
3
4      stationary = [x for x in eig_val if abs(real(x)) < 1 * 10^{-5}]
5
6      steady_state_pos = findall(x -> x == minimum(broadcast(abs, eig_val))
7      , broadcast(abs, eig_val))
8
9      steady_state = eig_vect[:, steady_state_pos]
10
11     steady_state = steady_state / (vac_left' * steady_state)
```

At this point, it is possible to calculate physical quantities, as discussed in section *4.3.3*. This is done in listing *10*. Since the Lindbladian does not contain any contributions that are spin specific, all quantities we calculate must be equal for both spin orientations. However, in cases in which it poses no additional effort, the calculation has been performed for both cases, since it offers an easy way to double check that the code works correct in that regard.

Listing 10: Function to calculate the occupation probability, and the electron current

```
1  for i in 1:sites
2      n_up[i] = vac_left' * N(steady_state, basis_states_s, 2*i - 1)
3      n_down[i] = vac_left' * N(steady_state, basis_states_s, 2*i)
4
5      n_up_t[i] = vac_left' * N_t(steady_state, basis_states_s, 2*i - 1)
6      n_down_t[i] = vac_left' * N_t(steady_state, basis_states_s, 2*i)
7  end
8
9  for i in 1:sites
10
11     inflow[i] = vac_left' *
12     N((L_inflow * steady_state), basis_states_s, 2*i) * 2
13     outflow[i] = vac_left' *
14     N((L_outflow * steady_state), basis_states_s, 2*i) * 2
15
16     right[i] = vac_left' * (J_right[:,:,i] * steady_state)
17     left[i] = vac_left' * (J_left[:,:,i] * steady_state)
18 end
```

Let us briefly discuss the function N, which corresponds to the number operator, and which is used in listing *10*. Listing *11* shows this function. The steady state consists of a superposition of many particle states. The number operator, in the basis we chose, must check for each state in this superposition, if a certain site, and spin combination is occupied. Therefore, we go through all the states in the relevant subspace of the superfermion basis, and apply the annihilation and then the creation operator. If the state survives, the respective coefficient of the original state remains unchanged. However, if the state is annihilated, then the entry becomes zero.

Listing 11: Function that corresponds to the number operator

```
1   function N(steady_state, basis_states_s, k)
2
3       steady_temp = copy(steady_state)
4
5       for (i, (state, state_t)) in enumerate(basis_states_s)
6
7           if create(k, ann(k, state)) == nothing
8               steady_temp[i] = 0
9           end
10      end
11      return steady_temp
12  end
```

The next function, shown in listing *12*, performs some consistency checks. When creating our simulation, we obviously want it to give physical results. This is only possible, if the correct implementation of the theory in the code is ensured. Since we know some conditions that must be fulfilled, we can check that this is indeed the case. Firstly, there must be a stationary state, which is checked in line 7, since, otherwise, all the other calculations do not make any sense. The variable stationary, introduced in listing *9*, contains all the eigenvalues which have an absolute value smaller than[10] 10^{-5}. Therefore, if this list has a length of more than zero, at least one stationary state exists. Line 12 checks if all the eigenvalues of the gamma matrices are equal to, or bigger than zero, since they must be positive semidefinite. In the lines 17 to 21, we apply the Lindbladian to the steady state from the right, and to the left vacuum from the left. Both results must give zero, therefore, the sum of all the components must be zero. This is checked in line 23. The last two checks in line 30 and 39 are regarding observables. For the occupation number it is checked that $n - \tilde{n} = 0$ is fulfilled, and since there is no magnetic field present, the result must be equal for both spins. In the steady state, the sum of all currents flowing into and out of each site must vanish. Another property of observables in general is, that they must be real valued. So we also check that the imaginary part is (up to numerical errors) zero in line 38.

Listing 12: Function for basic consistency checks.

```
1   function check_results(gam_in_up, gam_out_up, stationary, L_s, steady_state,
2   vac_left, n_up, n_down, n_up_round, n_down_round, n_up_round_t, n_down_round_t,
3   inflow, outflow, left, right)
4
5       x = 0
6
7       if length(stationary) > 0
8           x = x + 1
9           print("\n\n$(length(stationary)) stationary state/s has/have been found.")
10      end
11
12      if all(x -> x>=0, eigvals(gam_in_up)) && all(x -> x>=0, eigvals(gam_out_up))
13          x = x + 1
14          print("\n\nThe gamma matrices are positive definite.")
15      end
16
17      test_steady = L_s * steady_state
18      test_steady = [x for x in test_steady if abs(x) > 1e-12]
19
20      test_vac_left = vac_left' * L_s
21      test_vac_left = [x for x in test_vac_left if abs(x) > 1e-12]
```

---

[10]This is due to numerical errors, which may cause the results not to be exactly zero but very small.

```
22      if test_steady == [] && test_vac_left == [] && (abs(vac_left' \cdot steady_state)
23      - 1) < 1e-8
24          x = x + 1
25          print("\n\nThe steady state as well as the left vacuum annihilate L, and the
26          trace of the steady state is equal to one.")
27      end
28
29      if n_up_round == n_down_round && sum([abs(imag(x)) for x in n_up]) < 1e-8
30      && sum([abs(imag(x)) for x in n_down]) < 1e-8 && sum(n_up_round_t
31      + n_down_round_t - n_up_round - n_down_round) == 0
32          x = x + 1
33          print("\n\nThe particle density is real valued and equal for spin up
34          and spin down, and the particle number is conserved.")
35      end
36
37
38      if abs(sum(inflow + outflow + left + right)) < 1e-8 && abs(imag(sum(inflow)))
39      + abs(imag(sum(outflow))) + abs(imag(sum(left))) + abs(imag(sum(right)))
40      < 1e-8
41          x = x + 1
42          print("\n\nSum of currents over all sites is zero, and up to numerical
43          errors they are real valued.")
44      end
45
46      print("\n\n$x/5 checks worked out.")
47  end
```

As a next step, we will add an external time periodic electric field, which also has a spatial change of the magnitude. However, we can show that it is reasonable to neglect this spatial difference for typical physical systems. Since the gaps of semiconductors are of the order of eV[11], it is quite physical to choose this as the unit for our energy. Using this, it can be seen that we deal with systems in which at least $1eV$ is necessary to get from the lower to the higher band. This gives the minimal relevant wavelength λ as

$$\nu = \frac{E}{h} = \frac{1\text{eV}}{4 \cdot 10^{-15}\text{eVs}} = 2.5 * 10^{14}\text{s}^{-1} \rightarrow \lambda = \frac{3 \cdot 10^8\text{m/s}}{2.5 \cdot 10^{14}\text{s}^{-1}} = 1.2 \cdot 10^{-6}\text{m}. \tag{65}$$

Silicon, being a typical semiconductor, has a lattice constant of approximately 5Å. The longest chains with applied driving will certainly be shorter than 20 sites. The highest value for the slope is $\frac{2\pi E}{\lambda}$, with E the magnitude of the electric field. So let us compare the relative highest difference between the outermost sites:

$$\Delta = \frac{2\pi E}{\lambda} \cdot 20 \cdot \text{sites} \cdot 5 \cdot 10^{-10}\text{m/site} \cdot \frac{1}{E} = 5.2\%. \tag{66}$$

In our simplified model, the electric field changes only the on-site energy periodically in time. On-site energies are only relevant on the diagonal part of the Lindbladian matrix. Therefore, we can collect all the information related to the time dependency in a vector with the same number of entries as we have basis states. This vector corresponds to the one called p in listing *13*. We have to sum up all the particles in each state, that are influenced by the time periodic part. This is done in the for loop starting in line 10. Once for the normal space and another time for the tilde space. In line 16, we multiply this vector element wise with the identity, to create a matrix which has this vector on its diagonal, and add it to the Lindbladian. With this we can set up our system of differential equations as done in line 16, which is then solved numerically in line 18. What we get as a result, is a value of the density matrix in superfermion representation for each time step, from which we can extract the current.

---

[11]http://hyperphysics.phy-astr.gsu.edu/hbase/Tables/Semgap.html

Listing 13: Function for calculating the current as a function of time with applied periodic driving.

```julia
function get_current_t_direct(ω)
    p = complex(zeros(length(basis_states_s)))
    u_0 = complex(zeros(length(basis_states_s)))
    u_0 = steady_state

    time = (0.0, 100.0)

    for (i, (state, state_t)) in enumerate(basis_states_s)
        particles = sum([parse(Int, i) for i in
        [x for x in state][collect(Iterators.flatten([[x x] for x in driving]))]])
        particles_t = sum([parse(Int, i) for i in
        [x for x in state_t][collect(Iterators.flatten([[x x] for x in driving]))]])
        p[i] = -1im*(particles - particles_t)
    end

    ff(u,p,t) = (L_s + I(length(basis_states_s)).*p*α*cos(ω * t)) * u
    prob = ODEProblem(ff, collect(Complex{Float64}, u_0), time, p)
    sol = solve(prob, AutoTsit5(ABDF2()), adaptive=true, saveat = 0.1)

    inflow_t = []
    outflow_t = []
    right_t = []
    left_t = []
    current_temp = zeros(4, length(sol.t))

    for i in 1:length(sol.t)
        inflow_temp, outflow_temp, right_temp, left_temp = get_current(sol.u[i])
        append!(inflow_t, [inflow_temp])
        append!(outflow_t, [outflow_temp])
        append!(right_t, [right_temp])
        append!(left_t, [left_temp])
    end

    return inflow_t, outflow_t, right_t, left_t, sol.t, sol
end
```

A.2 Interacting Green's Functions

The next function we will discuss, which is split up into listings *14*, and *15*, is responsible for evaluating the interacting Green's functions using the Lehmann representation [*19*]:

$$G_{ij}^{>+}(\omega) = \sum_i \langle I| a_i |iR\rangle \langle iL| a_j^\dagger |\rho_\infty\rangle \frac{1}{\omega - iL_i}, \tag{67}$$

where L_i are the eigenvalues of the Lindblad operator, $\langle iL|$ are the left, and $|iR\rangle$ the right eigenstates of L, and all other parameters have the same meaning as described in the theory chapter. Eq. *67* shows the greater Green's function, for which we will exemplary show how it is obtained, since the lesser one, which can be found in [*19*] as well, is obtained similarly. We only need the subspace for which $n - \tilde{n} = \pm 1$ is fulfilled, since then the respective right eigenstate, and the left vacuum, as well as the steady state and the left eigenstate, have the same particle number after applying the annihilation/creation operator. The list `basis_states_s_plus` contains the states for $n - \tilde{n} = +1$ and `basis_states_s` the ones for $n - \tilde{n} = 0$. Our first step, shown in listing *14*, is to map which two states of these lists correspond to each other, after applying a creation or annihilation operator. In general, a state may consist of a superposition of many-bode states, and we have to apply the annihilation/creation operator to each individual state, and we either get a new one in the respective subspace, or the state is annihilated. An example of this procedure for such a generally defined state is given in figure *84*.
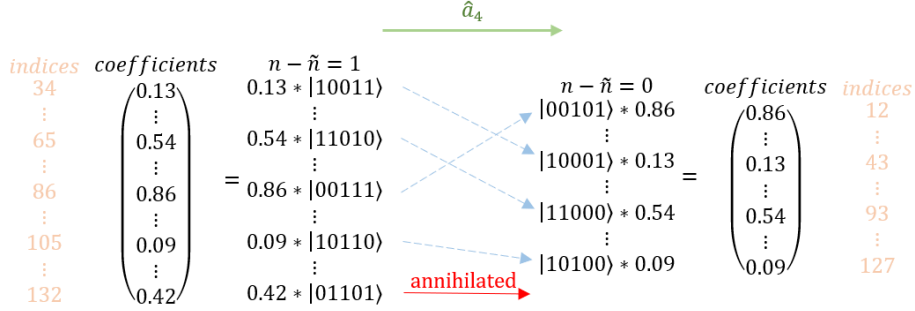
Figure 84: Mapping the states of the $n - \tilde{n} = \pm 1$ subspace to the $n - \tilde{n} = 0$ subspace after application of an annihilation operator. The states of the tilde space have been neglected.

To perform this computation, we apply the annihilation operator for the appropriate site, on each state in the respective basis, as shown in line 13. Our final goal is to multiply two states, one of which changes from one subspace to another, the other one stays in its subspace. So we first save the index position of the vector entry for the state which stays in its space in line 14. Then, in line 15, we must find the corresponding index position of the vector entry for the state, which after applying an operator is now in a new subspace. Lines 26 to 32 do precisely the same, just potentially with another state being annihilated.

Listing 14: Function to calculate the interacting Green's functions 1/2.

```
1   function get_G_greater(a_pos_mu, a_pos_nue, w, basis_states_s_plus,
2   vac_left, steady_state, basis_states_s, eig_vect_plus_l, eig_vect_plus_r,
3   eig_val_plus, spin)
4
5       G_greater_temp = zeros(length(w))
6       G_greater_plus_temp = zeros(length(w))
7       pos_R_plus = []
8       pos_L_plus = []
9       pos_vac_plus = []
10      pos_rho_plus = []
11      phase_1 = []
12      phase_2 = []
13
14      for (i, (state, state_t)) in enumerate(basis_states_s_plus)
15          if ann(a_pos_mu*2 - spin, state) != nothing
16              append!(pos_R_plus, i)
17              append!(pos_vac_plus, findall(x -> x ==
18              (ann(a_pos_mu*2 - spin, state), state_t), basis_states_s))
19              append!(phase_1, (-1)^sum([parse(Int, x)
20              for x in state[1:a_pos_mu*2 - spin - 1]]))
21          end
22      end
23
24      for (i, (state, state_t)) in enumerate(basis_states_s_plus)
25          if ann(a_pos_nue*2 - spin, state) != nothing
26              append!(pos_L_plus, i)
27              append!(pos_rho_plus, findall(x -> x ==
28              (ann(a_pos_nue*2 - spin, state), state_t), basis_states_s))
29              append!(phase_2, (-1)^sum([parse(Int, x)
30              for x in state[1:a_pos_nue*2 - spin - 1]]))
31          end
32      end
```

Now, in listing *15*, we can multiply the correct values with each other, by inserting the list of indices for both vectors, as is done in the code. The temporary variables, `term_i_j`, represent the different terms in this equation, and only serve the purpose of a better overview. We want to get the Green's function as a function of ω, and there is only one of the three terms that are being multiplied, that depends on ω. Therefore, the other two terms only have to be calculated once, and are then multiplied with the vector of results. The lesser Green's function is calculated similarly, and using the lesser and greater one, we can obtain the Keldysh and retarded Green's function.

Listing 15: Function to calculate the interacting Green's functions 2/2.

```
1       for i in 1:length(basis_states_s_plus)
2
3           term_1_1 =  broadcast(x -> 1/(x - eig_val_plus[i]), w)
4
5           term_1_2 = vac_left[pos_vac_plus]'
6           * (eig_vect_plus_r[pos_R_plus, i].* phase_1)
7
8           term_1_3 = eig_vect_plus_l[pos_L_plus,i]' * (phase_2.*steady_state[pos_rho_plus])
9
10          term_2_1 =  broadcast(x -> 1/(x - conj(eig_val_plus[i])), w)
11
12          term_2_2 = vac_left[pos_rho_plus]'
13          * (eig_vect_plus_r[pos_L_plus, i].* phase_2)
14
15          term_2_3 = eig_vect_plus_l[pos_R_plus,i]'
16          * (phase_1.*steady_state[pos_vac_plus])
17
18          G_greater_plus_temp = (term_1_1 * term_1_2 * term_1_3)
19          + G_greater_plus_temp
20      end
21      return G_greater_plus_temp
22  end
```

A.3 Non-interacting Green's Function

From [*19*], we also obtain an easy formula to calculate the non-interacting Green's function:

$$
\begin{aligned}
G_0^{>+}(\omega) &= U\bar{D}(\omega - \varepsilon)^{-1}U^{(-1)} \\
\bar{D}_{ij} &= \delta_{ij} - \delta_{ij}\Theta(Im(\varepsilon_i)), \\
U &= TV \\
T &= \begin{pmatrix} \mathbb{1} & 0 \end{pmatrix} \\
H &= \begin{pmatrix} E + i\Omega & 2\Gamma^{(2)} \\ -2\Gamma^{(1)} & E - i\Omega \end{pmatrix}, \\
\Omega &= (\Gamma^{(2)} - \Gamma^{(1)}).
\end{aligned}
\tag{68}
$$

where E is a tridiagonal matrix, which has the on-site energies on its diagonal and the hopping parameter on the two off-diagonal parts, V is the eigenvector matrix of E, and ε_i are the eigenvalues of E. In eq. *68* we showed the result for the greater Green's function, and for the lesser one it can also be found in [*19*]. In listing *16*, we performed this computation, and since this is, from an implementation point of view, a straightforward process, no specific explanation is provided.

Listing 16: Function to calculate the non-interacting Green's functions.

```julia
function get_Greens_Functions_0(w, gam_in_up, gam_out_up, t, e, sites)

    T = [float(I(sites)) zeros(sites,sites)]
    T_t = transpose(T)

    omega = gam_in_up - gam_out_up
    e_tri = e[1:2:end]
    t_tri = ones(sites-1)*t
    E = Tridiagonal(t_tri, e_tri, t_tri)

    h = complex(zeros(2*sites, 2*sites))

    h[1:sites, 1:sites] = E + 1im*omega
    h[1:sites, sites+1:end] = 2*gam_in_up
    h[sites+1:end, 1:sites] = -2*gam_out_up
    h[sites+1:end, sites+1:end] = E - 1im*omega

    eigen_value, V = eigen(h)
    V_inv = inv(V)
    eps = Diagonal(eigen_value)

    D = Diagonal(broadcast(x -> (sign(x)+1)/2, imag(eigen_value)))

    D_ = Diagonal(ones(sites*2)) - D

    G_greater_0 = [T * V * D_ * inv(x*I(sites*2) - eps) * V_inv * T_t for x in w]
    G_smaller_0 = [T * V * D * inv(x*I(sites*2) - eps)  * V_inv * T_t for x in w]
    G_greater_0_dag = [transpose(conj(x)) for x in G_greater_0]
    G_smaller_0_dag = [transpose(conj(x)) for x in G_smaller_0]

    G_K_0 = G_greater_0 + G_smaller_0 - (G_greater_0_dag + G_smaller_0_dag)
    G_R_0 = G_greater_0 + G_smaller_0_dag

    G_greater_0_full = G_greater_0 - G_greater_0_dag
    G_smaller_0_full = G_smaller_0 - G_smaller_0_dag

    return G_greater_0_full, G_smaller_0_full, G_R_0, G_K_0
end
```

A.4 Non-interacting equations of motion method

In the first piece of code, given in listing *17*, we will explain all the parameters being used. Our chain has three separate parts, and, using the parameter `broadness`, we can set their thickness. With `sites_x_split` we define the length of each part. The hopping parameter `t_hop` generally has four indices in 2D, since each entry is relevant for the coupling of two sites, with two indices needed for each. `e` defines the on-site energy. α and ω are the parameters for the applied periodic driving, $E(t) = \alpha \cos(\omega t)$, and the driving is applied to the sites for which `driving` is `true`. The interaction with the outside world is described by the parameters `gam_in`, and `gam_out`. Those last two parameters describe the inflow and outflow on the leftmost site, and we always use the swapped values for the rightmost site. Figure *85* visualizes our setup.

Listing 17: Parameters for equations of motion simulation.

```
1    broadness = [1 1 1]
2    sites_x_split = [7 14 7]
3    t_hop = ones((sites_x, maximum(broadness), sites_x, maximum(broadness)))
4    e = zeros((2, sites_x))
5    driving = zeros((2, sites_x))
6    α = 1.0
7    ω = 1.0
8    gam_in = 0.8
9    gam_out = 0
```
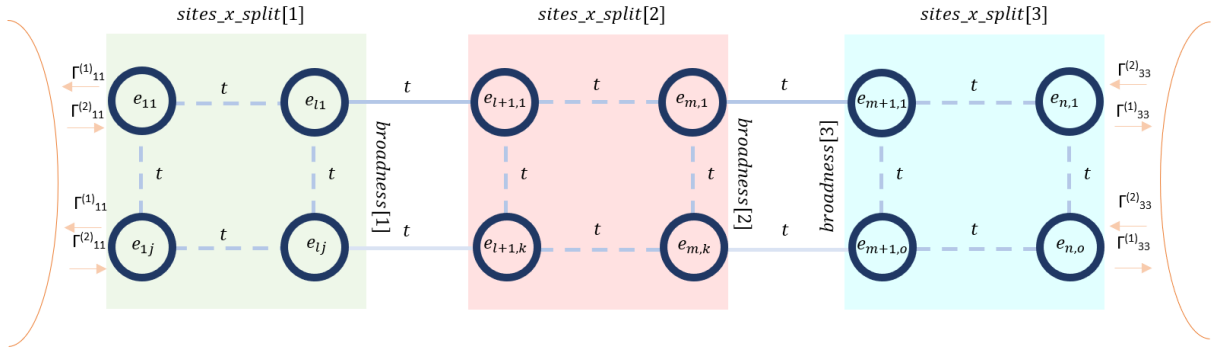

Figure 85: Visualization of the setup. The indices for the t have been left out, however, it is emphasized that each of them may have an individual value. Furthermore, the connections between the different areas on the very bottom, are in the general case not between the last site of each block, since they may have different broadness. To show this, the respective lines are more transparent.

The following substitutions have been made in figure *85*:

$$
\begin{aligned}
e[i,j] &\rightarrow e_{ij} \\
t\_hop[i,j,k,l] &\rightarrow t \\
gam\_out &\rightarrow \Gamma^{(1)}_{11} \\
gam\_in &\rightarrow \Gamma^{(2)}_{11}
\end{aligned}
\tag{69}
$$

Knowing all the necessary parameters, we can get to the actual code. We want the current flowing through our chain, and in all the setups for which we will use this code, the following statements are true:

1. Only for the left- and rightmost sites the parameters which determine in- and outflow of the system are non-zero.

2. The two left- and rightmost sites, do not have neighbours normal to the direction of chain extension.

Therefore, the current can always be obtained from $\left\langle c_{11}^{\dagger} c_{21} \right\rangle$, and $\left\langle c_{21}^{\dagger} c_{11} \right\rangle$. However, generally this still means we will have to solve for all the possible $\left\langle c_{ij}^{\dagger} c_{kl} \right\rangle$, since they are all coupled with one another, and there are n_{sites}^2 functions of this form. The variable `vars`, presented in listing 18, contains arrays of the form `[(i,j), (k,l)]` $\left(\rightarrow \left\langle c_{ij}^{\dagger} c_{kl} \right\rangle \right)$, where each one represents one function, and the `for` loop and its contained functions generate a list of all possible combinations. The idea for the function `get_functions` is very similar to the one given in listing 19, therefore, we will not discuss it in detail. The function `generic_non_interacting_chain()` creates the coefficient matrix, as well as the one for the periodic driving, and the inhomogeneous part.

Listing 18: Code implementation of the equations of motion method.

```
1   start = [[(1,1), (2,1)], [(2,1), (1,1)]]
2   append!(vars, start)
3   for var in vars
4
5       get_functions(var, vars, 1, 0)
6       get_functions(var, vars, -1, 0)
7       get_functions(var, vars, 0, 1)
8       get_functions(var, vars, 0, -1)
9
10  end
11
12  K_coef, K_val, K_t = generic_non_interacting_chain()
13
14  writedlm( "Koef_real.csv",  real(K_coef), ';')
15  writedlm( "Koef_imag.csv",  imag(K_coef), ';')
16  writedlm( "b.csv",  real(-K_val*complex(ones((length(vars), 1)))), ';')
17
18  ff(u,p,t) = (K_coef + K_t.*α*cos(ω*t))*u + K_val*complex(ones((length(vars), 1)))
19
20  u_0 = complex(ones((length(vars), 1)))
21  time = (0.0, 200.0)
22  beginning = 1000
23  prob = ODEProblem(ff, u_0, time)
24  sol = solve(prob, dt=0.04,adaptive=false)
```

The next function, listing *19*, shows the implementation of the algorithm, which we created in eq. (*53*). In the lines 3 to 5 we create three matrices. `A_coef` is the coefficient matrix for the $\left\langle c_{ij}^{\dagger} c_{kl} \right\rangle$, `A_val` is the matrix for the inhomogenous part[12], and `A_t` is the coefficient matrix for the $\left\langle c_{ij}^{\dagger} c_{kl} \right\rangle$ that are multiplied by the time periodic part. Figure *86* shows which position in the matrices corresponds to which function. Lines 10 and 11 set the entries for the on-site energy, and the time periodic part, and lines 24 to 44 set the entries for the gamma values. The hopping between sites is taken care of by the lines 17 to 22. Our algorithm, however, only takes into account nearest neighbour hopping. In one of the cases we want to look into, we need some additional hopping, which is realized by the lines 20 and 22.

Listing 19: Function to create the coefficient matrix for the eom method..

```
1   function generic_non_interacting_chain(vars, size, t_hop, star_points)
2       size = length(vars)
3       A_coef = complex(zeros(size, size))
4       A_val = complex(zeros(size, size))
5       A_t = complex(zeros(size, size))
6       constants = [[1 0], [-1 0]]
7
8       for (i, var) in enumerate(vars)
9
10          get_driving(var[1], var[2], A_coef, A_t, i, 1)
11          get_driving(var[2], var[1], A_coef, A_t, i, -1)
12
13          for (k, cons) in enumerate(constants)
14              get_hopping_eom(var, A_coef, i, cons[1], cons[2], t_hop, vars)
15          end
16
17          get_hopping_eom(var, A_coef, i, 1, 1, 1.0)
18          get_hopping_eom(var, A_coef, i, -2, 0, 1.0)
19
20          add_hopping_between(var, A_coef, i, 1, 1, t_hop, star_points[1:2], vars)
21
22          add_hopping_between(var, A_coef, i, 1, -1, t_hop, star_points[3:4], vars)
23
24          if var[1][1] == 1 && var[2][1] != 1 || var[1][1] != 1 && var[2][1] == 1
25              A_coef[i, i] = A_coef[i, i] + -gam_in/2
26              A_coef[i, i] = A_coef[i, i] + -gam_out/2
27          end
28
29          if var[1][1] == sites_x && var[2][1] != sites_x ||
30          var[1][1] != sites_x && var[2][1] == sites_x
31              A_coef[i, i] = A_coef[i, i] + -gam_in/2
32              A_coef[i, i] = A_coef[i, i] + -gam_out/2
33          end
34
35          if var[1][1] == 1 && var[2][1] == 1
36              A_coef[i, i] = A_coef[i, i] + -gam_out
37              A_coef[i, i] = A_coef[i, i] + -gam_in
38              A_val[i, i] = A_val[i, i] + gam_in
39
40          elseif var[1][1] == sites_x && var[2][1] == sites_x
41              A_coef[i, i] = A_coef[i, i] + -gam_in
42              A_coef[i, i] = A_coef[i, i] + -gam_out
43              A_val[i, i] = A_val[i, i] + gam_out
44          end
45
46      end
47
48      return A_coef, A_val, A_t
49   end
```

[12]Which will later be transformed to a vector

$$\begin{array}{c}\overset{\textit{vars}[1]\qquad\quad\textit{vars}[\textit{end}]}{\textit{vars}[1]}\\\textit{vars}[\textit{end}]\end{array}\begin{pmatrix} C_{11} & \cdots & C_{n1} \\ \vdots & \ddots & \vdots \\ C_{1n} & \cdots & C_{nn} \end{pmatrix}$$

Figure 86: Structure of the coefficient matrix.

We now discuss all the sub-functions mentioned in listing *19*, and start with the on-site energy, and periodic driving. This part is shown in listing *20*. In eq. (*53*) we established conditions under which on-site energy parts exist. Here we do precisely this, except that we split up the time periodic, and constant part. We first check if the on-site energy is nonzero, and if there is driving. If the latter is not true, then we check if there is only a constant on-site energy contribution. The driving component, if nonzero, is saved in A_t, and the on-site energy, again if nonzero, is saved in A_coef.

Listing 20: Function to create the on-site energy, and periodic driving entries..

```
1  function get_driving(var_1, var_2, A_coef, A_t, i, factor)
2      if driving[var_1[2], var_1[1]] == true && var_1 != var_2
3          A_coef[i, i] = A_coef[i, i] + factor * 1im*e[var_1[2], var_1[1]]
4          A_t[i, i] = A_t[i, i] + factor * 1im
5      elseif var_1 != var_2
6          A_coef[i, i] = A_coef[i, i] + factor * 1im*e[var_1[2], var_1[1]]
7      end
8  end
```

Listing *21* shows the part that takes into account the hopping between sites. The first `if` condition in line 3 checks for a case of the form $[c_i^\dagger c_j, c_j^\dagger c_i]$, and if so, we need the position at which we have to add a values to the coefficient matrix, as done in lines 4 and 7. If the commutator does not have this form, we only check if the boundaries are not violated, since then we increase or decrease the index of some creation or annihilation operator. Afterwards, we again need to search for the position at which entries must be added. The idea for the function `add_hopping_between` is the same, therefore, we will not repeat the explanation.

Listing 21: Function to create the entries for hopping between neighbouring sites..

```
1  function get_hopping_eom(var, A_coef, i, const_1, const_2, t_hop, vars)
2
3      if (var[1][1], var[1][2]) == (var[2][1] + const_1, var[2][2] + const_2)
4          j = findall(x->x==[(var[1][1],var[1][2]), (var[1][1],var[1][2])], vars)[1]
5          A_coef[i, j] = A_coef[i, j] + -1im*t_hop[var[2][1], var[2][2], var[2][1]
6          + const_1, var[2][2] + const_2]
7          j = findall(x->x==[(var[2][1],var[2][2]), (var[2][1],var[2][2])], vars)[1]
8          A_coef[i, j] =  A_coef[i, j] + 1im*t_hop[var[2][1], var[2][2], var[2][1]
9          + const_1, var[2][2] + const_2]
10     end
11
12     if var[2][1] + const_1 <= sites_x && var[2][1] + const_1 >= 1 && var[2][2]
13     + const_2 >= 1 && var[2][2] + const_2 <= sites_y[var[2][1] + const_1] &&
14     (var[1][1], var[1][2]) != (var[2][1] + const_1, var[2][2] + const_2) const_2)])
15         j = findall(x->x==[(var[1][1], var[1][2]), (var[2][1] + const_1, var[2][2]
16         + const_2)], vars)[1]
17         A_coef[i, j] = A_coef[i, j] -
18         1im*t_hop[var[2][1], var[2][2], var[2][1] + const_1, var[2][2] + const_2]
19     end
20
21     if var[1][1] + const_1 <= sites_x && var[1][1] + const_1 >= 1 && var[1][2]
22     + const_2 >= 1 && var[1][2] + const_2 <= sites_y[var[1][1] + const_1] &&
23     (var[1][1] + const_1, var[1][2] + const_2) != (var[2][1], var[2][2])
24         j = findall(x->x==[(var[1][1] + const_1, var[1][2] + const_2),
25         (var[2][1], var[2][2])], vars)[1]
26         A_coef[i, j] = A_coef[i, j] +
27         1im*t_hop[var[1][1] + const_1, var[1][2] + const_2, var[1][1], var[1][2]]
28     end
29  end
```

Having successfully created all our matrices, we can eventually set up our system of equations, as is done in listing *22*. `ff(u,p,t)` is the function, which we will set equal with the derivative of `u`, where `u` is the vector of $\left\langle c_{ij}^{\dagger} c_{kl} \right\rangle$, `p` is a constant that we do not need here, and `t` is the time. The equation reads:

$$\frac{\mathrm{d}c(t)}{\mathrm{d}t} = (A_{coef} + A_t \alpha \cos(\omega t))c(t) + b, \tag{70}$$

The vector `u_0` is the vector of starting values. It generally does not matter what we choose, because anything will lead to the same time periodic behaviour in the long term. We may think of this similarly as of the steady state. In all cases relevant to us, there is only one such state, and, therefore, we may expect that applying a time periodic perturbation will only allow for a single "stable" periodic signal, to which any starting state will converge. Line 6 uses the ode solver of DifferentialEquations.jl. The option `AutoTsit5(ABDF2())` sets a default explicit solver, and if the program notices that an implicit solver is more advantageous, it switches [13]. For our problem, after trying several step sizes without the adaptive option, it seems to be best to let the algorithm decide which step size to use. The `saveat` option saves values for specific steps by interpolation.

Listing 22: Function to calculate the evolution in time numerically..

```
1    ff(u,p,t) = (A_coef + A_t.*α*cos(ω*t))*u
2    + A_val*complex(ones((length(vars), 1)))
3    u_0 = complex(ones((length(vars), 1)))
4    time = (0.0, time_range)
5    prob = ODEProblem(ff, u_0, time)
6    sol = solve(prob, AutoTsit5(ABDF2()), adaptive=true, progress=false
7    , saveat = step_size)
```

---

[13]In https://diffeq.sciml.ai/stable/solvers/ode_solve/ this is recommended for systems with unknown stiffness. Tsit5 is also recommended for most non-stiff problems.

References

[1] Philipp Werner, Karsten Held, and Martin Eckstein. Role of impact ionization in the thermalization of photoexcited mott insulators. *Phys. Rev. B*, 90:235102, Dec 2014.

[2] Martin Eckstein and Philipp Werner. Thermalization of a pump-excited mott insulator. *Phys. Rev. B*, 84:035122, Jul 2011.

[3] Max E. Sorantin, Antonius Dorda, Karsten Held, and Enrico Arrigoni. Impact ionization processes in the steady state of a driven mott-insulating layer coupled to metallic leads. *Phys. Rev. B*, 97:115113, Mar 2018.

[4] Efstratios Manousakis. Photovoltaic effect for narrow-gap mott insulators. *Phys. Rev. B*, 82:125109, Sep 2010.

[5] John E. Coulter, Efstratios Manousakis, and Adam Gali. Optoelectronic excitations and photovoltaic effect in strongly correlated materials. *Phys. Rev. B*, 90:165142, Oct 2014.

[6] Elias Assmann, Peter Blaha, Robert Laskowski, Karsten Held, Satoshi Okamoto, and Giorgio Sangiovanni. Oxide heterostructures for efficient solar cells. *Phys. Rev. Lett.*, 110:078701, Feb 2013.

[7] William Shockley and Hans J. Queisser. Detailed balance limit of efficiency of p-n junction solar cells. *Journal of Applied Physics*, 32(3):510–519, 1961.

[8] Gernot Schaller. *Open Quantum Systems Far from Equilibrium*, volume 881. 11 2013.

[9] Crispin W. Gardiner and Paul Zoller. Quantum noise: A handbook of markovian and non-markovian quantum stochastic methods with applications to quantum optics. 2004.

[10] Carmichael and Howard J. *Statistical Methods in Quantum Optics 1*. 1999.

[11] Claude Cohen-Tannoudji, Jacques Dupont-Roc, and Gilbert Grynberg. *Atom—Photon Interactions*. 1998.

[12] Heinz-Peter Breuer and Francesco Petruccione. *The Theory of Open Quantum Systems*. 01 2006.

[13] Enrico Arrigoni and Antonius Dorda. *Master Equations Versus Keldysh Green's Functions for Correlated Quantum Systems Out of Equilibrium*, pages 121–188. Springer International Publishing, Cham, 2018.

[14] Maximilian Schlosshauer. Quantum decoherence. *Physics Reports*, 831:1–57, Oct 2019.

[15] Alan A Dzhioev and D S Kosov. Nonequilibrium configuration interaction method for transport in correlated quantum systems. *Journal of Physics A: Mathematical and Theoretical*, 47(9):095002, Feb 2014.

[16] Alan A. Dzhioev and D. S. Kosov. Super-fermion representation of quantum kinetic equations for the electron transport problem. *The Journal of Chemical Physics*, 134(4):044121, 2011.

[17] Alan A Dzhioev and D S Kosov. Nonequilibrium perturbation theory in liouville–fock space for inelastic electron transport. *Journal of Physics: Condensed Matter*, 24(22):225304, May 2012.

[18] J. Hubbard. Electron correlations in narrow energy bands. *Proceedings of the Royal Society of London. Series A, Mathematical and Physical Sciences*, 276(1365):238–257, 1963.

[19] Antonius Dorda, Martin Nuss, Wolfgang von der Linden, and Enrico Arrigoni. Auxiliary master equation approach to nonequilibrium correlated impurities. *Physical Review B*, 89(16), Apr 2014.

[20] Enrico Arrigoni. Handwritten lecture notes.

[21] Jakob Neumayer, Enrico Arrigoni, Markus Aichhorn, and Wolfgang von der Linden. Current characteristics of a one-dimensional hubbard chain: Role of correlation and dissipation. *Phys. Rev. B*, 92:125149, Sep 2015.

[22] Ch. Tsitouras. Runge–kutta pairs of order 5(4) satisfying only the first column simplifying assumption. *Computers Mathematics with Applications*, 62(2):770–775, 2011.